TUNIVERSIDADE TÉCNICA DO ATLÂNTICO
INSTITUTO DE ENGENHARIA E CIÊNCIAS DO MAR

WEST AFRICAN SCIENCE SERVICE CENTER ON CLIMATE CHANGE AND ADAPTED LAND USE

Master Thesis

AEROSOLS OPTICAL PROPERTIES PROFILE CHARACTERIZATION OVER SÃO VICENTE, CABO VERDE, DURING THE ASKOS CAMPAIGN

Samira Moussa Idrissa

Master Research Program on Climate Change and Marine Sciences

São Vicente
2022

UNIVERSIDADE TÉCNICA DO ATLÂNTICO
INSTITUTO DE ENGENHARIA E CIÊNCIAS DO MAR

WEST AFRICAN SCIENCE SERVICE CENTER ON CLIMATE CHANGE AND ADAPTED LAND USE

Master Thesis

AEROSOLS OPTICAL PROPERTIES PROFILE CHARACTERIZATION OVER SÃO VICENTE, CABO VERDE, DURING THE ASKOS CAMPAIGN

Samira Moussa Idrissa

Master Research Program on Climate Change and Marine Sciences

Supervisor | Prof. Dr. Nilton Évora do Rosário
Co-supervisor |Dr. Nickolaos Siomos

São Vicente
2022

UNIVERSIDADE TÉCNICA DO ATLÂNTICO
INSTITUTO DE ENGENHARIA E CIÊNCIAS DO MAR

WEST AFRICAN SCIENCE SERVICE CENTER ON CLIMATE CHANGE AND ADAPTED LAND USE

AEROSOLS OPTICAL PROPERTIES PROFILE CHARACTERIZATION OVER SÃO VICENTE, CABO VERDE, DURING THE ASKOS CAMPAIGN.

Samira Moussa Idrissa

Master's thesis presented to obtain the master's degree in Climate Change and Marine Sciences by the Institute of Engineering and Marine Sciences, Atlantic Technical University in the framework of the West African Science Service Center on Climate Change and Adapted Land Use.

Supervisor

Prof. Dr. Nilton Évora do Rosário

Federal University of São Paulo - Brazil

Co-supervisor

Dr Nikolaos Siomos

Ludwig-Maximilians-Universität,

São Vicente
2022

UNIVERSIDADE TÉCNICA DO ATLÂNTICO
INSTITUTO DE ENGENHARIA E CIÊNCIAS DO MAR

WEST AFRICAN SCIENCE SERVICE CENTER ON CLIMATE CHANGE AND ADAPTED LAND USE

AEROSOLS OPTICAL PROPERTIES PROFILE CHARACTERIZATION OVER SÃO VICENTE, CABO VERDE, DURING THE ASKOS CAMPAIGN.

Samira Moussa Idrissa

Panel defence

President

_____

Examiner 1

_____

Examiner 2

_____

São Vicente
2022

Financial support

The German Federal Ministry of Education and Research (BMBF) in the framework of the West African Science Service Centre on Climate Change and Adapted Land Use (WASCAL) through WASCAL Graduate Studies Programme in Climate Change and Marine Sciences at the Institute for Engineering and Marine Sciences, Atlantic Technical University, Cabo Verde.

Dedication

To my mother Aïssa Bana

Whatever I do or say, I couldn't thank you enough. Your affection covers me; your benevolence and your prayers guide me. Your presence has always been my source of strength to face different challenges.

To my father Moussa Idrissa

You have always been my model, my inspiration. Your support, your encouragement, and your prayers have always accompanied me.

May this work express my gratitude and affection.

Acknowledgements

I would start by thanking the almighty God for His unconditional blessings and who voluntarily allowed me to get to this position today,

I would like to express my gratitude to Prof. Dr Nilton Évora do Rosario and Dr. Nikolaos Siomos, who have accompanied me throughout this learning process. I thank them for their support, guidance, motivation and patience. They proved that " with some motivation and the right people around one can achieve significant and many things ". Working with them always motivated me to work hard, be diligent and do better.

Special thanks to the eVe team: Peristera Pachou and Dr Eleni Marinou, for their encouragement and for giving me the opportunity to discover this new field.

My Profound gratitude to the remote sensing team of Tropos for their availability and assistance during and after my internship at Tropos, especially to Dr Holger Baars, and Dr Julian Hofer.

I am equally thankful to the Director of WASCAL Cabo Verde, Dr. Corrine Almeida, the Deputy Director, Dr António Pinto Almeida, the Scientific coordinator Dr Estanislau Baptista Lima and the staff for all their support and constructive criticism during different stages of my studies.

Thanks to all my colleagues of the 2nd cohort, especially Emmanuel Tora, my family and friends for their encouragement, support and prayers during this process.

I would not complete this without an acknowledgement to the Federal Ministry of Education and Research (BMBF) that funded the West Africa Science Service Center on Climate Change and Adapted Land Use (WASCAL) which offered me the Master Research Program in Climate change and Marine Sciences fellowship.

And finally, my heartfelt gratitude to all the staff of the Institute of Engineering and Marine Sciences (ISECMAR) of the Atlantic Technical University and more so to all my lecturers for all forms of guidance they offered during my studies period.

Resumo

O estudo da distribuição vertical das partículas de aerossol é um aspecto muito importante para compreender a sua influência sobre o sistema climático. Uma forma de avaliar este aspecto dos aerossóis é discriminar a sua fonte e as propriedades ópticas na coluna atmosférica. O principal objectivo deste estudo foi caracterizar e analisar o perfil das propriedades ópticas do aerossol sob distintos cenários de mistura de aerossóis sobre a ilha de São Vicente, Cabo Verde, durante a campanha ASKOS que ocorreu em Julho e Setembro de 2021. Assim, foi aplicado o método de Extinção Elástica (ElEx) que permitiu a separação do perfil de retroespalhamento do aerossol por tipo e a estimativa do coeficiente de extinção total. A aplicação do método EIEx requer o retroespalhamento total e a razão de despolarização linear das partículas resolvidos verticalmente no mesmo comprimento de onda, obtidos do sistema LIDAR eVe, e da razão de despolarização linear e dos valores da razão LIDAR dos tipos de aerossóis puros, esses obtidos da literatura. O perfil do coeficiente total de extinção foi então estimado e comparado com os perfis obtidos pelo LIDAR eVe Raman e com os resultados de um sistema LIDAR PollyXT Raman, também operado em São Vicente durante o experimento ASKOS. Com base nesta metodologia, foram escolhidos três casos de estudo para discussão detalhada. O primeiro e terceiro casos consistiram em poeira pura do Sahara na troposfera livre, enquanto na Camada Limite Marinha (CLM) foram registados aerossóis marinhos puros e mistura de partículas de sulfato vulcânico e aerossóis marinhos, respectivamente. Relativamente ao segundo caso de estudo, foi encontrado um cenário misto de poeira do Saara e aerossóis marinhos tanto na troposfera livre como na CLM. No geral, a comparação entre os perfis de propriedades ópticas estimados pelo EIEx (Coeficiente de extinção, Razão LIDAR) e as inversões dos LIDARs eVe e PollyXT revelou uma boa concordância. No entanto, houve também diferenças importantes entre os resultados do EIEx e os produtos do eVe e do PollyXT, em particular na parte superior das camadas de aerossol e algumas divergências dentro da CLM. Estas diferenças na CLM podem ser atribuídas à presença de partículas de poluição ou às limitações dos sistemas LIDAR em representar corretamente as propriedades ópticas do aerossol na camada próxima da superfície, devido ao problema de sobreposição.

Palavras-chave: Aerossóis, Jatac/Askos, EIEx method, Razão de despolarização, Razão de lidar , Poeira do Saara, Propriedades ópticas.

Abstract

Studying the vertical distribution of aerosol particles is essential for understanding their influence on the climate system. One way to evaluate this aspect of aerosols is to discriminate their source and optical properties in the atmosphere column. The main objective of this study was to characterize and vertically analyze aerosol's optical properties profile under distinct aerosol mixture states over São Vicente Island, Cabo Verde, during the ASKOS campaign that took part in July and September of 2021. Thus, the Elastic Extinction (ElEx) method has been applied, which allows aerosol backscattering profile separations by type and estimation of total extinction coefficient. The EIEx application requires particles' complete backscattering profile and vertically resolved particles' linear depolarization ratio at the same wavelength. These values were taken from the eVe lidar system, linear depolarization ratio and lidar ratio values of pure aerosol types that were taken from the literature. The total extinction coefficient profile is then estimated and compared with eVe Raman retrievals and with the results of a PollyXT Raman lidar, also operated in São Vicente during the ASKOS experiment. Based on this method, three study cases have been chosen for detailed discussion. The first and third cases consist of pure Saharan dust in the free troposphere, while in the Marine Boundary Layer (MBL), pure marine and volcanic sulfate were recorded, respectively. Regarding the second study case, a mixed scenario of dust and marine aerosols were found across the MBL and free troposphere. Comparison between the EIEx estimated optical properties profiles (extinction coefficient, lidar ratio) and the eVe and PollyXT lidar retrievals revealed a good general agreement. Nevertheless, differences can be observed in regions where the signal to noise ratio is low, such as close to the top of the aerosol layer and also inside the MBL. These differences in the MBL could be attributed to the presence of pollution particles or the limited ability of the lidars to correctly represent the aerosol optical properties in the near range due to the overlap problem.

Keywords: Aerosols, Jatac/Askos, EIEx method, Depolarization ratio, Lidar ratio, Saharan dust, Optical properties.

Abbreviations and acronyms

AD-Net	Asian Dust Network
AE	Angstrom Exponent
AERONET	AErosol RObotic NETwork
AOD	Aerosol Optical Depth
AVHRR	Advanced Very High-Resolution Radiometer
CAL/VAL	Calibration and Validation
CALIOP	Cloud-Aerosol Lidar with Orthogonal Polarization
CALIPSO	Cloud-Aerosol Lidar and Infrared Pathfinder Satellite Observation
CCN	Cloud Condensation Nuclei
Dp	Depolarization ratio
EARLINET	European Aerosol Research Lidar Network
ElEx	Elastic Extinction
ESA	Europe Space Agency
GOCART	Goddard Chemistry, Aerosol, Radiation, and Transport
HLOS	Horizontal Line-of-Sight
HSRL	High spectral resolution lidar
IN	Ice-Nucleatine
JATAC	Joint Aeolus Tropical Atlantic campaign
Lr	Lidar Ratio
MBL	Marine Boundary Layer

MODIS	Moderate Resolution Imaging Spectroradiometer
NOA	National Observatory of Athens
OMI	Ozone Monitoring Instrument
OSCM	Ocean Science Center Mindelo
PLANET	Micro-Pulse Lidar NETwork
PLDR	Particle Linear Depolarization Ratio
PMTs	Photomultiplier Tubes
RCS	Range Corrected Signal
RH	Relative Humidity
SEVIRI	Visible and Infrared Imager
SSA	Single Scattering Albedo
SZA	Solar Zenith Angle
TROPOS	Leibniz Institute for Tropospheric Research
VLDR	Volume Linear Depolarization Ratio

General index

Figure Index

Table index

1. Introduction

1.1. Background and Context

The tropospheric aerosols are ubiquitous particles in the atmosphere. They are solid and liquid particles suspended in the atmosphere, except hydrometeors, and their size generally ranges from a few nanometers to hundreds of micrometers (Pio et al., 2014). Depending on their sources and atmospheric processes (e.g., chemical and physical transformations, transportation, and removal processes), aerosols may vary significantly in time and space (Milford et al., 2019). Aerosols can be of natural origin (e.g., from soil resuspension, biogenic, marine) or anthropogenic (from human activities). On a global scale, five main aerosols are most often encountered: biomass burning, volcano particles, industrial and urban pollution, desert dust, and marine aerosols. Furthermore, they are characterized by different chemical, physical, optical, and radiative properties (Kambezidis & Kaskaoutis, 2008). These aerosols are essential components of the climate system (Knippertz & Todd, 2012). They can influence climate in various ways. Due to their optical, radiative properties and their potential to act as cloud condensation nuclei (CCN) and ice nucleating (IN) particles, they play a central role in Earth's energy budget and hydrological cycle (Ramanathan et al., 2007). Additionally, the role of aerosol particles in the global terrestrial and oceanic biogeochemical cycles is vital (Winckler et al., 2008).

Concerning its nature, the aerosol radiative effects are usually divided into two categories; the direct radiative effect (DRE), which corresponds to the Earth's energy budget modification by aerosols directly via scattering and absorption of solar and terrestrial radiation (Pöschl & Shiraiwa, 2015). And the indirect radiative effect, that corresponds to the modification of the Earth's energy budget indirectly by acting as cloud condensation nuclei and ice nucleating particles, therefore, changing cloud microphysical, optical properties and lifetime (Haywood et al., 2011). Nevertheless, through the absorption of solar and terrestrial radiation, aerosols can influence the atmosphere temperature profile and its stability and, consequently, the formation of clouds (Bates et al., 2008). This effect has been called the semi-direct effect (Ackerman et al., 2000; Koren et al., 2004).

Regarding the impact on the global biogeochemical cycles, it has been shown that aerosols, mineral dust, are a significant source of nutrients and trace metals for terrestrial and oceanic ecosystems (Saltzman, 2009). Additionally, they affect the optical properties of ocean

surface (Moutin et al., 2002) and can significantly influence marine trace element biogeochemistry. Deposition of aerosol is an important factor influencing the ocean surface biological productivity by increasing the nutrient in low chlorophyll regions of the oceans (Saltzman, 2009). Regarding land ecosystems, previous studies show that the atmospheric transport of Saharan dust results in substantial iron bioavailability across the Amazon rainforest canopy (Rizzolo et al., 2017).

Atmospheric aerosol systems present large spatial and temporal variability in their geographical distribution, vertical profile, and chemical and physical properties, representing a challenge to monitoring and modelling aerosol radiative effects. Despite the described aerosol's importance and relevance in the climate system, they are still considered a major source of uncertainty to our understanding of climate processes and, consequently, in the Earth system and climate models simulations (Stocker et al., 2013). Aerosol radiative effects, in particular, are still an important source of uncertainty in recent global climate change assessments and predictions. Large uncertainties exist in current estimates of aerosol particle's radiative forcing because of incomplete knowledge concerning the distribution of their concentration and radiative properties (Baars et al., 2017). To reduce these uncertainties, coordinated and strategic integration of data from multiple platforms (e.g., ground-based networks, satellite, ship, and aircraft) and techniques (e.g., in-situ measurement, remote sensing, numerical modelling, and data assimilation) are highly required.

Within this perspective and focusing on the Saharan dust aerosols plume traversing the Atlantic Ocean, the ASKOS experiment, which took place from July to September of 2021 at São Vicente Island of Cabo Verde. This experiment deployed advanced ground-based remote sensing and surface/airborne *in situ* instrumentation to provide a comprehensive observation of aerosol, clouds, water vapor, and wind. The Sahara Desert contributes to more than 50% of global emissions of dust aerosols with environmental effects that span from radiative balance, visibility, and air quality, to deliver nutrients to the oceans (Dunion & Velden, 2004). The ASKOS campaign was planned to take place during the period when dust aerosols above Cabo Verde are expected to be at their maximum. Among the planned scientific objectives, the experiment aims to: a) characterize columnar and vertical profiles of the aerosol optical properties (scattering, backscattering, absorption, extinction, Lidar ratio, depolarization ratio) under marine, dusty and mixed scenarios; b) Evaluate and validate satellite-based (Aeolus) aerosol retrievals under these distinct scenarios and estimate the uncertainty associated with the dust aerosol's non-sphericity. The unparalleled set of instruments operating simultaneously

during ASKOS[1] integrating ground-based and satellite-based passive and active remote sensing provides a unique opportunity to study the complex dynamic of aerosol load, profile, optical, and microphysical properties over São Vicente Island under dominant marine aerosols scenario and during Saharan dust aerosols outbreaks. This was a key motivation for this investigation.

1.2. Problem Statement

Historically, passive remote sensing instruments (ground-based and onboard satellites) have helped characterize the long-term variability of the columnar aerosol loading, optical and radiative properties over the Cabo Verde region during both pure marine aerosol scenario and dusty conditions (Dubovik et al., 2002). However, they provide limited information on the mixing state and vertical distribution of dust, urban industrial, smoke, pollution, volcano and marine aerosols. Among the aerosols retrievals based on passive remote sensing instruments available during the ASKOS campaign, it is worth highlighting the products from the ground-based AERONET (AErosol RObotic NETwork) CIMEL Sun Photometer, which are widely used as reference columnar data to validate retrievals from satellite instruments (Holben et al., 1998). Despite its focus on the columnar aerosol properties, the ratio of the extinction-to-backscatter coefficient (often referred to as the Lidar Ratio) of the AERONET has also been crucial in the context of the aerosol retrievals of active remote sensing instruments, namely lidar systems.

The main advantage of lidar systems is their ability to retrieve the vertical aerosol distribution and their optical properties, depending on the lidar type. Therefore, lidars provide a unique perspective to evaluate aerosol transportation and radiative effects along the atmosphere column. The Raman-based lidar technique allows the retrieval of the Lidar Ratio, from which it is possible to infer the aerosol type and mixed state (Ansmann et al., 2002; Giannakaki et al., 2010). On the other hand, the multiwavelength elastic backscatter lidars can detect the presence of coarse aerosols, and the simple elastic Lidar can use a priori assumptions of the aerosol type or combination via the Lidar Ratio (Lr) property to identify the aerosol based on the particle backscatter coefficient retrieval (Klett, 1981). Another technique applied in lidars is the polarization technique, which allows the retrieval of the aerosol depolarization ratio (Dp) (Weitkamp, 2006). A polarization lidar emits polarized light and can detect the depolarization of the backscattered light, which can be significant when the scatterers have a non-spherical

[1] https://askos.space.noa.gr/about/instruments/

shape, such as desert dust, ice crystals, volcanic ash, and even pollen. The combination of polarization and Raman techniques can be used to separate the desert dust aerosol from other aerosol components using Depolarization Ratio (Dp) and Lidar Ratio measurements (Tesche et al., 2009). Unlike marine aerosols mixtures, desert dust causes high backscattered light depolarization (Althausen et al., 2009). On this basis, a recently developed method, called ElEx (elastic extinction, Giannakaki et al., 2020), allows the estimation of the aerosol extinction coefficient profiles using only the information provided by the elastic and polarization channels of an elastic depolarization lidar system. This technic used the particle backscatter profiles and the vertically resolved particle linear depolarization ratio measurements at the same wavelength.

The ElEx method is limited to cases where only two basic aerosol types are observed, and the mixing state of the atmosphere is well known. The first aerosols have a high capacity of light depolarization, while the second do not depolarizes the light. A scenario usually reported over the Cabo Verde region involves marine and Saharan dust aerosols. ASKOS instrumentation setup in São Vicente Island provides a strategic framework to apply and evaluate the ElEx method since a combination of lidar systems that include a single-wavelength polarization Raman lidar system (Paschou et al., 2022) and a multiwavelength polarization Raman Lidar (Baars et al., 2016) has been operated simultaneously during the campaign. This represents a motivation for the more specific goals of the present study. ElEx method's potential to expand extinction coefficient profiles retrievals to non-Raman lidars represents an important and valuable contribution to aerosol characterization (Giannakaki et al., 2020). Therefore, the continuous evaluation/validation method is essential especially under the unique context of ASKOS.

1.3 Research Questions

Focusing on the understanding of aerosol optical properties in the atmosphere column of Mindelo and on the performance of the EIEx method to resolve and characterize the vertical optical properties of the aerosol's components, below are listed the main questions that summarize the aim of the present study:

- How did aerosol loading and optical properties characterize Mindelo's atmosphere during the ASKOS first campaign period?
- Is the EIEx method able to consistently resolve the vertical contribution of aerosol species over Mindelo city?

1.4. Objectives of the work

Considering the above-described context, the main objective of this investigation is to characterize the aerosol's optical properties and types over São Vicente Island, Cabo Verde, during the ASKOS campaign from July to September 2021.

To achieve the general goal, some specifics objectives were defined:

- Use the AERONET sun photometer retrieval over São Vicente to analyze and contextualize the total atmosphere column for the ASKOS campaign period.
- Use the eVe lidar system measurements collected over São Vicente during the ASKOS campaign to identify aerosol vertical structure scenarios (case studies) where the ElEx method can be applied, i.e., dust and non-dust particles are observed, and their mixing state is well characterized.
- Link backward trajectory analysis of the air masses arriving over São Vicente with regional maps of aerosol optical depth from MERRA-2 reanalysis to identify the origin and nature of aerosol layers for the studies cases.
- Focusing on the target cases, to perform the aerosols discrimination profiles over São Vicente by applying the ElEx method using the eVe lidar dataset.
- Validation of the ElEx (elastic extinction) extinction coefficient profiles against the retrievals from eVe and PollyXT, an independent multiwavelength depolarization Raman lidar system also operated in São Vicente during the ASKOS experiment.

1.5. Structure of the work

This thesis is organized as follows: The conceptual framework and literature review in section two which describe the previous study and research did in the study area, data, and methodology used are presented in section three; the results and discussion are described in section four. The conclusion and future work recommendations are shown in section five.

2. Literature review

2.1. The importance of dust

Atmospheric aerosols significantly affect the radiation budget (Stocker et al., 2013). They can absorb or scatter incoming and outgoing solar radiation, thereby heating or cooling the climate system depending on their type. According to their size and chemical composition, they can also serve as condensation nuclei of clouds, thus altering their physical and radiative properties (Kaufman et al., 2002). Mineral dust has emerged as a critical aerosol of particular concern in the Earth system due to its influence on radiation, clouds, atmospheric dynamics, chemistry, air quality, and biogeochemical cycles (Knippertz & Todd, 2012). It represents the most abundant and dominant aerosol species in terms of mass (Textor et al., 2006). The assessment of global dust emissions revealed that the Sahara Desert is the largest source of dust in the world by a wide margin ((Prospero et al., 2002), with an average emission of 22,000 tons per year, seconded by the East Asian deserts, which contribute nearly 600 tons of particles annually (Huang et al., 2008).

Saharan dust is the product of natural erosion of soils by wind and is estimated to contribute at least (Bates et al., 2008) 80% of the total dust budget and more than half of the global aerosol load (Textor et al., 2006). Consequently, studying and understanding Saharan dust is very important since it affects the environment and atmosphere differently. Its ability to scatter and absorb the shortwave and longwave solar radiation is considered a direct radiative effect (Knippertz & Todd, 2012). Additionally, dust aerosols can also indirectly affect the radiation budget by impacting the cloud microphysical processes (Haywood et al., 2011). For instance, they can operate as cloud nuclei, thus indirectly moving the radiation through albedo, rainfall efficiency, cloud lifetime, and size (Klüser & Holzer-Popp, 2010; Rosenfeld et al., 2001). It is also important to mention their semi-direct influence, which is the uptake of heat (within the dust layers), which affects the humidity, vertical dynamics, cloud formation precipitation (Klüser & Holzer-Popp, 2010), and even the development of tropical cyclones (Dunion & Velden, 2004).

Mineral dust is the aerosol most involved in ocean biochemistry. SWAP et al. (1992) was the first who suggested the contribution of Sahara Dust to the nutrient budgets of Amazonian environments, which has been further validated in more current studies (Bristow et al., 2010; Koren et al., 2006) and reinforced by the study of the carbon cycle impact of Saharan dust conducted by the Nasa (NASA, 2022). Mineral dust is considered a relevant indicator of the feedback of climate in glacial/interglacial processes (Krinner et al., 2006; Winckler et al.,

2008). Thus, the quantity and composition of dust deposited in sediments and glacial soils are used as markers of climatic and ecosystem changes over long duration time scales (Lambert et al.,2008; Sima et al.,2009).

Moreover, dust particles present a severe risk to human health, mainly in countries close to dust sources and downwind areas (Meningococcal Meningitis, 2022). Several illnesses have been linked to dust particulate matter, especially cardiovascular and respiratory difficulties caused by breathing submicron particles, as these can be absorbed deeper into the human respiratory system (Yoon et al., 2012). Ocular diseases such as meningitis and valley fever have been documented in some areas during and after heavy dust events (Meningococcal Meningitis, 2022; Polymenakou et al., 2008).

However, despite all these climatic implications and environmental impacts, the monitoring and simulation of Saharan dust emission and transport across the world are incredibly challenging given the complex meteorology, removal processes and sparse monitoring network. Despite that, historical and recent developments in spectral viewing and polarization capabilities have allowed the extraction of aerosol properties (dust) from many remote sensing techniques and sensors using both ground-based (Sun photometers, Lidar systems) and satellite (MISR, MODIS, PARASOL, CALIPSO, OMI, ATSR, or AEOLUS) systems. These sets of remote sensing techniques and platforms provide, via complex algorithms and models, a more exhaustive overview of the critical phenomena involving dust transport in the atmosphere (Molero et al., 2020). They provide vital information on mineral dust's spatial and temporal distribution, especially over regions where in situ monitoring is sparse or unavailable (over remote areas, including ocean regions).

2.2. Dust remote sensing-based monitoring

2.2.1. Satellites

Satellite-based remote sensing can provide almost complete spatial coverage of the dust distribution. The instruments aboard satellites are being used to monitor different aspects of the atmospheric particles, including optical properties, for instance, aerosol optical depth, mass concentration, and vertical distribution (Knippertz & Todd, 2012). Aerosol visual depth (AOD), an indirect measurement of the aerosol load, is estimated from cloud-free reflectance measurements at the top of the atmosphere (Milford et al., 2019). Other satellite products related to dust monitoring include absorption AOD (Marais & Chance, 2015). In fact, throughout the last decades, considerable progress has been observed with the improvement of satellite sensors'

abilities to survey dust, e.g., the second-generation of Meteosat (MSG) spinning enhancements Visible and Infrared Imager (SEVIRI) (Brindley & Ignatov, 2006; Thomas et al., 2007). The Multi-Angle Imaging Spectroradiometer (MISR) and Cloud-Aerosol Lidar with Orthogonal Polarization (CALIOP) (Hu et al., n.d.) as well as some novel approach for other satellite data have been applied to improve our knowledge on the critical phenomena of the dust balance, emission, transportation, and deposition. One case is the quantification of the AOD on high spatial resolution above the bright desert surfaces from MODIS data in the Nadir view performed by Hsu et al. (the "Deep Blue" algorithm of Hsu et al., 2004). Another case is the deduction of AOD at a 15-minute time scale from the SEVIRI infrared and optical channels (Brindley & Ignatov, 2006; Thomas et al., 2007). The AOD is combined with the SEVIRI dust product (see "Best practices for RGB compositing of multispectral imagery", a guideline of the European Organization for the Exploitation of Meteorological Satellites[2]).

Among additional examples of approaches to advance aerosol monitoring from satellites, targeting application is the retrieval of aerosol optical properties, there are the satellite Polarization and Anisotropy of Reflectance for Atmospheric Sciences coupled with Observations from a Lidar (PARASOL, Wang et al., 2014). The Multi-Angle Imaging Spectroradiometer (MISR, Diner et al., 1998), which monitors backscattered radiation from the Earth/atmosphere system from the visible to near-infrared bands. Or, the remarkably detailed vertical profiles of aerosol backscattering from the CALIOP space lidar (and to a lesser extent ICESat), although the temporal range is restricted (Rogers et al., 2014). The Aeolus satellite of the European Space Agency (ESA) provides global profiles of the Horizontal Line-of-Sight (HLOS) wind component in the troposphere and the lower stratosphere (Tan et al., 2008) through ALADIN, a sophisticated Doppler Wind Lidar. This instrument (ALADIN) used a circularly polarized emission and a multiple-interferometer to retrieve the particle (i.e., aerosols and clouds) backscatter coefficient, the extinction coefficient, and the backscatter-to-extinction ratio.

Several studies can be mentioned highlighting the information delivered by these instruments. For instance, the analysis of the aerosol type distribution over the globe is based on five-year CALIPSO retrieval (Huang et al., 2008). As well as the three-dimensional (3D) models of the occurrence of dust and smoke in China based on CALIPSO, MODIS (Moderate Resolution Imaging Spectroradiometer) and OMI (Ozone Monitoring Instrument) conducted by Guo et al. (2016), or the study performed by Liu et al., (2019) on the temporal-spatial

[2] http://oiswww.eumetsat.org/SDDI/html/doc/best_practices.pdf

distribution of dust over East Asia utilizing CALIPSO dust frequency occurrence (FDO), dust top layer height (TH) and aerosol subtype profile.

However, it is worth emphasizing that no satellite sensor or retrieval algorithm is without limitations. This refers to the multiple uncertainties coupled with cloud contamination and assumptions about the optical characteristics of the aerosol, with variability in the albedo and emissivity of the Earth's surface. Currently, no satellite sensor can detect aerosols under thick cloud layers and thick dust or distinguish cirrus clouds at visible wavelengths (Roskovensky & Liou, 2005). For example, 15 satellite algorithms built to monitor Saharan dust were correlated with AERONET's AOD, and the results revealed that these standard satellites error varied from 0.1 to 0.5 (Knippertz & Todd, 2012). There is an obvious need for more quantitative cross-comparison and analysis of the uncertainty sources, especially in areas highly exposed to desert dust. For this reason, satellite data requires ground-based data to be validated.

2.2.2. Ground-based instrument

Ground-based sensors play an important role in validating and calibrating space-based instruments by providing well-characterized reference information (Holben et al., 1998). The surface instruments generally give more accurate observations of aerosol properties (Huang et al., 2008). Still, they are spatially limited because they allow only a representation of an area near the observation site. The organization of identical ground-based instruments into observational networks, with standardized data processing procedures, extends such data into larger geographical scales. For example, the AERONET (AErosol RObotic NETwork) (Holben et al., 1998) has almost 500 surface-based sun photometers and provides high-quality retrievals of AOD and aerosol physical characterization. These instruments are ground-based and use passive remote sensing techniques focusing on spectral solar radiation measurements for aerosol properties monitoring worldwide. They are designed to measure at multiwavelength channels and collect the solar irradiance directly. This irradiance is complemented with angular radiance measurements (almucantar measurements, with a constant zenith angle equal to solar zenith angle (SZA)) and are routinely inverted to retrieve the microphysical and optical properties of aerosols for the entire atmospheric column. From such measurements, AERONET retrieves aerosol microphysical properties, namely size distribution and refractive index, and spectral optical properties, such as aerosol optical depth (AOD), Angstrom Exponent, single scattering albedo; asymmetry factor; and phase function (Huang et al., 2008; Naeger et al., 2016). The AERONET algorithms have been tested and upgraded for more than two decades (Liu et al.,

2019), and it has been implemented successfully in the worldwide network of instruments, providing useful information for satellite validation (Zhang et al., 2003) and climate studies. However, sun photometers collect information integrated into the atmosphere column, so they are largely limited because they do not offer information on the vertical distribution of aerosol particles.

The vertical distribution of aerosols, particularly dust, is relevant because it determines its climate effects, residence, and transport into the atmosphere (Bourgeois et al., 2015). Regarding the remote sensing monitoring of aerosol properties vertical profile, the lidar (light detection and ranging) technique has the potential to provide detailed information on the vertical distribution of particles in the atmosphere. This instrument of high vertical resolution is a powerful tool that provides a better characterization of the aerosol profiles by taking advantage of the additional information collected by the wavelength dependence of the backscatter and extinction coefficients (Molero et al., 2020). Lidar is an active remote sensing system capable of obtaining information on the atmospheric structure and constituents (gases, particles and cloud droplets), gathered by an appropriately designed optical receiver from the interaction between transmitted laser light and these atmospheric constituents (Mona et al., 2012).

Currently, there are several lidar instruments worldwide that have been employed by regional networks to provide long-term, accurate and consistent measurements of the vertical distribution of aerosol parameters. These have included the European Aerosol Research Lidar Network[3] ,which offers good spatial coverage of optical aerosol properties with high vertical resolution. The PLANET[4] (Micro-Pulse Lidar NETwork, Qiu et al., 2003), is a system designed to measure aerosol and cloud vertical structure (Ackerman et al., 2000). There is also Asian Dust Network[5] (AD-Net), formed in 1998 to provide 4D outlooks of dust movement using lidar sites around the Asian countries (Murayama et al., 2001).

Several techniques have been further elaborated to extract aerosol profiles based on the backscattering and extinction coefficient of the particles. Among them we have the algorithms suggested by Léon et al., (2003); Nishizawa et al., (2007) and Huneeus & Boucher, (2007) which are based on dual-wavelength backscattering lidar applications and pre-determined lognormal aerosol models. The lognormal models consist of fine and coarse modes with stationary size distributions and reflectance characteristics but varying concentrations

[3] http://www.earlinet.org/

[4] http://mplnet.gsfc.nasa.gov/

[5] http://www-lidar.nies.go.jp/AsiaNet/

throughout the vertical column. The technique of Nishizawa et al., (2007) uses a dual-wavelength lidar detection at 532 nm and 1064 nm, and a complementary measurement of the depolarization ratio of aerosol at 532 nm, to determine the type of the coarse mode (desert dust or sea salt) present in the atmosphere column. Shimizu et al., (2004), Sugimoto et al., (2003), and Sugimoto & Lee (2006) utilized the particle depolarization ratio and the backscatter coefficient quantitatively by making certain assumptions. they considered 0.35 for the dust depolarization ratios at 532 nm and 1064 nm, and the dust backscatter coefficient contribution in the total backscatter volume in Asia. Tesche et al. (2009) performed the same method as Sugimoto et al. (2003) by using particle depolarization ratio to separate dust and non-dust particles in the total volume of backscatter at 532 nm. Then, to reduce the uncertainties they employed the signal of a multiwavelength Raman to get, for the first time, the particle backscatter coefficients at 355 nm, 532 nm, and 1064 nm with the extinction coefficients at 355 nm and 532 nm at Praia city, in Cabo Verde.

The POLIPHON method, developed by Mamouri & Ansmann, (2017) provides separation of dust aerosol particles from other aerosol components (for the step I) and the separation of course and fine dust from the non-dust particles (step II) by using three wavelengths, at 355, 532, and 1064 nm, of a polarization lidar, complemented by the volume conversion factors obtained from an AERONET sun photometer and dust extinction coefficient for all three wavelengths. Giannakaki et al., (2017) recently developed a method called EIEx (elastic extinction), further applied by Giannakaki et al., (2020). This method performs the characterization of vertical profiles of dust and non-dust aerosols using the information provided by the elastic and polarization channels at 532 nm of a lidar system under some assumptions to specify the extinction coefficient profile. This last method is the focus of the present study. However, we investigate the inelastic Raman channel at 355 nm instead of using the elastic and polarisation channels to apply and validate the method.

.

3. Materials and methods

Cabo Verde archipelago is a country located around 570 km of the West African coast in the eastern portion of the Tropical Atlantic Ocean, as shown in Figure 1. Due to its strategic location, Cabo Verde has been a place of many experimental campaigns on dust aerosols that aim to study Saharan dust outbreaks over the Atlantic Ocean, e.g., AMMA and DABEX (Haywood et al., 2008; Rajot et al., 2008). And taking advantage of the Cabo Verde locations and in the framework of the AEOLUS CAL/VAL campaign, the National Observatory of Athens (NOA), aiming to evaluate the quality of the aerosol and cloud products of the Aeolus satellite, selected the island of São Vicente, during the summers of 2021 and 2022 to deploy the ASKOS experiment[6]. The country is composed of 10 volcanic islands. São Vicente, the second-largest city (Mindelo) of Cabo Verde, is located in the northern part of the archipelago. This area is characterized by the strong trade winds from the northeast that regulate the transport of different types of aerosols towards the country, especially from the Sahara, which makes the location a hot spot for investigations of aerosol dust interaction with atmospheric dynamics. The air mass recorded in Mindelo is relatively free of local anthropogenic pollution, with dust and marine aerosols being the dominant types of particles (Fomba et al., 2014). The aerosol mixture at this location is spatially and temporally variable depending on meteorological conditions. Usually, at the surface level, São Vicente receives clean marine air masses from the North Atlantic Ocean in late autumn and summer. In contrast, it receives dust-laden air masses from the Sahara in late autumn and winter (Fomba et al., 2014). Meanwhile, Saharan dust is transported to the region at higher altitudes during summer, resulting in high aerosol optical depths (Gama et al., 2015).

Although the tropical Atlantic significantly affects the global climate, there is still limited scientific data from this region. Furthermore, Cabo Verde lies directly on the path of sandstorms and bushfire smoke that migrated westwards from the North Africa region to the open Atlantic, thus exposing the local population to severe health risks. Overall, there is a need to enhance atmospheric dust monitoring capacity in the region, and São Vicente Island is becoming a reference in the monitoring of dusty airflow from Africa towards the Atlantic. And by the way to understand the dust role in the atmospheric processes, ocean biogeochemical cycles, and also its transportation towards the remote ecosystems of the Americas. Therefore,

[6] https://meetingorganizer.copernicus.org/EGU21/EGU21-13781.html

studies in the region targeting advancing current knowledge on mineral dust optical properties and its climate effects are highly important.

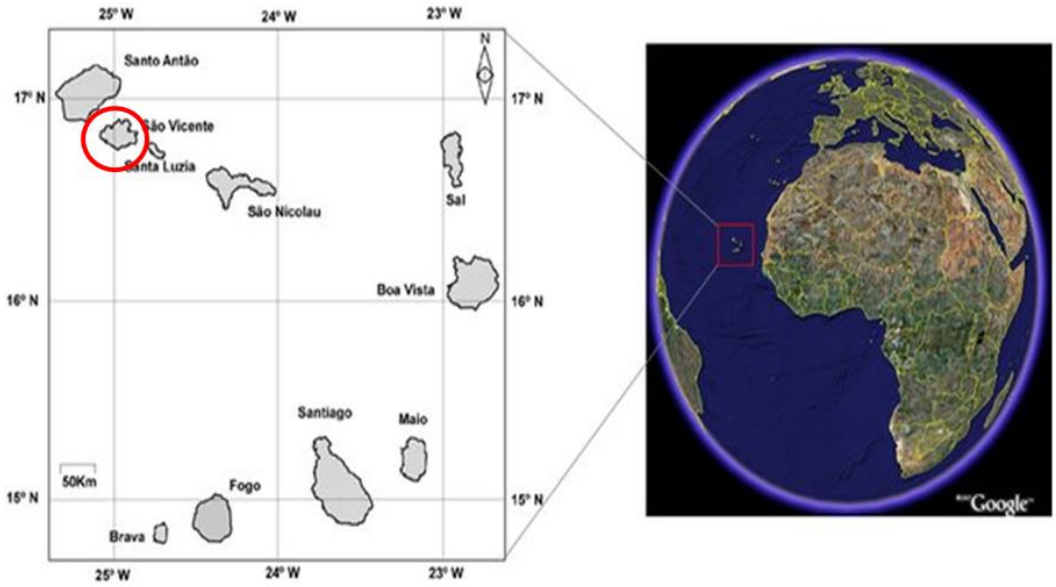

Figure 1: An overview of the study area, showing the localization of the 10 islands that constitute the Cabo Verde archipelago, on the West coast of Africa, and the São Vicente Island (highlighted using the red circle) where the ASKOS experiment occurred.

3.2. Data collection - ASKOS campaign

The primary dataset considered in this investigation was collected at São Vicente Island during the ASKOS campaign in the summer of 2021 by the three instruments described below, the eVe lidar system (Paschou et al., 2022), the PollyXT Raman lidar (Baars et al., 2016) and a CIMEL sunphotometer from the AERONET (Holben et al., 1998). The eVe measurements represent the reference dataset for this study. It was collected during the joint Aeolus Tropical Atlantic campaign (JATAC) from July to September 2021 at Cabo Verde. The JATAC/ASKOS experiment was organized by ESA in collaboration with European and US Partners; the aim is to characterize and understand the dynamic of clouds, winds, and aerosols in the Tropics and to validate the AEOLUS products (profiles of wind and aerosol-cloud optical properties). The site for the campaign is OSCM (Ocean Science Center Mindelo), located on the North-West coast of Mindelo at 16.878° N; -24.995° W. The two other instruments are installed on the rooftop of the OSCM and assure continuous measurement. The lidar system PollyXT from the Leibniz Institute for Tropospheric Research (TROPOS) has been operated since 29 June 2021, and the sunphotometer began collecting data around January 2021.

3.3. Instruments

3.3.1. Cimel sun photometer

AERONET is a network of sun photometers focusing on aerosol properties and precipitable water retrievals (Holben et al., 1998). These sun photometers, manufactured by CIMEL Electronic in collaboration with LOA and NASA, are installed worldwide and allow continuous and simultaneous measurements to characterize atmospheric aerosols. These ground-based remote sensing instruments are described in detail in the user manual of AERONET (CIMEL, 2014) and briefly in other studies (Diarra & Ba, 2014; Dubovik & King, 2000). A radio transmitter relays the data in the sun photometer's memory to the geostationary METEOSAT satellite and then forwards it to a ground receiving station (Holben et al., 1998). The CIMEL sun photometers are programmed to perform direct solar radiation measurements at a 15-min resolution and sky radiation at a 1-hr resolution. The instrument takes direct solar radiation measurements at eight different channels of 340, 380, 440, 500, 675, 870, 940, and 1020 nm, with the 940 nm band used for measuring columnar water vapor (Adesina et al., 2019). These observations retrieve the refractive index and the volume size distribution using an inversion algorithm. The obtained refractive index and size distribution are used to obtain the aerosol's optical properties: single scattering albedo (SSA), asymmetry parameter, extinction and backscattering coefficients, phase function, etc.

Information on uncertainties and calibration protocols has been reported by Dubovik et al. (Dubovik et al., 2002; Dubovik & King, 2000). AERONET data are provided at three quality levels: level 1.0 for raw data, level 1.5 for cloud-filtered observations, and level 2.0 for quality-assured data to which post-field calibration has been carried out. The main retrieval, namely Aerosol Optical Depth (AOD), is based on the Beer-Lambert-Bouguer law, via which the attenuation of spectral direct solar radiation through the Earth's atmosphere can be described as follow. The uncertainty in the AOD retrieval under cloud-screen conditions for the wavelengths above 440 nm is $< \pm 0.01$ and for shorter wavelengths $< \pm 0.02$ or less than $\pm 5\%$ uncertainty in the sky radiance measurements. Particle recovery errors in the size range ($0.1 \leq r \leq 7\mu m$) do not surpass 10%, except for tiny sizes below 0.1µm and sizes above 7µm. The SSA has an uncertainty of about 0.03 - 0.05 according to aerosol type and loading. The real and imaginary parts of the refractive index have uncertainties of about 0.3 - 0.5 and ± 0.04, respectively (Alam et al., 2012; Dubovik et al., 2002). The main retrieval, namely Aerosol Optical Depth (AOD), is based on the Beer-Lambert-Bouguer law, via which the attenuation of spectral direct solar radiation through the Earth's atmosphere can be described as follow:

$$I_\lambda = I_{0\lambda} D^{-2} \exp^{-\tau_\lambda \mu} \qquad \textbf{Eq (1)}$$

Where:

- I_λ is the intensity of the light at the wavelength λ at the observation site,
- $I_{0\lambda}$ is the intensity of the light at the top of the (TOA),
- D is the Sun-Earth distance in astronomical units at the time of observation,
- τ_λ is the total optical thickness, which includes the effect of all atmosphere radiatively active components at λ,
- and $\mu = \sec \theta$ is the air mass, where θ is the solar zenith angle (SZA).

The Angstrom coefficient **α** can be calculated using the following equation

$$\alpha = - \frac{ln\,(\,\tau_1 / \tau_2\,)}{ln\,(\,\lambda_1 / \lambda_2\,)} \qquad \textbf{Eq (2)}$$

Where:

- τ_1 is the aerosol optical depth (AOD) at a reference wavelength λ_1 and τ_2 is the AOD at another wavelength λ_2.
- α is closely related to the size distribution of the aerosol population; large values of α indicate a relatively high ratio of small particles to large particles. Meanwhile, under large particle dominance α should approach 0.

Moreover, of particular interest to the present investigation are the AERONET relatively new parameters obtained from the inversion of sun/sky radiometer measurements. Hence, the particle lidar ratio and the particle linear depolarization ratio for different aerosol types, which allows aerosol typing and aerosol-type separation in lidar measurements (Shin et al., 2018).

3.3.2. Lidar

There are different techniques for studying aerosols when it comes to using lidar systems, from elastic backscatter lidar, the simplest and most commonly used, to complex and sophisticated multi-wavelength Raman lidar, or the high spectral resolution lidar (HSRL). The lidar equation that describes the measured signal that is elastically backscattered from the atmosphere is presented below (Mona et al., 2012).

$$P(R) = P_0 \frac{E0\eta L}{R^2}\, O(R)\, \beta_{(R)} exp\left\{-2 \int_0^R \alpha_r dr\ '\right\} \qquad \textbf{Eq (3)}$$

Where:

- P (R) = the measured signal
- P_O= the number of photons in the laser pulse
- E_O= The emitted laser pulse energy,
- η and L = lidar parameters describing the efficiencies of the optical and detection units,
- O(R)= the overlap function of the telescope
- β(R)= the backscattering coefficient
- α_r =the extinction coefficient

For the purpose of this work, we focused on two types of lidars: a depolarization lidar system that utilizes both elastic and Raman channels, named Eve (Paschou et al., 2022), and an independent Depolarization Raman lidar system, termed as PollyXT. Both are ground-based systems operated during the ASKOS campaign in São Vicente Island.

-Lidar ratio

$$L_{aer(R)} = \frac{\alpha_{aer\,(R)}}{\beta_{aer(R)}} \qquad \textbf{Eq (4)}$$

Where:

- $\alpha_{aer(R)}$ = The extinction coefficient of aerosol
- $\beta_{aer(R)}$ = the backscattering coefficients of aerosol

e*Ve lidar system*

The eVe lidar was designed by Raymetrics S.A(Athens, Greece) in cooperation with the National Observatory of Athens and the Ludwig-Maximilian's-Universität, Munich, Germany. The system was developed to be a mobile and flexible ground-based lidar system, capable of functioning in an extensive range of environmental situations. The system employs two lasers for the emission of linearly and circularly polarized light-emitting lasers, respectively, and two telescopes, each gathering the backscattered light from both lasers. The eve transmitter consists of two lasers that emit polarized laser pulses at 355 and 532 nm and elliptically polarized pulses at 1064 nm. The eVe lidar system is a Depolarization Raman lidar (Paschou et al., 2022).

The advantage of the combined procedure is that it can determine aerosol extinction profiles with no significant assumptions during night-time measurements. Consequently, the aerosol backscatter coefficient profile can be established with much higher accuracy than simple elastic backscatter lidar (Ansmann et al., 1992). Consequently, the eVe system allows the retrieval of the following optical properties: the particle extinction coefficient, the particle

backscatter coefficient, the particle depolarization ratios and the volume depolarization ratios. Moreover, it is possible to directly measure the lidar ratio profile from the independent measurement of the aerosol extinction and backscatter profiles. The lidar ratio is a very relevant parameter for aerosol identification and typing. With the assistance of transport models, this type of measurement allows a detailed analysis of aerosol characterization and mixing patterns (Villani et al., 2006). The eVe system has all the needed information to perform and evaluate the ElEx method.

PollyXt lidar system

The PollyXT is a sophisticated portable lidar system (the one with interest is fixed) with the capabilities of advanced EARLINET lidars and EARLINET quality standards but dedicated to stand-alone operation in remote places. This Raman lidar was initially conceived in 2003 by TROPOS and FMI. In the preceding years, these systems have been successfully applied within EARLINET. They are relatively robust, as they can function unsupervised and autonomously 24 hours a day, seven days a week (24/7) (Wandinger et al., 2012). One more advantage of Polly Lidar is the consistent data structure and thus the simple possibility to update and adjust the software. All PollyXT lidars are operated in a network called PollyNET (Baars et al., 2016), which provides data backup, monitoring of instruments and an internationally accepted knowledge transfer. Since 2006, two multiwavelength polarization and Raman lidar systems with expanded functionalities (PollyXT, second generation) have been developed and operated by the same institutions (TROPOS and FMI).

These systems allowed the measurement of particle backscatter coefficients at 355, 532 and 1064 nm and extinction coefficients at 355 and 532 nm. The backscatter and extinction coefficients are used to characterize the optical properties of aerosols (Müller et al., 2007) by an inversion algorithm to deduce the size distribution and particle concentration. Additionally, a polarization-sensitive channel has been set up to determine the particle shape from a linear depolarization ratio (Kanitz et al., 2013), to distinguish dust and non-dust particles in mixed aerosol layers (Baars et al., 2011) and to examine mixed phase of clouds (Kanitz et al., 2011).

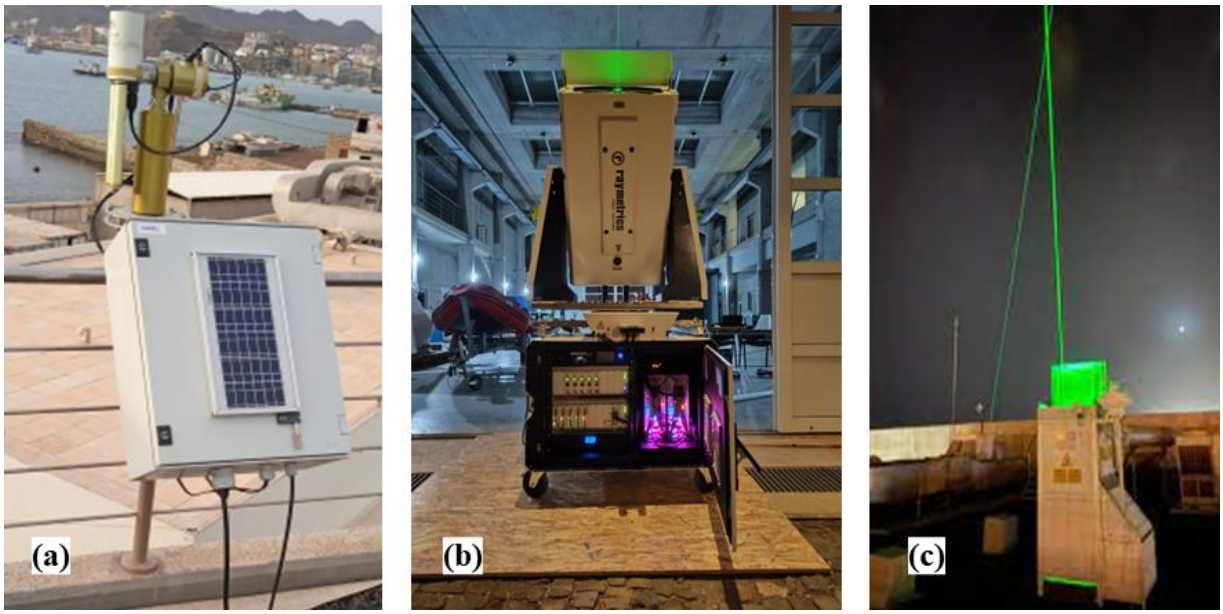

Figure 2: The set of instruments used in this project: (a) a sun photometer from the AERONET; (b) the Eve lidar system from The National Observatory of Athens (NOA); and (c) The PollyXT lidar from Leibniz Institute for Tropospheric Research (TROPOS). All of them are being operated at the OSCM (Ocean Science Center of Mindelo), in São Vicente Island during the ASKOS campaign in 2021.

3.4. Data Analysis

3.4.1 Lidar ratio and Depolarization ratio

Understanding the relationship between the different optical properties is key to aerosol characterization. The main parameters that will be considered during this study will be the particle backscatter coefficient, the lidar ratio, the depolarization ratio, and the particle extinction coefficient. The relationship between extinction and backscatter coefficients is expressed by the lidar ratio, as shown previously. It depends on the particle's size distribution, shape, and chemical properties; therefore, Lidar ratios constitute an essential factor for aerosol characterization. Regarding the depolarization ratio, it depends on the polarization state of the backscattered light retrieved by the lidar (Kaduk,2017). With polarization, the lidar particle depolarization ratio is derived from the volume depolarization ratio by measuring the parallel and cross-polarized signal component of the backscattered light. The emitted laser light is linear polarized; therefore, if the backscattered light is depolarized by non–spherical scattering particles, such as dust particles, a significant cross-polarized signal component can be registered by the lidar telescope (Seifert, 2010). The particle depolarization ratio δ_v (R) is the ratio of the cross-polarized to parallel–polarized signal. From the particle depolarization ratio, information about the sphericity of the scattering particles can be inferred. Spherical particles, such as smoke, pollution and marine aerosols produce very low depolarization. Hence the

particle linear depolarization ratio for spherical aerosol particles is almost zero (δ_p (R) ~ 0). In the case of non–spherical particles, such as dust and volcanic ash, the emitted light is strongly depolarized during the backscattering process (δpar(R) > 0). Considering the aspects described here, the combination of lidar ratio and depolarization ratio has been used to identify aerosols type when these two optical properties are available. In this study, lidar and depolarization ratio measurements taken over São Vicente Island during the ASKOS campaign and obtained from literature were fundamental to the characterization and discussion of the profiles of aerosol types transported over the study region.

Retrieval uncertainties

An overview of the lidar ratio and particle linear depolarization ratio is shown in Figure 3. The lidar ratio and linear depolarization ratio values at 355 nm for different aerosol types and mixtures are plotted against each other (Illingworth et al., 2015). Ground observations with Raman polarization lidars have been made at Cabo Verde Islands, Leipzig, Munich, the Amazon basin and over the North Atlantic (Baars et al., 2011; Groß et al., 2012). The linear particle depolarization ratio presents the most significant differences among the different aerosol types. The difference extends from low values of 2-5% for marine aerosol, pollution, and smoke to the highest values for volcanic ash (37%). Dust and dust mixtures range from 15 to 28%. The lidar ratio has its lowest values for marine aerosol (15-30 sr) and the highest values for smoke and dust/smoke mixtures (50-95 sr). All other aerosol types are in the range of 35-70 sr.

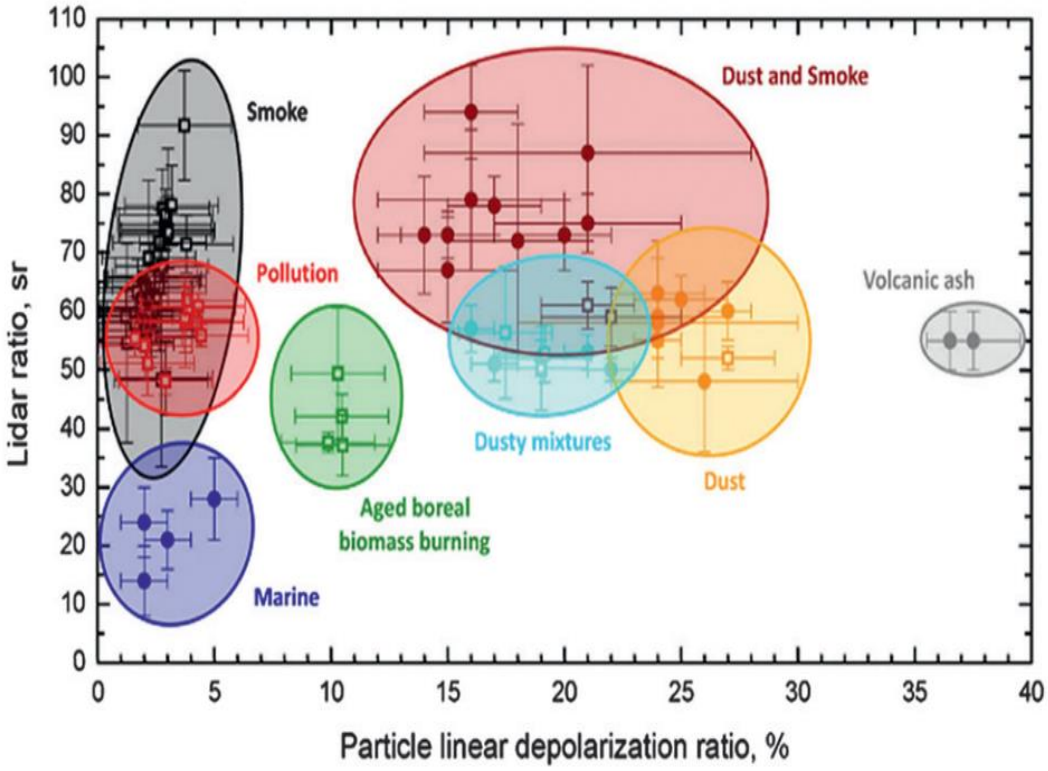

Figure 3: Lidar ratio as a function of particle linear depolarization ratio at 355 nm obtained by a different institution, TROPOS (squares) and University of Munich (dots), for different regions across the world: at Cabo Verde, Leipzig, Munich in the Amazon Basin and over the North Atlantic (Illingworth et al., 2015).

For the EIEx application, the assumed lidar ratio and depolarization ratio chosen from the literature (see Table 1) agree with the general analysis performed by Illingworth et al. (2015).

Table: Mean value and the standard deviation of aerosol lidar ratio, particle linear depolarization ratio taken from the literature.

Aerosol	Lidar ratio	Depolarization ratio	Source
Dust	54±7 sr	0.21 ± 0.01	(Kaduk et al., 2017)
	55 sr		(Groß et al., 2015)
	50 - 60 sr	0.27 ± 0.03	(Mamouri & Ansmann, 2017)
	53 ± 10 sr	0.26 ± 0.06	(Tesche, Müller, et al., 2011)
	53 ± 7 sr	0.26 ± 0.06	(Freudenthaler et al., 2009 ; Tesche et al., 2009)
	55 ± 6	0.30 – 0.35	(Müller et al., 2007)
	61±4 sr	0.25 ± 0.01	(Bohlmann et al., 2018.)
	48–70 sr	0.24 – 0.27	(Groß et al., 2011)
	58 ± 7	0.25 ± 0.03	(Groß et al., 2011)
Volcano ash	64 ± 12.7 sr		(Chouza et al., 2020.)
	60 sr	0.35	(Prata et al., 2017)
	50 < Lr < 60 sr	0.35 < Dp < 0.38	(Groß et al., 2012)
	63 ± 21 sr		(Lopes et al., 2019)
Volcano sulfate	60 < Lr < 80 sr	0.01 < Dp < 0.02,	(Groß et al., 2012a)
	30–60 sr	0.1–0.2	(Vaughan et al., 2021)
	40–50 sr	<5%	(Prata et al., 2017)
Marine	21±1 sr	0.03±0.01	(Kaduk, 2017)
	15–25 sr	0.05	(Mamouri & Ansmann, 2017)
	23±2 sr	around zero	(Bohlmann et al., 2018)
	22±1 sr	around zero	(Bohlmann et al., 2018)
	18 ± 4 sr	0.02 ± 0.01	(Groß et al., 2011)
Pollution	58 ± 12 sr	<0.05	(Müller et al., 2007)
	44±5 sr	0.015±0.01	(Kaduk, 2017)

Uncertainties in the basic lidar-derived optical properties retrieval and the EIEx method are extensively analyzed and discussed by Giannakaki et al. (2017), Mamouri & Ansmann (2017), and Tesche et al. (2009). Typical uncertainties in the fundamental particle optical properties were analyzed over several experiments. Figure 4 shows the gaussian distributions of the depolarization ratio (Fig.4 (a)) and the lidar ratio (Fig.4 (b)) used in Monte Carlo error simulation for the EIEx method retrievals. The assumed depolarization ratio and the lidar ratio average and standard deviation values for each pure aerosol type are 53 ± 10 sr and 0.26 ± 0.06 for dust (Tesche, Müller, et al., 2011), 70 ± 10 sr and 0.02 ± 0.05 for volcanic sulfate (Groß et al., 2012b), 18 ± 4 sr and 0.02 ± 0.01 for marine (Groß et al., 2011), and finally 44±5 sr and 0.015± 0.01 for pollution (Kaduk,2017).

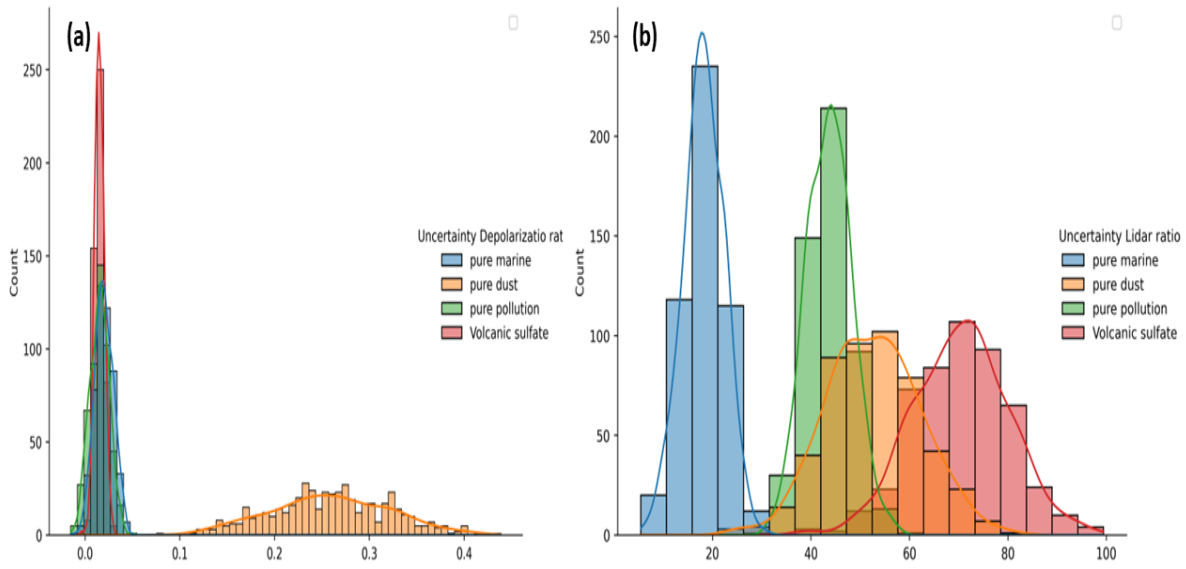

Figure 4: Summary of the gaussian distributions applied to (a) literature taken particle depolarization ratio and the (b) lidar ratio~~,~~ and their respective uncertainty. Used in the Monte Carlo uncertainty analysis of the EIEx method retrievals.

The analysis of Figure 4-a for the depolarization ratio variation indicates that values between 0 and 0.05 would make it challenging to identify the nature of the particle, as it could be either marine, sulfate, or pollution aerosols. This is also valid for certain mixture states. Concerning the lidar ratio, Figure 4-b reveals certain similarities among the particle's natures. The uncertainty of Sahara dust, which can be ± 10 with a reference of 53 sr at 355 nm, means that dust values can be similar to those of pollution or sulfate. Therefore, a careful study of the possible mixed state of the atmosphere through understanding the origin of air masses is important for the separation process.

Mamouri et al. (2017) reported an additional source of uncertainty in the case of marine particles in layers with low relative humidity (RH). As sea salt is hygroscopic, the salt particles absorb water to form droplets when the RH exceeds the deliquescence relative humidity (DRH). If the RH reduces to the relative crystallization humidity (CRH), the particle crystallizes from the droplet. At RH above CRH, sea salt particles are in solution with water and exhibit low $\delta \approx$ 3% values (Tesche, Gross, et al., 2011). When the RH is lower than the CRH, sea salt particles crystallize and exist as non-spherical particles due to the cubic shape of NaCl, the main constituent of the sea salt aerosol. As non-spherical particles, they cause higher depolarization ratios. In this case, the dried sea salt particles caused depolarization ratios of 10% at 355 nm. During the 2014 winter campaign of the Saharan Aerosol Long-range Transport and Aerosol-Cloud-interaction Experiment (SALTRACE) in Barbados, Haarig et al., (2017). detected an increase in particle depolarization ratios of up to 12% at 355 nm when the relative humidity

drops below 50%. In a laboratory chamber experiment, Sakai et al. (2010) found linear depolarization ratios at 532 nm of 1± ≤0.1% for droplets, 8±1% for sea salt crystals, and 21±2% for NaCl crystals. Marine particles are transported over the top of the MBL; as they get dried and crystallized, their depolarization ratio increases, even though the backscatter is low compared to the MBL. We can conclude that marine aerosol can cause depolarization of the lidar signal when the RH is low. However, for the purpose of this work, we just focus on the humidity condition of the MBL.

3.4.2. The selection of the Study case

In this study, we also use the AOD field from MERRA-2 Reanalysis, and back trajectory analysis from HYSPLIT[7] model taken from AERONET synergy tool MERRA-2 is NASA's most recent global atmospheric reanalysis product. Worldwide natural and anthropogenic aerosols are simulated in MERRA-2 with the Goddard Chemistry, Aerosol, Radiation, and Transport (GOCART) model (Randles et al., 2017). MERRA-2 reanalysis also assimilates aerosol optical depth (AOD) from a variety of ground-based and remote sensing platforms, including AOD measurements from AERONET, bias-corrected AOD retrievals from Advanced Very High-Resolution Radiometer (AVHRR) instruments, and AOD retrievals from MISR and MODIS on bright surfaces (Yang et al., 2021). The aim of combining the AOD field and back trajectory is to characterize the origin of the air masses arriving over São Vicente during the target's days. Indeed, the case study was selected based on several criteria:

- The analysis of the air masses origin: mainly focusing on dust transport from the Saharan region and possible mixing of another type of aerosol, marine aerosols in particular;
- AERONET sun photometer data are used to quantify the atmosphere in terms of aerosol load and optical properties variability during the ASKOS experiment.
- The linear depolarization ratio values of the particles are between 5% and 30%, which reveals a mixture of dust and another aerosol type (marine, volcanic, pollutants);
- Moreover, finally, the availability of the Raman measurement for eVe and PollyXT lidar systems for comparing the EIEx methodology with the well-established Raman extinction coefficient profiles.

[7] https://gmao.gsfc.nasa.gov/reanalysis/MERRA-2/data_access/

3.4.3. The EIEx (Elastic extinction) method

Assumptions

To perform EIEx method (Giannakaki et al. 2020), we need to consider two main assumptions:

- There are only two types of aerosols in the atmosphere column above Mindelo and their individual depolarization ratio as well as their lidar ratio values are known from the literature.
- The second assumption is about the relation between the backscatter coefficient and the particle's extinction coefficient. Ended assume that there is a constant and height relation between aerosol extinction and backscatter coefficient.

These assumptions generate some errors in the retrieval, which will be analyzed throughout this investigation.

The First step: Backscatter coefficient and particle depolarization

The Klett– Fernald (Klett, 1981) equation is used to retrieve the backscatter coefficient of the particles assuming a priori lidar ratio information from literature, similar to Giannakaki et al., (2020).

Second step: Separation of the backscatter profile

To distinguish the two types of aerosols in the atmosphere mixture, we need to use the equation of the particle depolarization ratio which is automatically computed from the lidar signals detected in the cross-polarized and co-polarized channels. Since we already assume that the distinguishable aspect of the two types of aerosols is the depolarization ratio.

-The particle depolarization ratio equation

$$\delta p = \frac{\beta_1^{\perp} + \beta_2^{\perp}}{\beta_1^{II} + \beta_{2II}} \qquad \textbf{Eq (5)}$$

-The backscatter coefficient for the first particle

$$\beta_1 = \frac{\beta_t\,(\delta_t - \delta_2)\,(1 + \delta_1)}{(\delta_1 - \delta_2)\,(1 + \delta_t)} \qquad \textbf{Eq (6)}$$

- δp= the depolarization ratio of the particle
- $\beta^{\perp}$ =Cross polarized particle backscatter coefficients
- β^{II} =Co -polarized particle backscatter coefficients

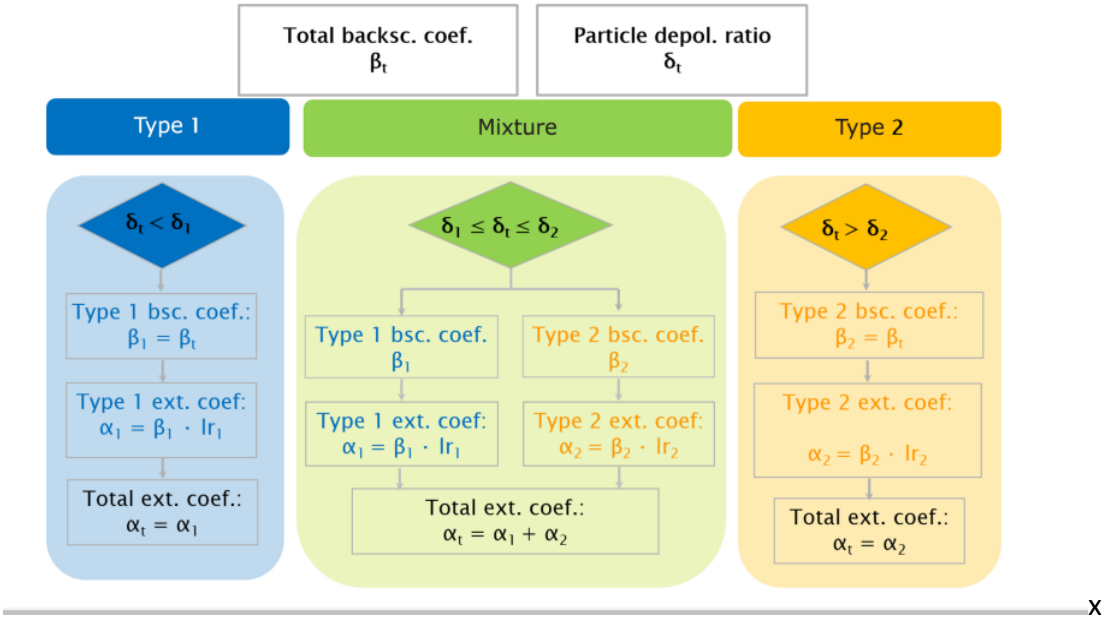

Figure 5: The proposed EIEx methodology for the retrieval of extinction coefficient profile using backscattering coefficient and depolarization data (Giannakaki et al., 2020).

Third step: Estimation of extinction coefficient profile

The separation of the backscatter profile gives us the opportunity to calculate the total extinction coefficient by applying the correct lidar ratio to each aerosol component.

-Equation for the Extinction estimation

$$a_t = a_1 + a_2 = \beta_1 \cdot lr_1 + \beta_2 \cdot lr_2 \qquad \textbf{Eq (7)}$$

3.4.4. Elastic extinction retrieval: EIEx validation

At the final stage of the project, independent extinction coefficient profiles from eVe and PollyXT based on Raman method are used to validate the estimated extinction coefficient via EIEx. To carry out this validation we proceed to a comparison between the profiles of the lidar ratio and the extinction profiles obtained from the Eve lidar and the PollyXT products.

4. Results and discussion

4.1. Overview of the ASKOS campaign

The aerosol optical properties time series from the sunphotometer over Mindelo during the 2021 campaign indicated significant variability resulting from the different sources dynamic (ex. Saharan dust, marine), types of aerosols and meteorological scenarios. The instantaneous retrievals of aerosol optical depth from AERONET at 500 nm (AOD) are analyzed and represented in Figure 6. During the campaign period, July to September 2021, the AOD over Mindelo varied from values below 0.2 to 2.0 during extreme dust transport events. These events occurred throughout the year, with significantly higher values, as can be seen, based on both Sal Island and Mindelo AERONET retrievals. That indicates a hazy aspect of the atmosphere. In addition, a reduction in the value of the Angstrom coefficient ($\alpha_{440\text{-}870}$) is usually recorded whenever a substantial increase in AOD occurs. In particular, the period from July to mid-September experiences the lowest values of $\alpha_{440\text{-}870}$, over Mindelo, fluctuating between 0.2 and 0.6. This fluctuating suggests an increase of the coarse particles in the atmosphere column above Mindelo, mainly transported from Saharan regions to the island and with the contribution of marine coarse mode aerosols from the Atlantic. Nevertheless, a regional (Sal Island and Mindelo) remarkable increase of this parameter is observable towards the end of September up to 1.6, which is indicative of a reduction in the number of coarse mode aerosols and dominance of air masses with a new mixture of particles during this brief portion of time.

On the other hand, the analysis of the lidar ratio for the campaign period (July and September) shows a decrease in its variability (40 - 80 sr) compared to the values by the end of the year (40 - 110 sr) similar to that seen for $\alpha_{440\text{-}870}$. Identical patterns can be distinguished for the depolarization ratio, which recorded mostly high values from the beginning of the summer season until mid-September (Fig.7). This situation indicates the presence of an air mass with non–spherical scatterers such as mineral particles (almost-pure dust conditions) as indicated by an increase in the particle depolarization ratio, and potentially mixing with spherical scatterers such as sulphates and pure sea salt particles. Towards the end of September, the lidar ratio is significantly larger than the values observed. The depolarization ratio decreases in contrast to what was observed over most of the experiment period (July-September). One can also see that there is an increase in $\alpha_{440\text{-}870}$. This cooperative behavior in aerosol optical properties over Mindelo at the end of September indicates the influence of air masses with distinct mixing of aerosol types compared to what was seen in the previous days of the experiment. It is worth

mentioning that at this time, there was a major volcanic eruption in the Canarian Island region, upwind of Mindelo, which will be further discussed.

Under the conditions described above, it is possible to characterize distinct scenarios of the aerosol mixture over Mindelo, which provide exciting options to test the consistency of results obtained by applying the EIEx method to discriminate the contribution of different types of aerosols. Next, we present a selection of cases of aerosol mixing scenarios over Mindelo where the EIEx method was performed.

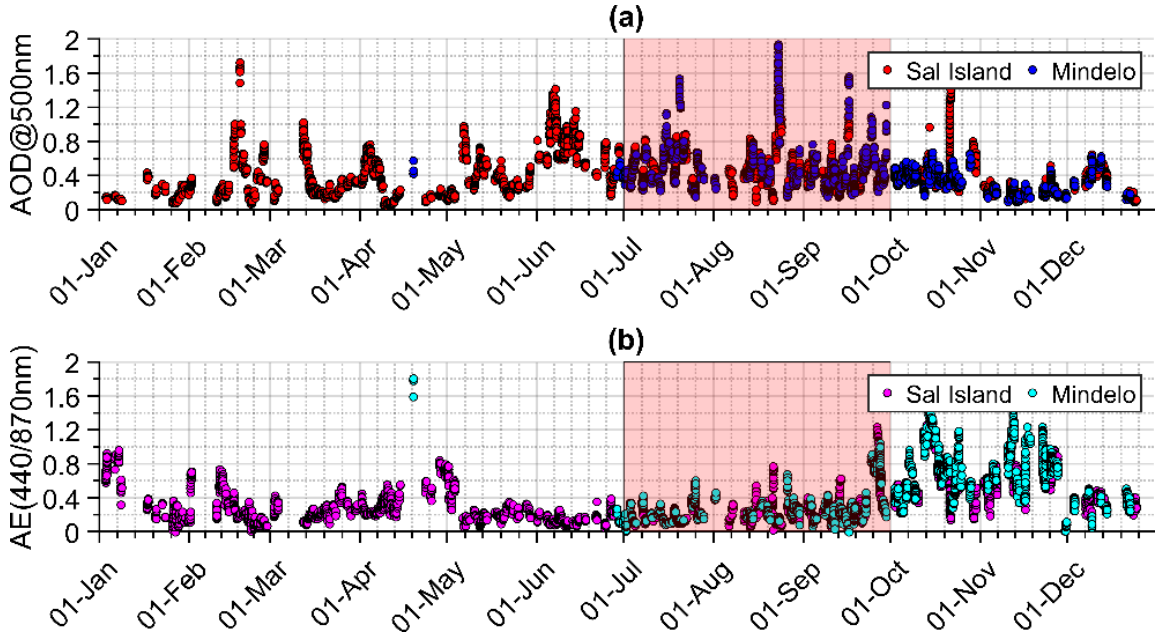

Figure 6: Variability of Aerosol Optical Depth at 500 nm (AOD@500nm) and Angström Exponent based on 440 and 870 nm (AE 440/870 nm) over Mindelo and Sal Island for 2021 based on AERONET sun photometer retrievals. The ASKOS campaign period is highlighted in red**.**

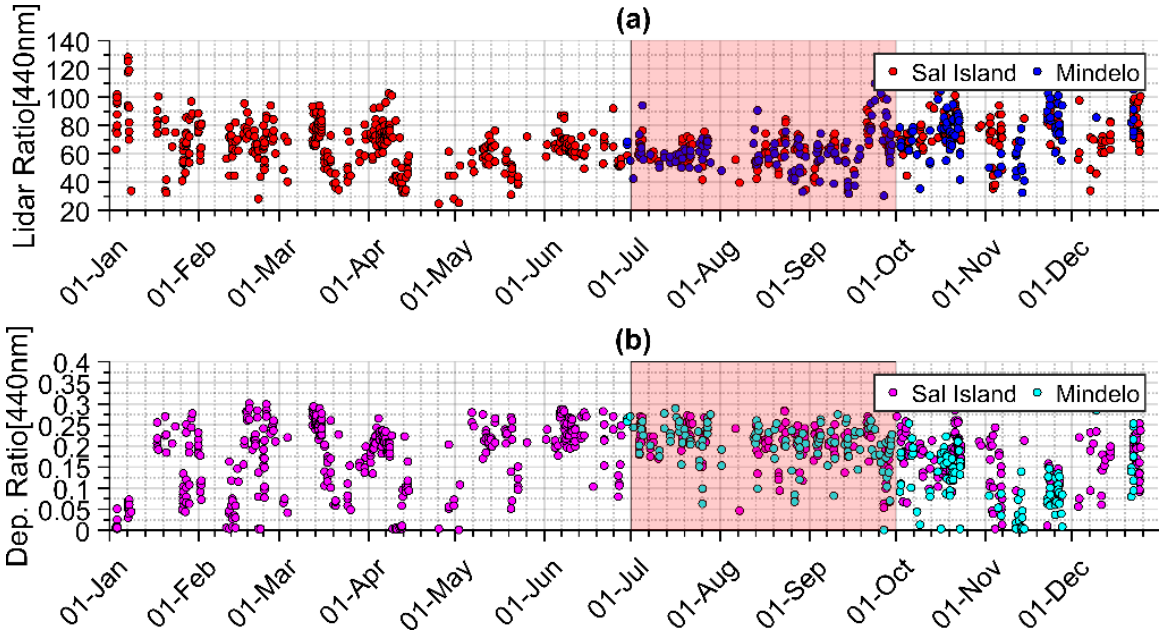

Figure 7: Variability of columnar Lidar ratio and particles Depolarization ratio at 440 nm over Mindelo and Sal Island for 2021 based on AERONET sun photometer retrievals. The ASKOS campaign period is highlighted in light red.

4.2 Study cases selected

Three cases within the ASKOS campaign were selected and subjected to examination using the EIEx method. These cases were selected based on the evaluation of specific predefined parameters outlined previously in the methodology (section **3.4.2.**). Pure dust and marine case occurred on 10 September, a case of high mixing state of dust and marine on 13 September, and a case with pure dust and volcanic particles underlying the marine boundary layer on 24 September.

For each study case, the same approach was followed: First, the parameters from the sunphotometer inversion products at 440 nm, the Lidar time-height plots of the range-corrected signal and the volume linear depolarization, measured at 355 nm with eVe, were analyzed with a critical observation of aerosol layers and clouds. Then, an analysis of the back trajectories of air masses over Mindelo at different altitudes integrated with maps of the MERRA-2 Aerosol Optical Depth (AOD) was used to investigate the origin of the observed aerosol layers. Specifically for the case where volcanic particles were suspected, instead of the MERRA-2 AOD map, additional information based on the SO_2 columnar concentration from OMI was used. Finally, for a detailed analysis of the optical properties, a separation of the aerosol mixture profiles was obtained from the eVe Raman products and the EIEx method by considering the

backscatter, depolarization ratio, and lidar ratio profiles. In order to perform this separation method, several Lidar and depolarization ratios from aerosol species taken from the literature are considered according to the atmospheric condition observed over the Mindelo for the study cases. The assumed lidar ratio and depolarization ratio, and respective uncertainties values: are 53 ± 10 sr and 0.26 ± 0.06 for dust (Tesche et al., 2011), 70 ± 10 sr and 0.02 ± 0.05 for volcanic sulfate (Groß et al., 2012),18 ± 4 sr and 0.02 ± 0.01 for marine (Groß et al., 2011), and finally 44 ± 5 sr and 0. 015 ± 0.01for pollution from Kaduk, (2017).

4.2.1. The first case: The 10 September 2021

The first case is the pure dust and marine aerosol combination scenario on 10 September 2021**.** The AERONET AOD at 500 nm observations, in Figure 8, show an increase in aerosol loading during this day over both stations Sal and Mindelo, with values mainly around 0.5 for the station of Mindelo. The Angstrom exponent decreases, indicating the presence of more coarse particles compared to the previous and subsequent days (9th and 11th September). Additionally, Figure 9 exposes an increase in the depolarization ratio up to 0.23 for the station of Mindelo. From these features, we can affirm that there was an increase in coarse mode particles (dust and marine).

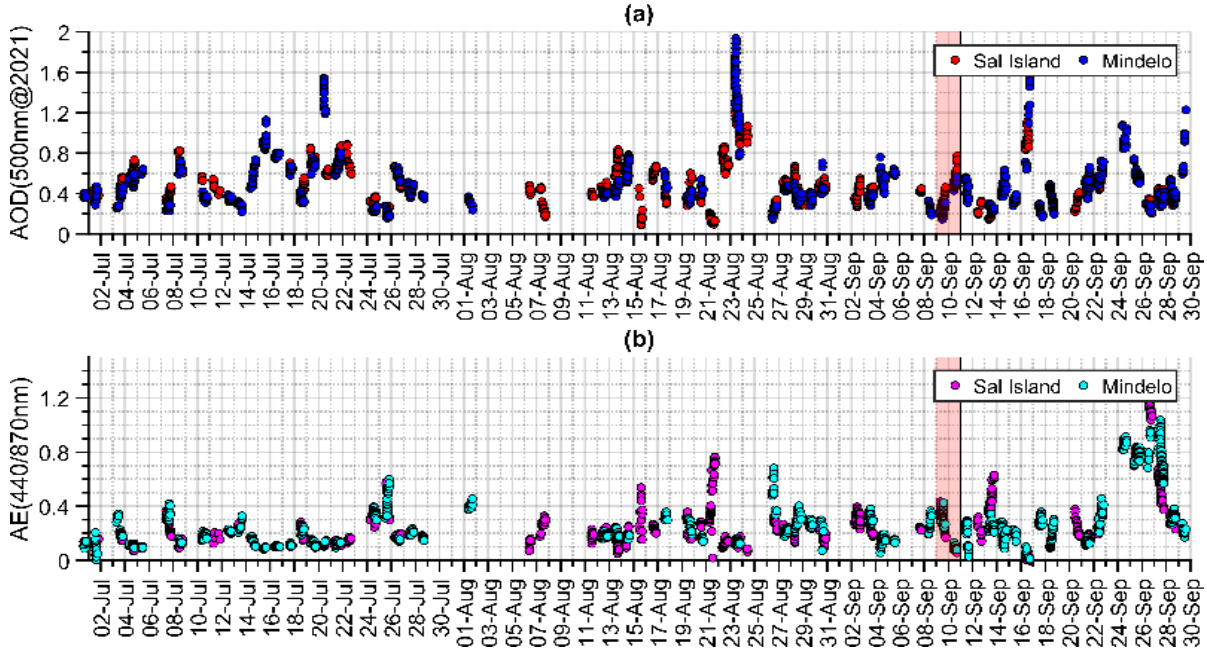

Figure 8: Variability of aerosol optical depth (AOD) and Angstrom exponent (AE) over Mindelo and Sal Island from AERONET retrievals products during the ASKOS experiment. The period highlighted (red) corresponds to the conditions before, during and after the 10 September 2021 study case.

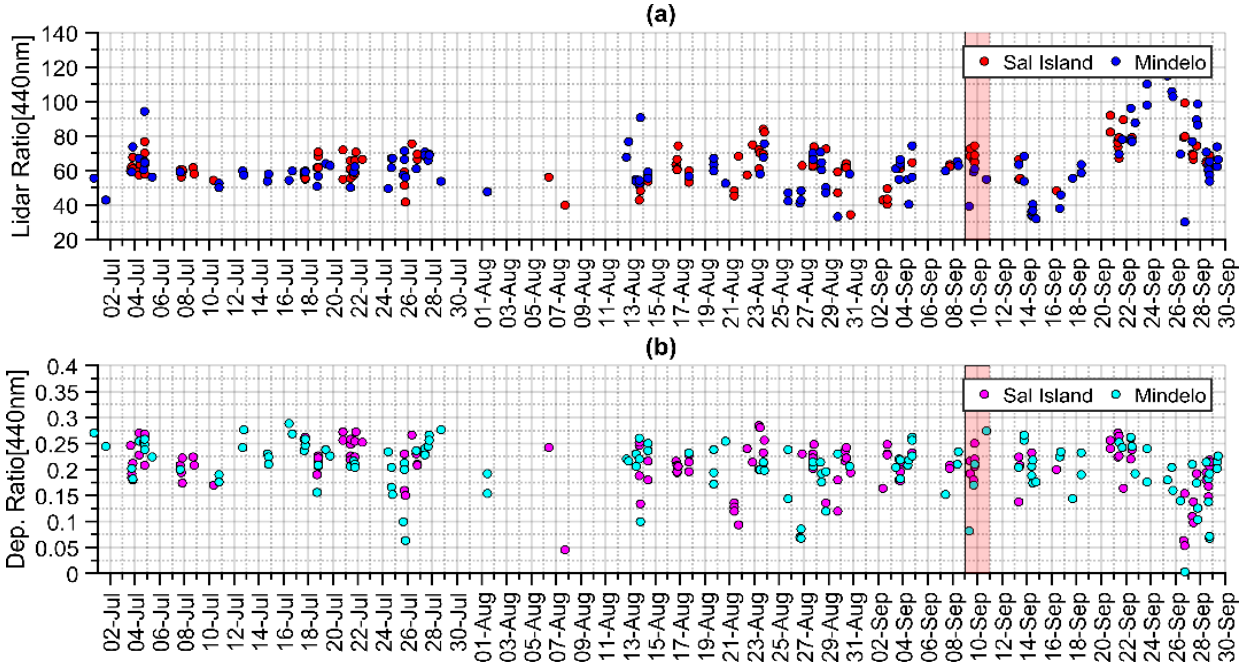

Figure 9: Variability of lidar and linear depolarization ratio at 440 nm over Mindelo and Sal Island from AERONET retrievals products during the ASKOS experiment. The period highlighted (red) corresponds to the conditions one day before, during and one day after the 10 September 2021 (1st study case).

Figure 10 shows the time–height displays of the range-corrected signal (RCS) and the volume linear depolarization ratio (VLDR) at 355 nm measured with eVe on the evening of 10 September, where the cloudless period from 20:41 to 21:09 UTC is highlighted. According to the VLDR structure, aerosol layers from the surface up to 4 km and a low-level cloud layer around 500 m can be seen. From RCS, these observed aerosol layers can be separated into two parts: a layer confined to the marine boundary layer (MBL) up to 1 km, and an aerosol layer above the MLB, in the free troposphere, from 1km up to ~ 4 km. However, from the VLDR structure, it is possible to identify a well-mixed layer characterized by a higher volume depolarization ratio (> 0.07) extending from 2.5 km to 5.0 km (red colors in Fig.10-(b)), indicating the presence of non-spherical particles. Just below, from 2.5 km to the top of MBL (~ 0.8 km), there is another homogeneous layer of VLDR with values varying between 0.05 and 0.07. On the other hand, the lidar observations of VLDR in the lowermost part of the atmosphere (< 0.04), 0.5 – 1.0 km above the ground, suggest the presence of more spherical particles, such as marine aerosols that are expected within the marine boundary layer.

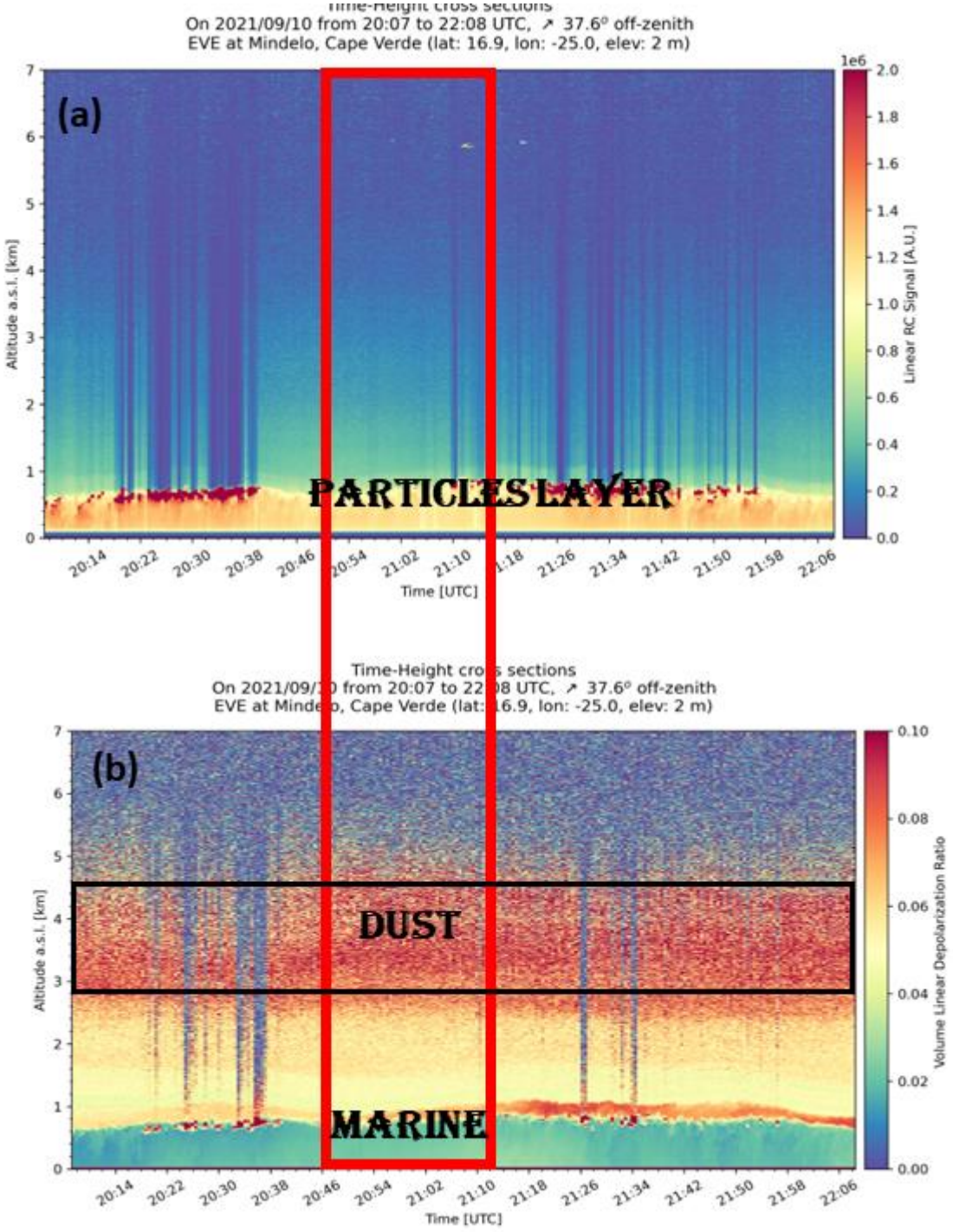

Figure 10: Range-corrected signal at 355 nm (a) and volume depolarization ratio (b) at Mindelo during the ASKOS campaign for the day of 10 September 2021 from eVe instrument located at Ocean Science Center Mindelo.

The back trajectories of air masses arriving at Mindelo on 10 September, combined with the Aerosol Optical Depth at 550 nm (AOD@550 nm) map from MERRA-2 reanalysis, at the

heights of 100, 1000, 2000, 3000, and 4000 m are presented in Figure 11. The trajectories analysis suggests that the air masses arriving at Mindelo within the marine boundary layer travelled all their way close to the ground, from the Canary Islands to Mindelo during the previous three days; hence mainly particles within MBL are expected in this layer. In contrast, the air masses that arrived over Mindelo in the layers above (1000, 2000, 3000, and 4000 m) originated from the West Africa coast and continental areas. In fact, the air mass that arrived at 2000, 3000 and 4000 m was over the Saharan desert at the beginning of the trajectory. So, aerosol dust layers between 1.1 km to 4 km are therefore expected, as suggested by VLDR. Additionally, the AOD map shows a Saharan dust plume extending from the North-West of Africa towards Mindelo.

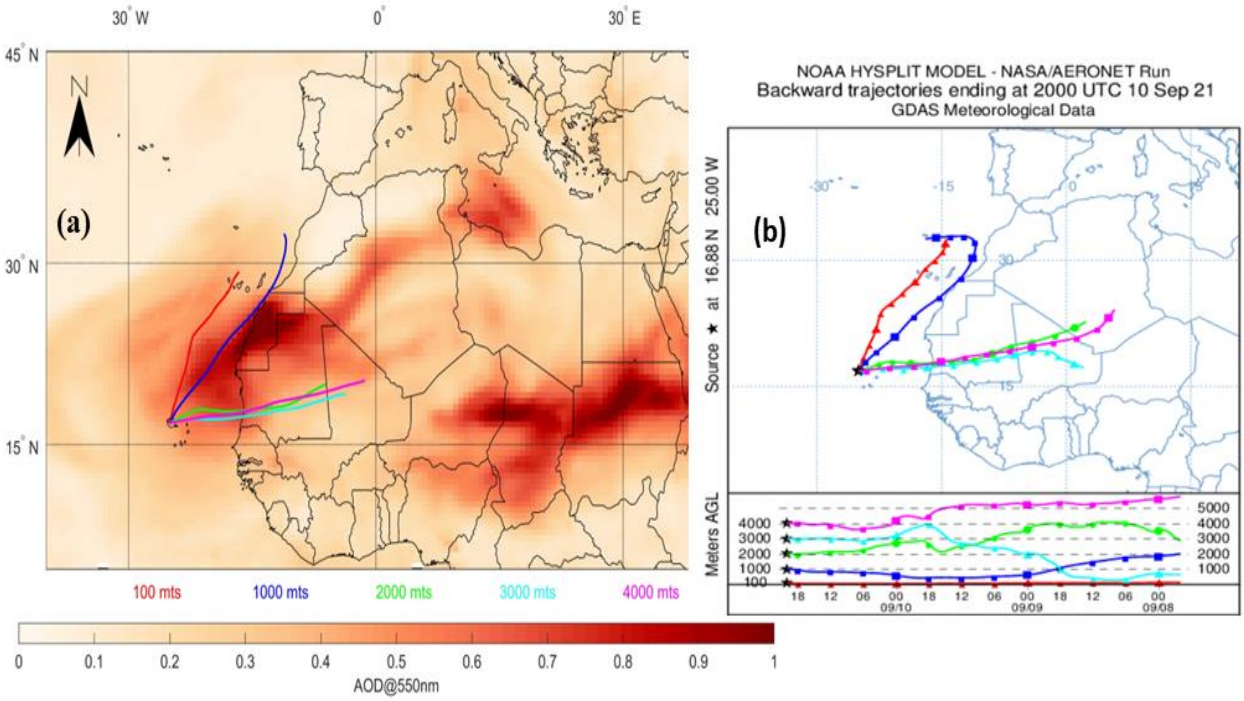

Figure 11: (a) Back trajectories of air masses arriving over Mindelo at different altitudes and map of Aerosol Optical Depth at 550 nm (AOD@550nm) distribution across North Africa and Atlantic Ocean on 10 September 2021. (b) The arrival heights are set to 100 m, 1000 m, 2000 m, 3000 m, and 4000 m.

Following Mindelo atmosphere vertical structure and air mass origins, applying the ElEx methodology for the measurement obtained on 10 September was performed considering averaged lidar profiles between 20:41 and 21:09 UTC. The advantage of this method is its applicability in both daytime and nighttime conditions. And accuracy even for a small SNR (signal near range) in the extinction retrievals despite the small temporal averaging frame. In Figure 12, profiles of the reference backscatter (from eVe) and resolved backscatter profiles for

different mixtures of aerosols applying the method, as well as the Lidar and particle linear depolarization ratio obtained by eVe system and taken from literature for each aerosol type, are shown.

These results are obtained by the good agreement between the near range profile and the far range profile at 355 nm. It is worth mentioning that there is an overlap problem. This overlap is inherent in near range lidar measurements (Wandinger et al.,2002). Concerning eVe, the full overlap range is 450m. So, the optical parameters above this high range (450m) are not influenced by the overlap issue.

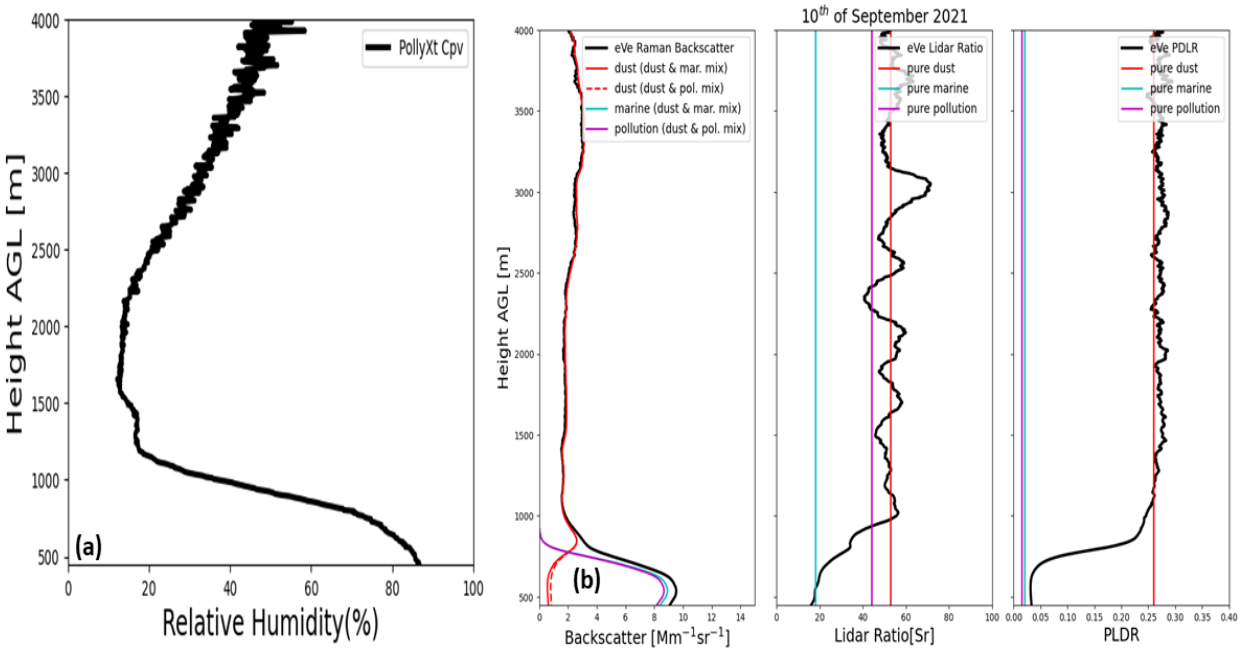

Figure 12: (a) Relative humidity from PollyXT lidar system, (b) backscatter coefficients from eVe (black) for the case of 10 September 2021 and resolved for aerosol types (dust, marine and pollution) considered in different assumptions of aerosol mixtures applying EIEx method, lidar and depolarization ratios from eVe and taken from the literature for the types of aerosols considered in the mixture. The red line represents the dust component, the light blue for marine, and purple for pollution at 355 nm.

Figure12-(a) illustrates the relative humidity profile of the atmosphere over Mindelo computed through the PollyXT system measurements from 20:00 to 20:59 UTC on 10 September 2021. It is important to underline that this study's particular interest lies in the humid condition of the lower atmospheric layers. Mindelo location, in the middle of the Atlantic Ocean, and because the analysis of the air masses demonstrated that marine particles, whose depolarization ratio is dependent on the ambient humidity, are probably the dominant type of aerosols in the MBL. According, to Mamouri et al. (2017), as long as relative humidity (RH) is above 50–60%, the particle depolarization ratio of marine particles is in the range of 0.05 ±

0.02. In this way, the RH observed in the lower layers of the atmosphere in Mindelo for this study case decreases from 85% near the ground to 50 % around 1000 m. Therefore, we can assume that the marine depolarization ratio is within the literature ranges.

Furthermore, Figure12-(b) presents the retrieval of the eVe optical parameters using the Raman method (with the black line) and the results from the profiles separation using the EIEx method. The separation of the two aerosol types was applied using the EIEx separation technique, and the resolved dust and marine optical properties were presented. The lidar ratio profile for 355 nm obtained by applying the Raman lidar method indicates two aerosol layers: the primarily first confined to the MBL (< 1.0 km) and the second in the aerosol layer (from 1.0km to 4km). The eVe profile indicates values of Lidar ratio (Lr) close to 53 sr from ~1.0km to 4 km height, which is typical for dust. Below about 1 km height, the Lr decreases to values around 17-18 sr (355 nm) within the MBL. This reduction of the Lr values from 53 sr to 18 sr points out marine aerosols as the major non-dust component in the MBL. Minor contributions to particle backscattering by pollution origin cannot be excluded. The eVe PDLR shows similar features. The depolarization ratio values indicated by the eVe profile above the MBL were around 0.28 and then declined towards 0.03 in the MBL. These values are consistent with the pre-selected averages based on the literature, which are 0.26 for pure dust and 0.02 for pure marine. Despite their difference from the assumption, they are still in the range frame of the selected pure species. Indeed, Kaduk (2017), in her investigation of pure particle classification and mixture state in Leipzig, obtained precisely the same value (0.03) for the depolarization ratio of pure marine.

4.2.2. The second case: 13 September 2021

Figure 13 presents AOD500nm and AE, while Figure 14 shows lidar ratio and particle linear depolarization ratio distribution during the 13 September, based on AERONET retrievals. On 13 September, AOD500nm was about 0.3, representing a much lower value compared with 10 September, when dusty conditions were prevalent. Although relatively low, AE presented an increase, especially over Sal Island. The lidar ratio shows an average value of 50sr, and the particle depolarization ratio was again high at 0.26. Based on these optical properties, the following points can be derived: the aerosol load is probably lower compared to the previous case and may be composed of a distinct mixture of aerosol particles.

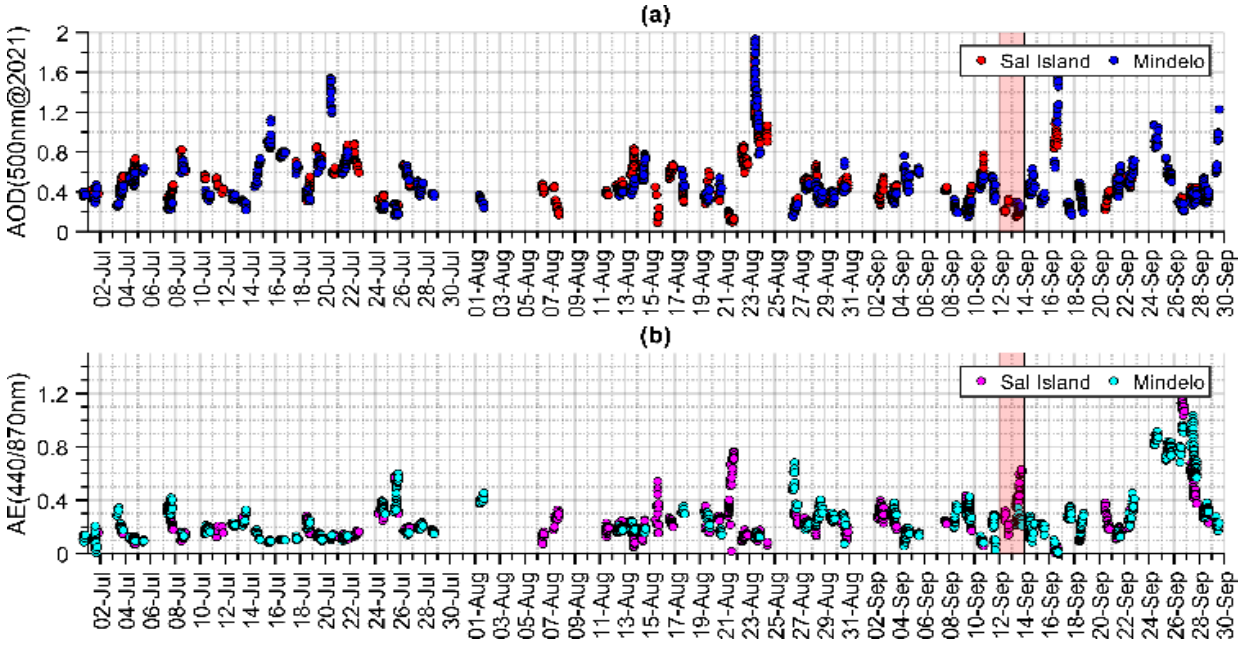

Figure 13: Variability of aerosol optical depth (AOD) and Angstrom exponent (AE) over Mindelo and Sal Island from Aeronet retrievals products during the ASKOS experiment. The period highlighted(red) corresponds to the conditions before, during and after the 13 September 2021 study case.

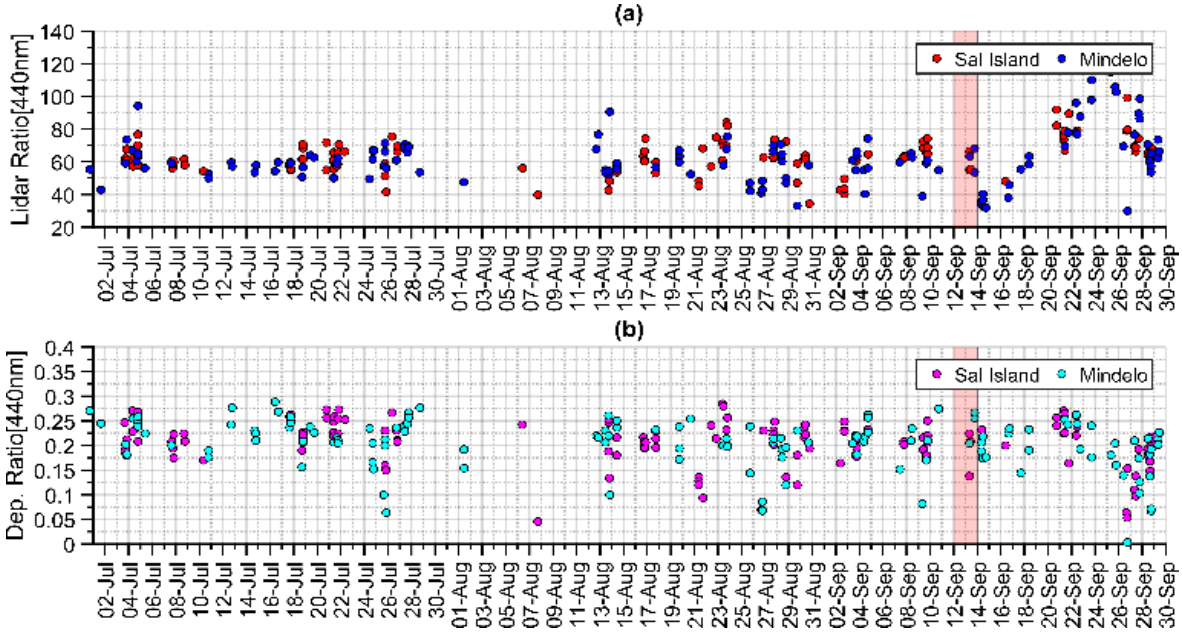

Figure 14: Variability of the lidar ratio and linear depolarization ratio at 440 nm over Mindelo and Sal Island from Aeronet retrievals products during the ASKOS experiment. The period highlighted(red) corresponds to the conditions one day before, during and one day after the 13 September 2021 (2nd study case).

This second case represents a mixture of coarse and fine aerosols in the considering atmosphere column. The range-corrected signal (RCS) and the VLDR performed from the eVe (Fig.15) measurement from 20:17 to 21:17 UTC reveals some cloud contamination at different altitudes between 1 km and 2 km. The VLDR suggests a single compact layer of mixed aerosols

throughout the profile from the ground to 3 km. The VLDR intermediate values (~ 0.02 - 0.04) suggest that the layer is not pure Saharan dust and neither could be of pure marine, pollution, or volcanic origin. Consequently, a thoroughly mixed state of different types of aerosols in the atmosphere on all layers from MBL to 3 km can be assumed. This mixture could be interpreted (consider the main species) as either dust with marine or dust and pollution.

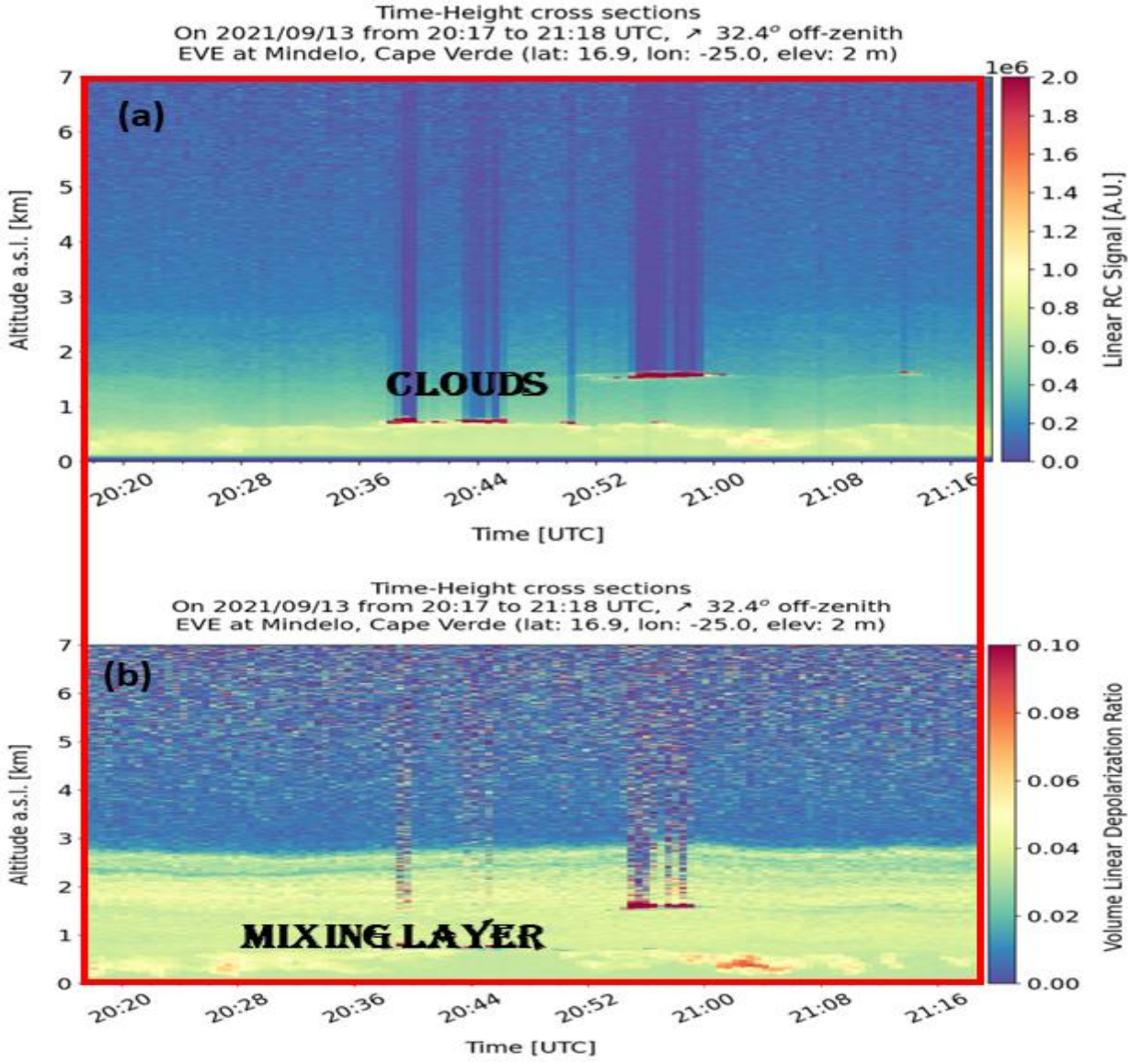

Figure 15: Range-corrected signal at 355 nm (a) and volume depolarization ratio (b) at Mindelo during the ASKOS campaign for the day of 13-September 2021 from eVe instrument located at Ocean Science Center Mindelo.

The three days back trajectory of air masses arriving over Mindelo at different levels (Fig.16) indicates that, during the referred period, all air masses were coming from the ocean in the southern part of Cabo Verde, implying a lower dust contribution and higher dominance of marine aerosols compare to the case of 10 September. An analysis of the AOD spatial

distribution from MERRA-2 reveals moderate values between 0.3-0.4, relatively high for marine particle, suggesting the presence of dust previously transported. Consequently, the dust aerosols could have been mixed with marine and/or pollution aerosols.

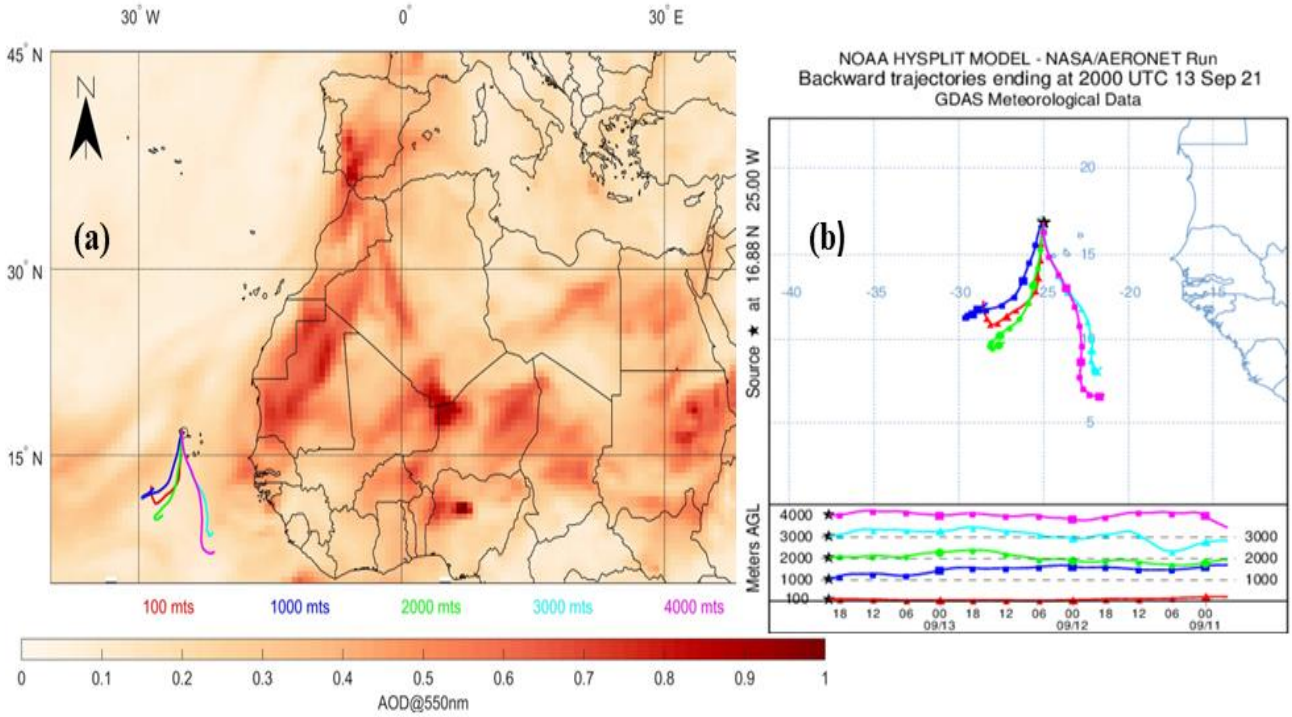

Figure 16:(a) Back trajectories of air masses arriving over Mindelo at different altitudes and map of Aerosol Optical Depth at 550 nm (AOD@550nm) distribution across North Africa and Atlantic Ocean on 13 September 2021. (b) The arrival heights are set to 100 m, 1000 m, 2000 m, 3000m, and 4000 m.

Considering the information provided by these previous analyses, we proceed with applying the EIEx method taking into account the optical properties (lidar and depolarization ratio) of dust, marine, and pollution based on the literature. In fact, the optical parameters revealed a very different scenario from the first case study. For this situation, the estimated values of the lidar ratio of the different species are maintained: 53 sr for the dust, 18sr for the marine, and 45 sr for the pollution. These values were respectively combined with the depolarization ratio of 0.26, 0.02, and 0.015 for the three aerosol species considered. The calculated dust, marine, and pollution backscatter coefficients profiles are presented in Figure17-(b). However, before analyzing the optical properties profile derived from the EIEx method, the humidity conditions of the atmosphere are first examined to verify the structural aspect of the marine particles. The RH profile of PollyXT retrieval from 19:55 to 20:51 UTC presented in Figure 17-(a) indicates a layer with enhanced and varying RH (around 85% - 60%) from the surface to 1.8 km height. From this level (1.8 km) to the upper levels, the RH varied

from 60% (ground) to ~50% in the upper layer. Therefore, the RH is still > CRH in the identified aerosol mixing layer, so spheric marine particles are likely. Hence, from the point of view of the humidity scenario, the assumed values for marine aerosol are consistent for this atmosphere condition.

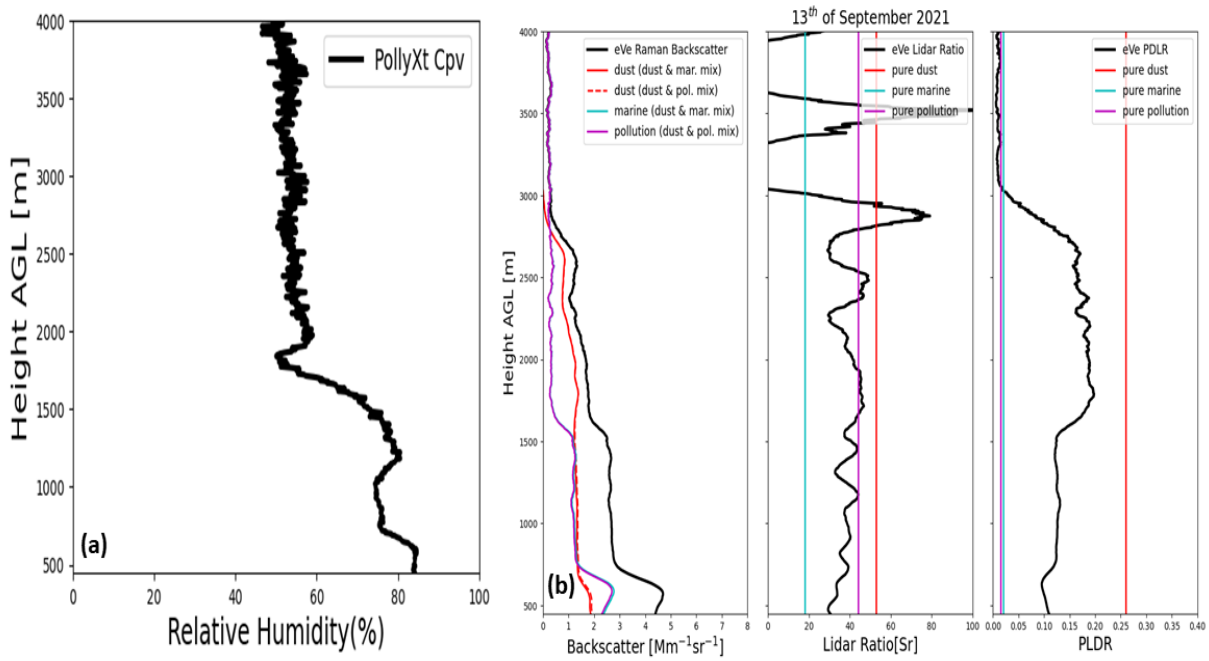

Figure 17: (a) Relative humidity from PollyXT lidar system, (b) backscatter coefficients from eVe (black) for the case of 13 September 2021 and resolved for aerosol types (dust, marine and pollution) considered in different assumptions of aerosol mixtures when applying EIEx method, lidar and depolarization ratios from eVe and taken from the literature for the types of aerosols considered in the mixture. The red line represents the dust component, the light blue for marine, and purple for pollution at 355 nm.

Inspection of the particle depolarization ratio profile demonstrates values between 3% and 15% (Fig.17-(b)). A layer extended from the MBL to 1.5 km with a depolarization ratio of around 0.03. Upward, from 1.5 km to 2.8 km, another layer with a higher depolarization ratio ~0.15-0.20 was found. This structure indicates a different degree of mixing, with dust being more dominant in the second layer. These values are significantly lower than the ones considered for the most depolarizing species (dust) by 15%. The prior assumption of lidar ratio (53 sr and 18 sr) and depolarization ratio (0.02 and 0.26) for the pure species reveal extreme values for this case. This situation illustrates the mixed state of the atmosphere across all layers. To produce adequate profiles and to readjust the separation method, it will be necessary to consider a combination of the estimated values for the different pure species to derive adequate and predictable profiles.

4.2.3. The third case: 24 September 2021

For the case of 24 September 2021, the AERONET sunphotometer retrievals indicate a substantial increase in both AOD and AE over Mindelo (Fig.18,19) to values close to 1.0 for both parameters. While the AOD increase indicates an increase of the aerosol load over the city, the increase of the AE signifies a change in the aerosol mixing state of the atmospheric in terms of aerosol particles' nature and mixture state. An increase in the AE indicates a higher contribution of fine mode aerosols. Most interesting is the lidar ratio increase, which equals 80-90 sr, with a depolarization ratio around 0.2. These characteristics are not typical for any of the 3 aerosol species examined so far (dust, marine, and pollution). So, we can assume a different type of aerosol exists in the atmospheric column.

The time–height plot of RCS at 355 nm (Fig.20) shows a mostly cloudless atmosphere. The measurement was performed from 19:55 to 21:25 UTC. The detailed analysis of the aerosol optical property profiles based on the volume depolarization allows the characterization of two different aerosol layers. The first layer above the MBL (1.5 km to 3km) is characterized by higher depolarization ratios, which can be associated with the presence of dust. The second layer is within the MBL < 1.5 km exhibits a meagre depolarization ratio, almost close to 0. This depolarization value is lower than the previous observations presented here. It suggests that the marine particle is no anymore the main species in this layer.

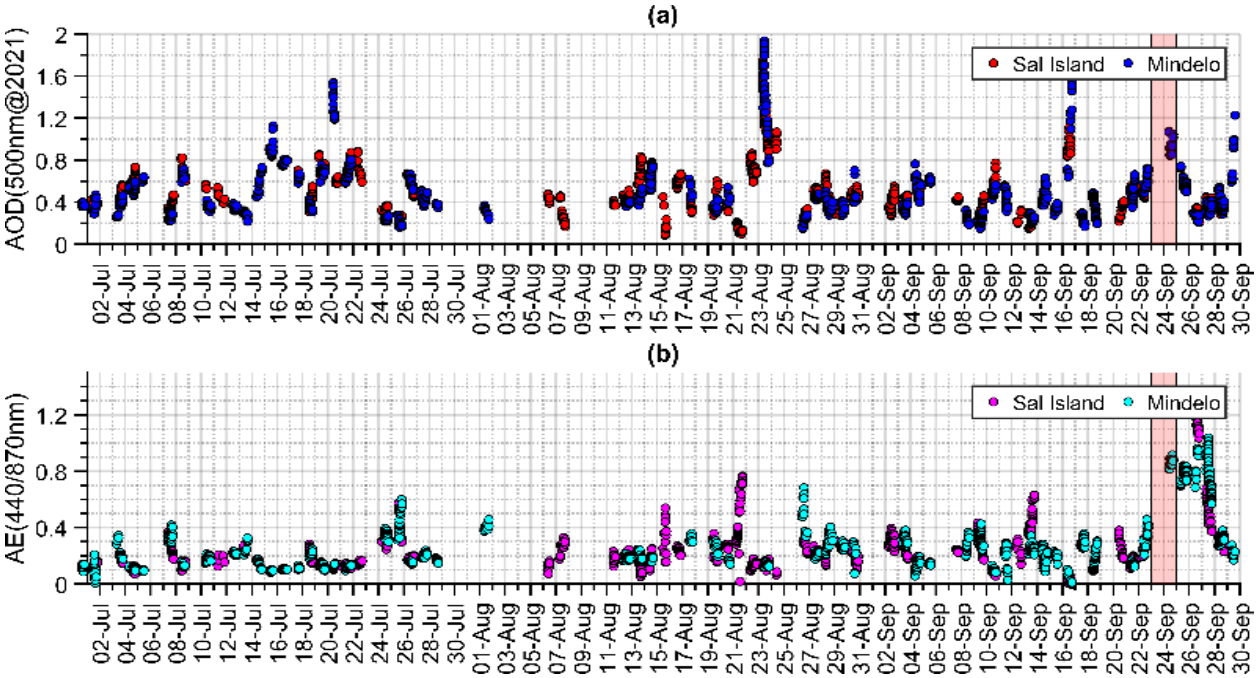

Figure 18: Variability of aerosol optical depth (AOD) and Angstrom exponent (AE) over Mindelo and Sal Island from Aeronet retrievals products during the ASKOS experiment. The period highlighted (red). corresponds to the conditions before, during and after the period highlighted(red) corresponds to the conditions before, during and after the 24 September 2021 study case.

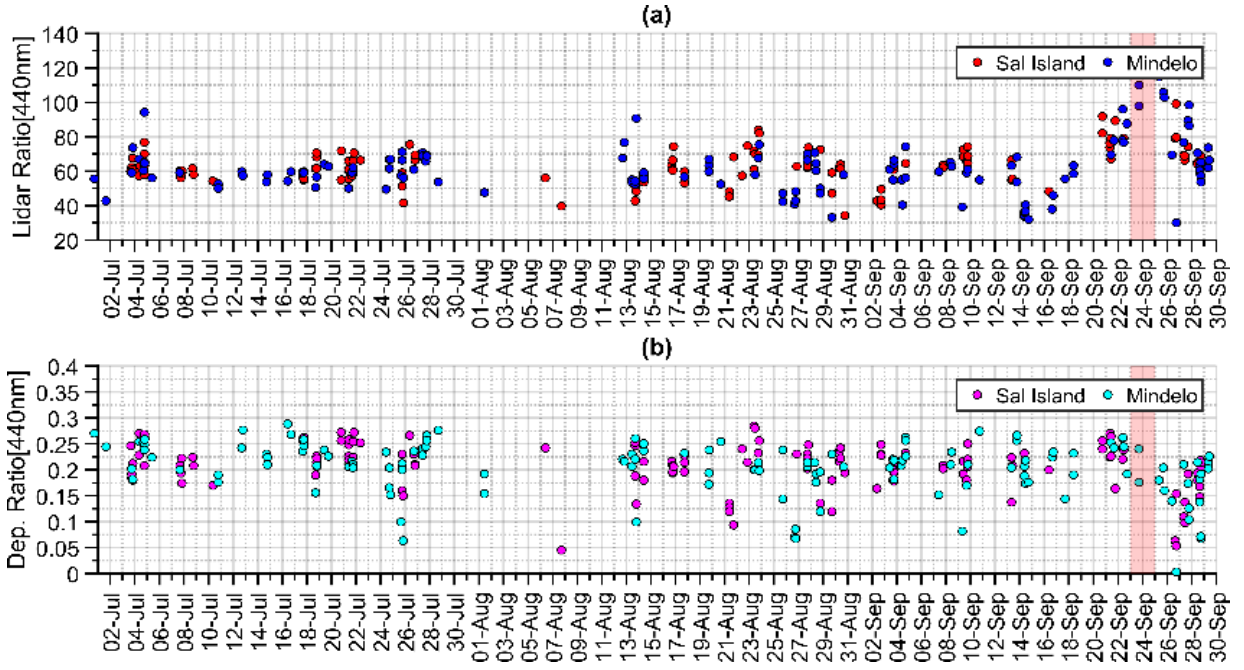

Figure 19: Variability of the lidar ratio and depolarization ratio at 440 nm over Mindelo and Sal Island from Aeronet retrievals products during the ASKOS experiment. The period highlighted (red) corresponds to the conditions one day before, during and one day after the 24 September 2021 (3 study case).

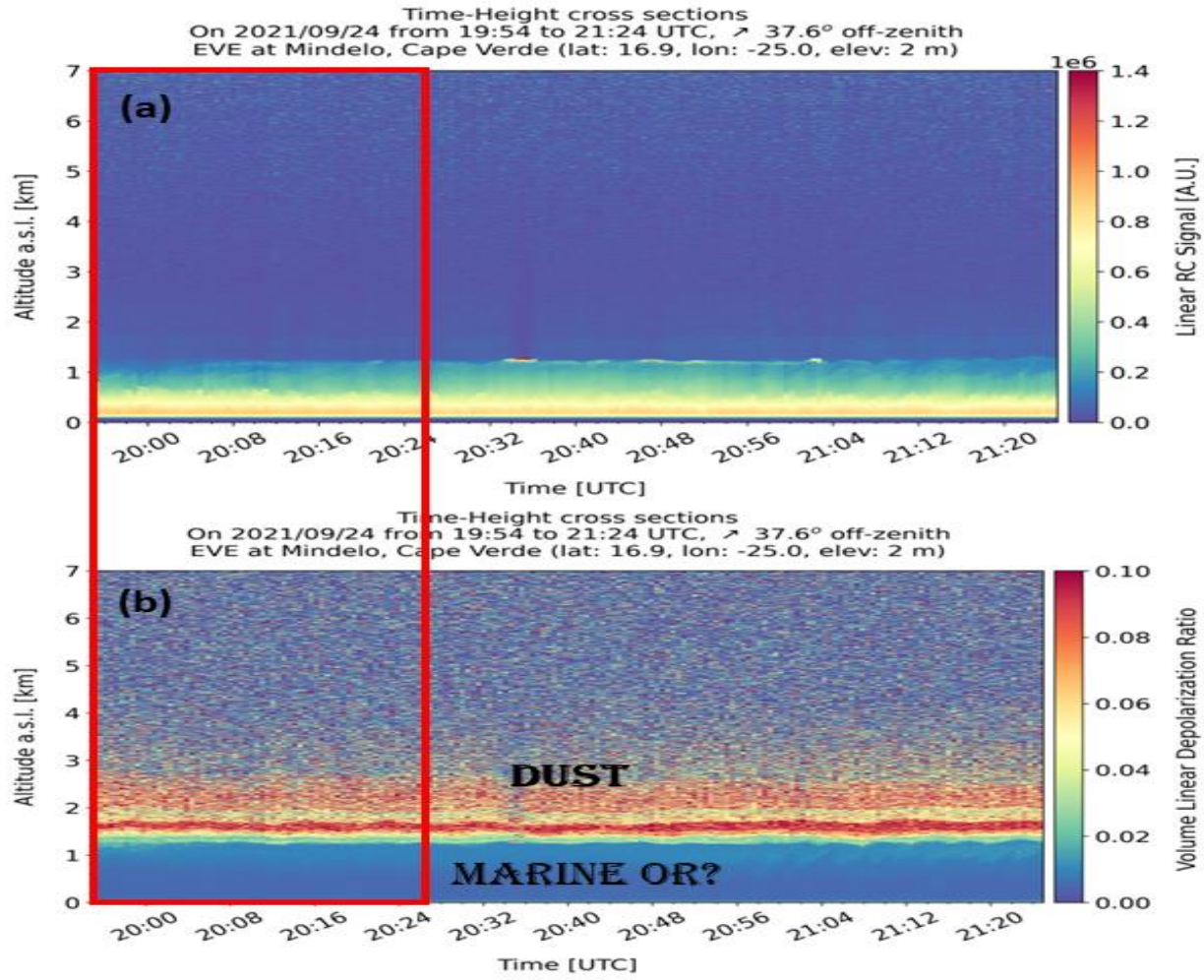

Figure 20: Range-corrected signal at 355 nm (a) and volume depolarization ratio (b) at Mindelo during the ASKOS campaign for the day of 24-September 2021 from eVe instrument located at Ocean Science Center Mindelo.

The analysis of 3-days backward trajectories in Figure 21-(a) reveals that the air masses arriving over Mindelo at levels 2000, 3000 and 4000 m height originated from the Saharan regions. The air masses were travelling from Mauritania, a region at this period affected by a dust plume, as can be seen in the AOD map from MERRA-2 reanalysis. This helps to explain the high dust particles load and depolarization ratio of around 2-4 km in this case. The air masses arriving within the marine boundary layer, at 100 m and 1000 m, originated from areas over the Atlantic Ocean, so it may inevitably carry marine particles and were less contaminated by dust. The trajectory of these air masses indicates that they mainly come from the Canary Islands region. At the time of the case analyzed here, the observation based on the Ozone Monitoring Instrument (OMI) aboard AURA satellite revealed a large plume of SO_2 (Fig 21-(b)) above Canary Island. The plume was a result of the Cumbre Vieja volcano eruption at Las Palma that sent large plumes of Sulfur dioxide into the atmosphere over North Africa and Europe, and

which started on 19 September 2021, according to Copernicus Atmosphere Monitoring Service (D'Auria et al.,2022). The SO_2 is emitted by volcanic eruptions. Therefore, the sulphate aerosols of volcanic origin is expected over Mindelo, considering the volcanic eruption that took place in Las Palmas during this period and the air mass trajectory discussed.

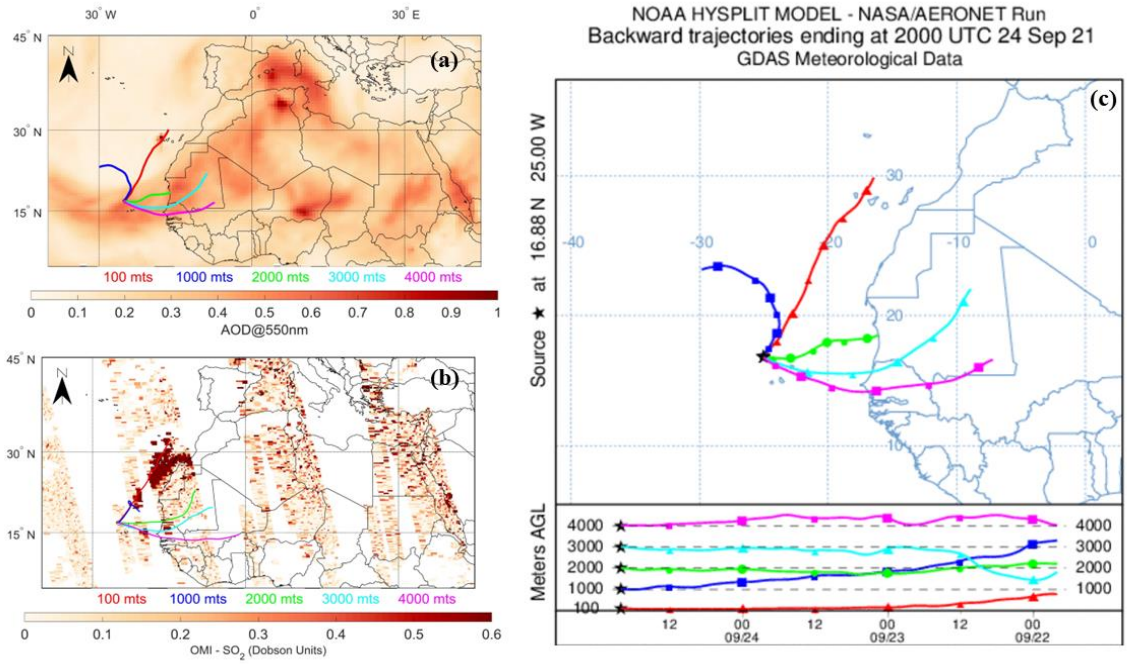

Figure 21: (a) backward trajectories of the air masses and AOD at 550 nm distribution on 24 September 2021 at Mindelo, São Vicente. (b) The arrival heights are set to 100 m, 1000 m, 2000 m,3000 m and 4000 m, and (c) the back trajectories combined with columnar sulfur dioxide (SO2) content from the OMI sensor aboard AURA satellite, which is a strong component of volcano eruption.

For this case apart from the literature values that we already applied for dust, sea salt, and urban pollution, we will include also volcanic sulphate particles in the calculations (70 ± 10 and 0.02 ± 0.05, Groß et al., 2012). The calculated backscatter profiles for each species using measurements from eVe are displayed in Figure 22. The analysis of Figure 22-(b) found the particle depolarization ratio from eVe between 0% and 30%, fluctuating with altitude from one extreme to another. It is around 0.25–0.27 in the aerosol layer between 1500 m to 400 m, which corresponds to the prevalence of dust particles. Between 800 m to 1500 m, the depolarization value varied from 0.03 to 0.0, which explained the mixed state between marine and volcanic contribution. The analysis of the atmospheric relative humidity from 21:00 to 21h:59 UTC (Fig.22-(a)) exposes a high humidity condition in the lower part of MBL, from 70% to 90%, and variation between 30% to 50% in the upper region of the atmosphere.

Here it is important to emphasize that sulfate is a hygroscopic species, so its structure becomes more spheric when the RH is high (like the marine particle). Indeed, Groß et al. (2012), during their investigation of the ash plume of the Eyjafjallajökull eruption, demonstrated that a great change in the depolarization and lidar ratio could be related to the modification of the micro-physical properties of the particle-induced by humidity condition of the atmosphere layer. Thus, this value of depolarization ratio close to 0 result from the morphological change of the sulfate due to its humidification.

Considering the lidar ratio profiles, different aspects can be detected. The values obtained from eVe are around 68 sr in the MLB and are in agreement with the typical values of volcanic sulfate gotten from Groß et al. (2012) and Vaughan et al. (2021) during their study on the stratosphere ash plume based on the Raikoke volcano eruption in a marine condition (Kuril Island). However, in the upper atmosphere (> 1200 m), the Lr varied from 60 sr to 90 sr, which is either lower or higher than the lidar ratio chosen from the literature. These results require further investigation to understand the atmosphere structure and its component aspects at these high levels. More analysis will be undertaken in the next part with the method's validation.

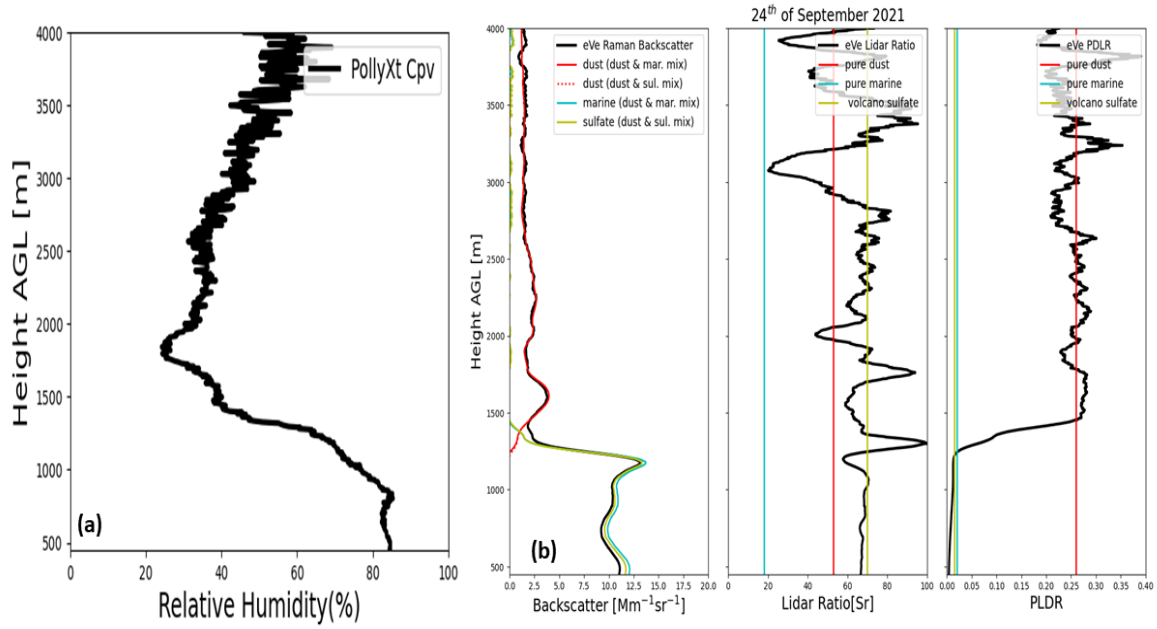

Figure 22: (a) Relative humidity from PollyXT lidar system, (b) backscatter coefficients from eVe (black) for the case of 24 September 2021 and resolved for aerosol types (dust, marine, and pollution) considered different assumptions of aerosol mixtures when applying EIEx method, lidar and depolarization ratios from eVe and taken from the literature for the types of aerosols considered in the mixture. The red line represents the dust component, the light blue for marine, and purple for pollution at 355 nm.

4.3. Validation of the EIEx method and discussion

4.3.1. Validation with the eVe Raman retrieval

After the application of the EIEx method to separate the aerosol type contribution to the backscattering profile and the discussion of the results obtained, we proceed in this part to the validation of the method by performing a comparison between the extinction coefficient profiles and the lidar ratio derived from Eve's and Polly's Raman lidar systems with the one calculated from the EIEx application. The lidar and depolarization ratio uncertainties taken from the literature are applied for a Monte Carlo simulation in order to quantify the uncertainties in the retrievals.

4.3.1.1 The first case: 10 September 2021

Figure 23 shows the species backscatter profiles from eVe calculated with EIEx by assuming a mixture of 2 species (dust and marine; dust and pollution). Using the Monte Carlo method, we estimate the uncertainty in the species profiles due to the variability of the lidar ratio and depolarization ratio values reported in the literature

The Raman backscatter retrieval error is also included in figure 23 (shaded black). For the particle backscatter coefficient, the eVe retrieval uncertainties at 355 nm range 5%. Nevertheless, the range is higher for the parameters derived from the nitrogen Raman signal, with 10% for the extinction and 20% for the lidar ratio. However, it is interesting to emphasize that the derived extinction coefficient profile using the proposed methodology was pretty noisy, because it is not necessary to calculate the derivative of the Raman signal, a necessary step for the Raman retrieval that inevitable increase the noise. This is one of the advantages of the EIEx methodology (Giannakaki et al.,2020).

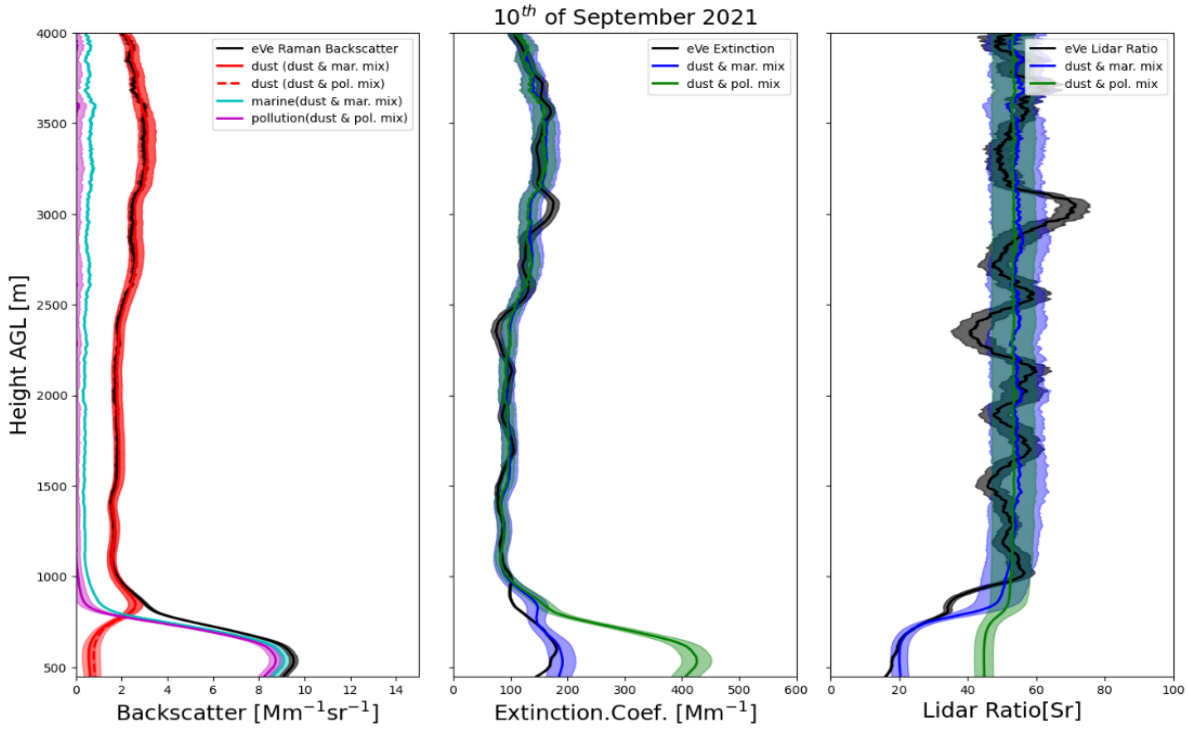

Figure 23: Comparison of the eVe Raman-derived profiles (black) with the EIEx profiles of backscatter coefficients, lidar ratio and extinction coefficient for the 10 September 2021, considering different aerosol mixtures (dust/marine and dust/pollution).

The analysis of the extinction profiles reveals piling up of all profiles in higher layer of the aerosol layers. This means matching of the eVe profiles with the dust/pollution mixtures and the dust/marine profile. The excellent agreement seen at these higher levels is because dust particles are predominant, as can be seen in the resolved backscattering profiles. But in the MBL, the dust/pollution profile is offset from the eVe profile while the dust/marine combination systematically follows the eVe profile. This is explained by the consistency of the different aerosol layers: above the MBL, the pure dust contribution is dominant, and in the MBL that is the case for marine particles. In general, taking into account the estimated uncertainty for the derived extinction profile from EIEx, throughout the layers, the comparison between the eVe Raman and the EIEx extinction profile's shows a very good agreement.

Similarly, the comparison of the profiles shows that the particles Lidar ratio profile obtained with the Raman lidar technique is in better agreement with the EIEx retrieval for the mixture of dust and marine particles than for the mixture of dust and pollution particles. For the aerosol layers in the upper levels above 1.5km, the results obtained for the pure dust contribution corroborate with the result obtained during the campaign of SAMUM2 around Praia city in Cabo Verde (Groß et al., 2011). However, the values are different from that recorded during the Polarstern cruise around Canary Island (61 ±4 sr) in a dust plume event. Although within the

MBL, the Polarstern cruise results for the pure marine case (Bohlmann et al., 2018.) are slightly higher (23 ± 2 sr at 355) than the values assumed in the present study for the method (18 ± 4 sr).

This region is a transition layer between a layer dominated by marine particles (MBL) and layers above dominated by dust particles, which can be a challenge for consideration of depolarization and lidar ratios. Furthermore, a looking carefully at the EIEx extinction profiles reveals a small difference between the EIEx and the Raman extinction coefficient profiles at the top of MBL (0.5-0.7 km). Giannakaki et al. (2020) found a similar issue, which they attributed to an influence of particles of anthropogenic origin, which are more probable to be at the top of MBL. Given that pollution aerosols do not depolarize the light, thus, they evaluated that the value used for the depolarization ratio fits well for the separation of dust and non-dust particles in general, which would be similar to the present study. For their specific scenario, they found the aerosol-type-dependent lidar ratio assumption as the main reason for the observed difference between the method and the reference extinction profile. In the present study, as can be seen in the eVe lidar ratio profile around the levels between 700 and 900 m, a lidar ratio between 30 and 40 sr would be adequate for this particular layer. According to the values found in the literature, this lidar ratio interval represents a transition from marine to smoke or pollution aerosol types (Fig.3). The back trajectory for this case study suggests that air mass arriving at Mindelo at 1000 m was travelling from an ocean region close to Western Sahara, therefore, out of the typical biomass burning areas in the southern portion of Sahara.

4.3.1.2. The second case: 13 September 2021

The analysis of the backscatter and the depolarization ratio profiles revealed a mixed atmospheric condition from the MBL up to the free troposphere for this particular case (section **4.2.2**). The comparison between Raman and the EIEx extinction profiles also shows a good correlation for the combination of dust and marine particles for all atmospheric layers analyzed. However, it is observable that above 1.7 km, the combination of dust and pollution is also consistent with the eVe profile. Two mechanisms may explain this observation. First, the presence of anthropogenic particles (as discussed in the previous section), and second, the similarity of particle depolarization ratio of both types of aerosols (marine and pollution) at a certain atmospheric condition. Indeed, according to some laboratory investigation, Sakai et al. (2010) showed that pollution and marine particle depolarized light at the same range of values of 0.01 ± 0.001, especially under adequate humidity conditions. For this case, over Mindelo,

there was a deeper layer characterized by high levels of relative humidity (Fig.17) as a result of air masses travelling from the moist regions southward of Cabo Verde. Nevertheless, this consistency between the profiles of eVe and the EIEx results for dust and pollution combination in higher levels is not discerned in the estimated lidar ratio profiles. Despite the noisy profile from eVe in higher layers, the EIEx results for dust and marine combination present better agreement implying that the atmosphere is dominated by a rather heterogeneous mix of dust and marine with a principal value of 33±3 sr. These values are following those obtained by Kaduk. (2017), which was around 34 ± 12 sr.

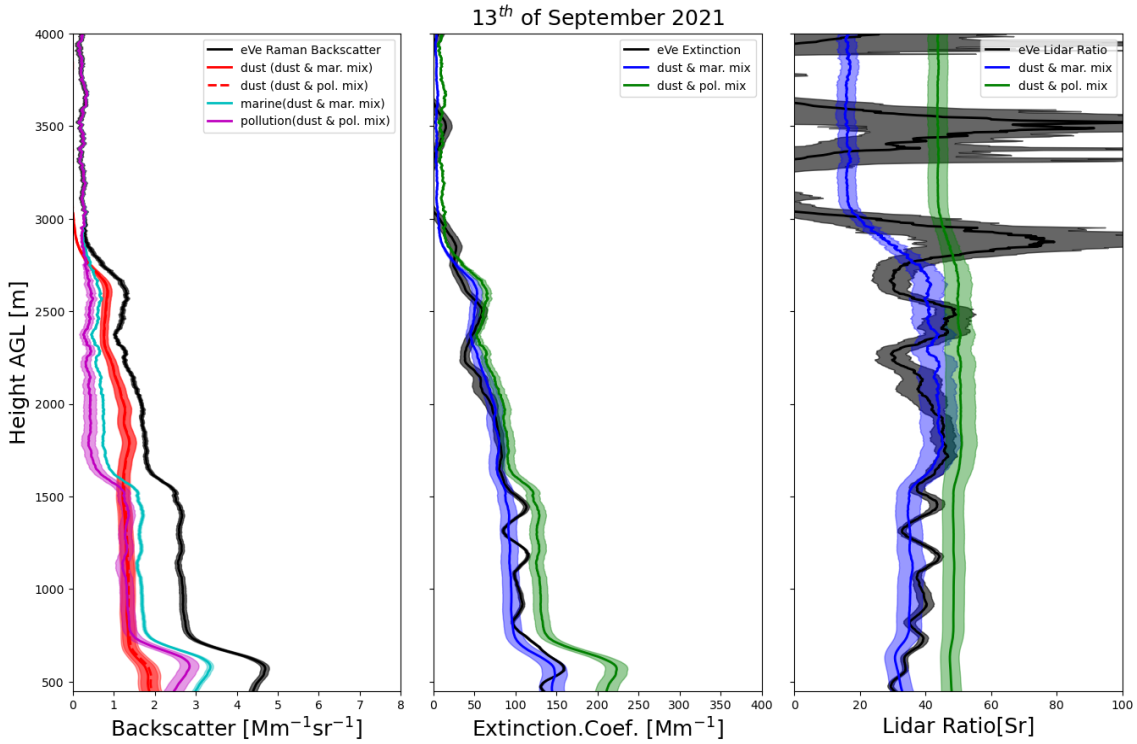

Figure 24: Comparison of the eVe Raman-derived profiles (black) with the EIEx profiles of backscatter coefficients, lidar ratio and extinction coefficient (red, blue and green) for the 13 September 2021 considering different aerosol mixtures (dust/marine dust/pollution).

4.3.1.3 The third case: 24 September 2021

In this case, the atmospheric conditions regarding aerosol types and vertical structure are quite different. The particles types chosen for profile discrimination are dust, marine (assuming the same literature-based lidar and depolarization ratios as in the first two cases), and volcanic sulfate, for which was assumed a lidar ratio of 70 ± 10 sr and 0.015 ± 0.005 for the depolarization ratio (Groß et al., 2012). The analysis of the extinction profiles from the assumed mixtures (dust/marine and dust/sulfate) shows a close agreement between the eVe profile in the

free troposphere, particularly for the layer from 1.5 km to 4 km. The dust-sulfate mixture and the dust-marine combination both overlap with the eVe profile at these altitudes. This is mainly due to the strong presence of dust in the upper aerosol layer, as can be seen in the backscattering resolved profiles. Meanwhile, unlike the previous cases, the marine/dust extinction profile is far from that of the eVe product in the marine boundary layer environment. The volcanic sulfate/dust mixture proposed to resolve the profile of the aerosol types via EIEX presented a good agreement with eVe, which is consistent with the transportation of aerosols from the Canarias towards Cabo Verde within the MBL.

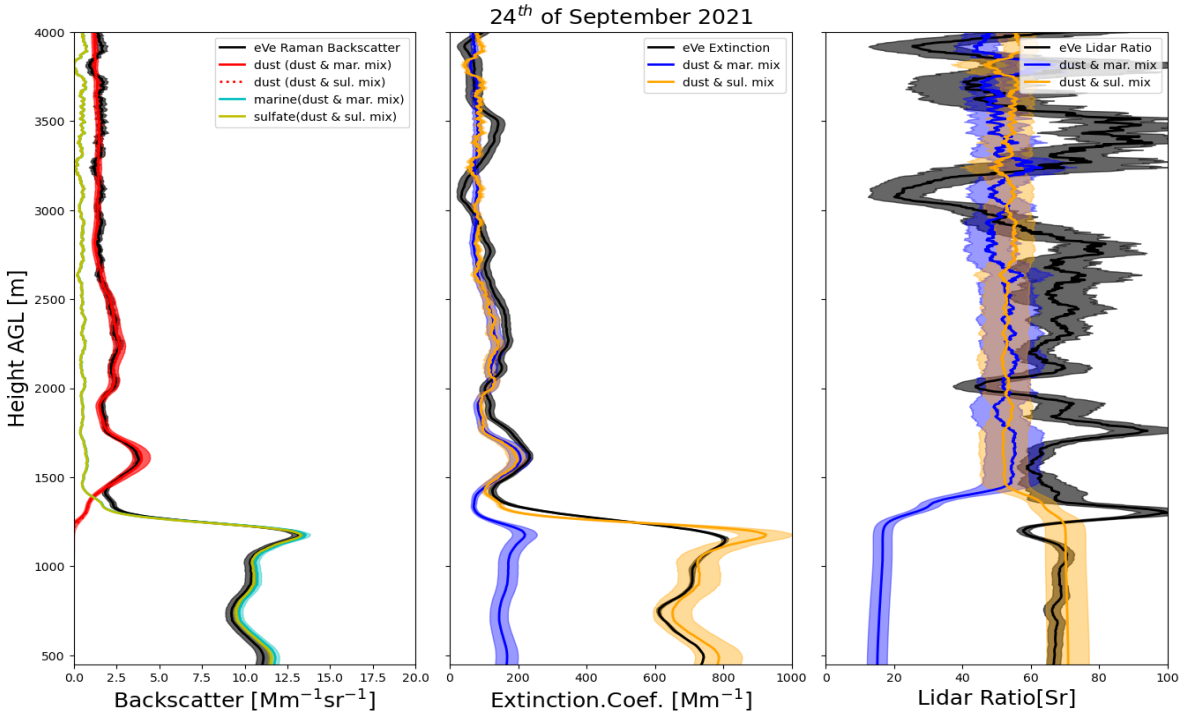

Figure 25: Comparison of the eVe Raman-derived profiles (black) with the EIEx profiles of backscatter coefficients, lidar ratio and extinction coefficient (red, blue and orange) for the 24 September 2021 considering different aerosol mixtures (dust/marine and dust/sulfate).

The comparison of the lidar ratio products shows a similar behavior, with the sulfate/dust combination performing better in the MBL. These mismatches could be due to layers of dust mixed with volcanic sulfate. It is important to mention that the selected lidar and depolarization ratio values from the literature for sulfate do not necessarily reflect the optical properties of pure sulfate. Indeed, Groß et al. (2012), in the process of volcanic aerosol detection during the Eyjafjallajökull eruption have found that the optical properties of pure volcanic sulphate are challenging to obtain. Especially in the marine conditions in which we currently operate, so

these values represent a mixture of sulphate and marine, although sulphate should still be predominant. Therefore, the average lidar ratio obtained from the Raman method within MBL is around 65-68 sr, which is slightly lower than the value of 70 sr assumed from the literature for this case but still within the range of uncertainty (± 10sr).

For the upper levels of the atmosphere, on average, the lidar ratio value from the Raman method is higher than that obtained by the EIEx method for any of the two mixtures. the EIEx method for any of the two mixtures, given the eruption at the time. Still, at these high levels, air mass was travelling from the Sahara region to Mindelo. Volcanic ash has the same optical properties as dust in terms of lidar ratio (63 ± 21 sr: (Lopes et al., 2019) and (Chouza et al.,2020)) but should be more depolarizing than dust (0.35 < Dp < 0.38, Ansmann et al., 2021; Groß et al., 2012). However, it is not possible here to perform a separation of three aerosol species using only the depolarization ratio and the backscatter coefficient, as mentioned in the methodology (section**3.4.3**).

4.3.2. Validation of EIEx with the PollyXT lidar retrievals

In this section, a brief evaluation of the results from the application of the EIEx methodology on PollyXT data is presented. Unfortunately, due to the lack of data, the uncertainties related to the PollyXT measurement will not be included. However, those related to the particle properties and the EIEx application will be discussed.

The application of EIEx based on the Raman products of PollyXT demonstrates a dependence of the optical properties according to the atmospheric layer. Figure 26 represents the quicklook of the volume depolarization ratio at 532 nm for the three cases chosen. For 10 September, the measurements were performed from 20:00 to 20:59 UTC (Fig.26-(a)). During this time frame, cloud contamination at around 1.7 km of altitude is observed. The timeframe considered for the second case (13 September) is from 19:55 to 20:51 UTC, with significant cloud contamination at 1 km and 1.5 km levels (Fig.26-(b)). The last case, whose retrieval time extends from 20:00 to 20:59 UTC, presents a cloudless sky (Fig.26-(c)). The aerosol layers identified by the volume depolarization ratios are similar to those highlighted by the eVe measurements, so we will not focus on them in this section. Therefore, it is inevitable that both eVe and PollyXT observe the same atmosphere during these selected periods.

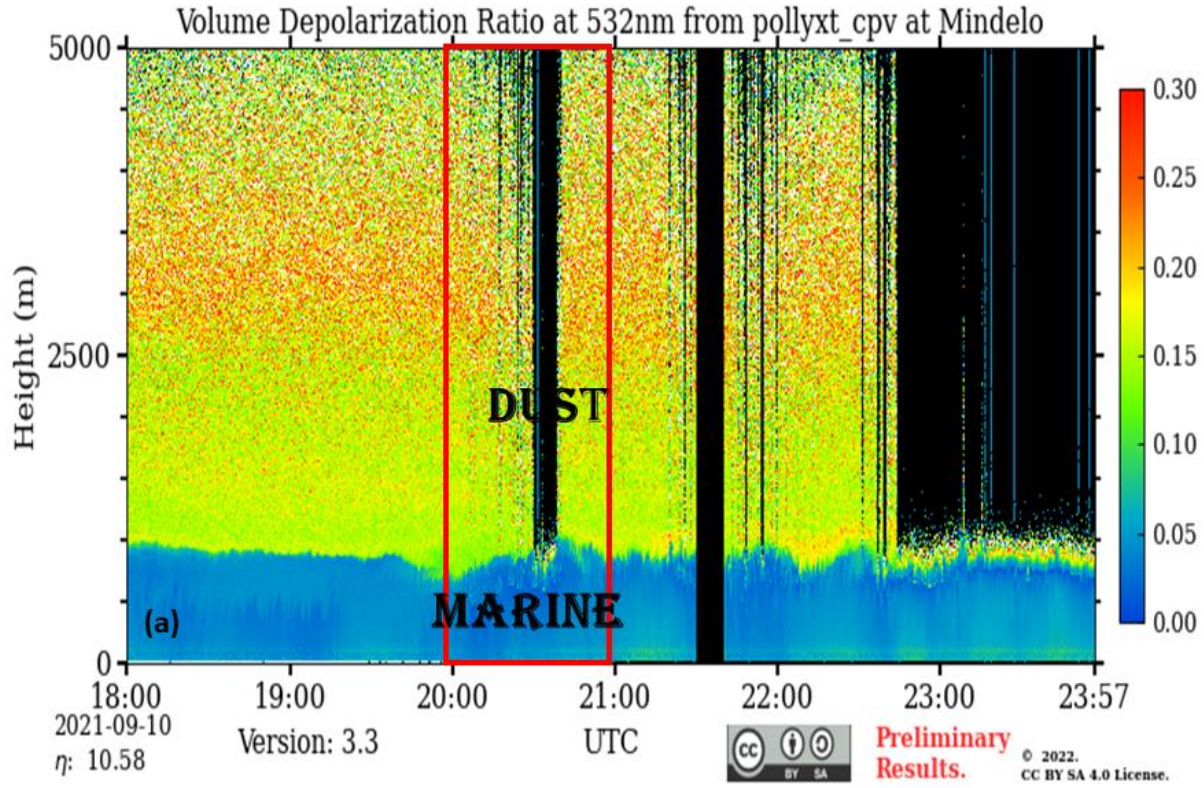
Volume Depolarization Ratio at 532nm from pollyxt_cpv at Mindelo
Height (m)
5000
2500
0
DUST
MARINE
(a)
18:00
19:00
20:00
21:00
22:00
23:00
23:57
2021-09-10
η: 10.58
Version: 3.3
UTC
0.30
0.25
0.20
0.15
0.10
0.05
0.00
Preliminary Results.
© 2022. CC BY SA 4.0 License.

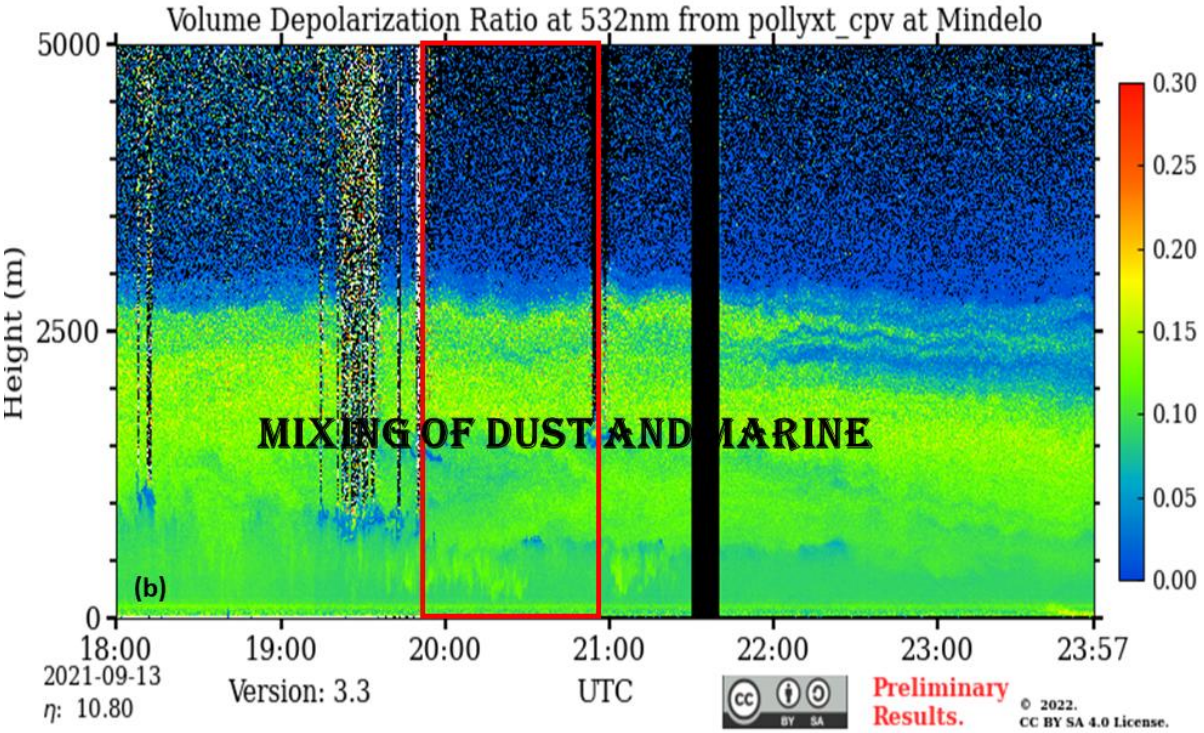
Volume Depolarization Ratio at 532nm from pollyxt_cpv at Mindelo
Height (m)
5000
2500
0
MIXING OF DUST AND MARINE
(b)
18:00
19:00
20:00
21:00
22:00
23:00
23:57
2021-09-13
η: 10.80
Version: 3.3
UTC
0.30
0.25
0.20
0.15
0.10
0.05
0.00
Preliminary Results.
© 2022. CC BY SA 4.0 License.

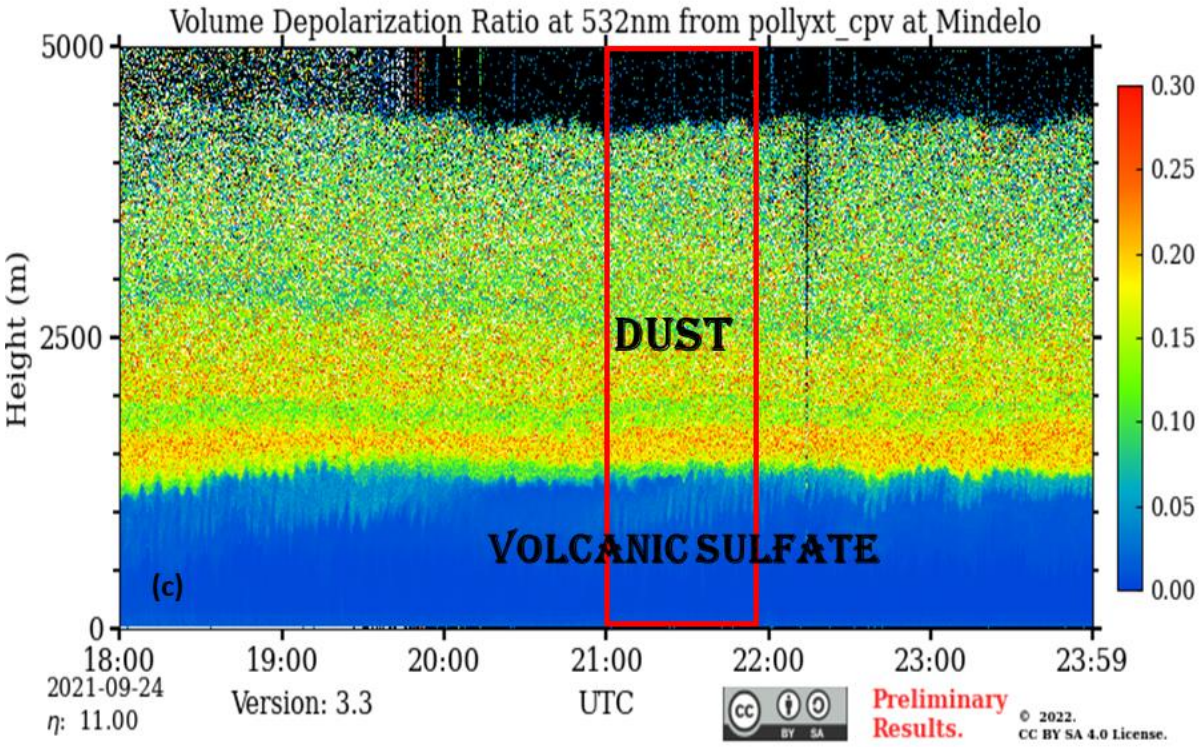

Figure 26: Aerosols volume depolarization ratio at 532 nm retrieved with PollyXT lidar system over Mindelo, Cabo Verde during ASKOS campaign, a) For 10 September 2021. (b) for 13 September 2021 and c) for 24 September 2021.

The results obtained from the application of the EIEx method on the pollyxt data to characterize the optical parameters of the particles reveal different scenarios. For the first case (10 September 2021), the extinction coefficient profiles (Fig.27-(a)) from the dust/marine and dust/pollution combinations show a good agreement with the PollyXT extinction profile in the higher free troposphere (above 1.5 km). Nevertheless, the dust/marine mixture performed better. However, the analysis within the MBL shows a difference between the PollyXT profile and the two extinction profiles obtained from the EIEx method, especially regarding the mixture of dust/pollution. The values found by the PollyXT retrieval in this part of the atmosphere are much lower than those obtained from the estimated EIEx products. The lidar ratio profiles showed a good agreement between the PollyXT profile and the dust-marine mixture profiles in the free troposphere, with values between 38 sr-50 sr in the aerosol layer. But a considerable decrease is observed in the MBL, with an average of 15 sr for PollyXT lidar ratio and 20 sr for the dust-marine profile. The results obtained above 1.5 km can be related to the presence of a relatively homogeneous layer of dust, despite the lidar ratio having lower values than those usually attributed to Saharan dust.

The second case included here, also shows a good agreement between the PollyXT and the dust-marine mixture profiles (Fig.26-(b)) for both optical properties, extinction profile and lidar ratio. The lidar ratio is typical for marine/dust mixtures between 28-32sr.

Figure 27-(c) shows the last study case, 24 September, which indicates a good agreement between PollyXT profiles and the one from the dust-marine and dust-sulfate mixtures for both extinction coefficients and lidar ratio in the aerosol layer higher than (<1.5 km). The mean value of the lidar ratio provided by PollyXT is estimated to be 60±10 sr which is well within the range of values considered in the literature (Groß et al., 2011). However, we notice a mismatch of the profiles in the MBL. We also noted that the PollyXT profiles are located between the two profiles resulting from the application of the EIEx method (for extinction and lidar ratio). The products of the dust-marine mixture are lower than the PollyXT, while the dust-sulfate mixture shows higher values.

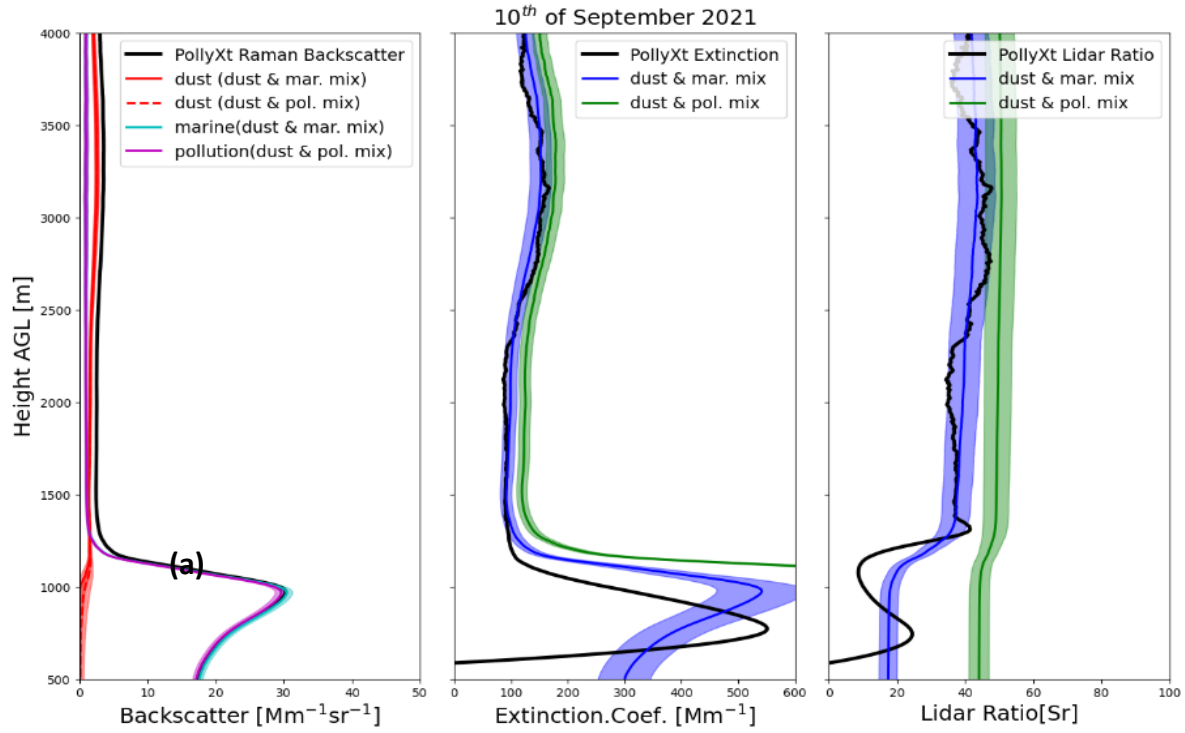

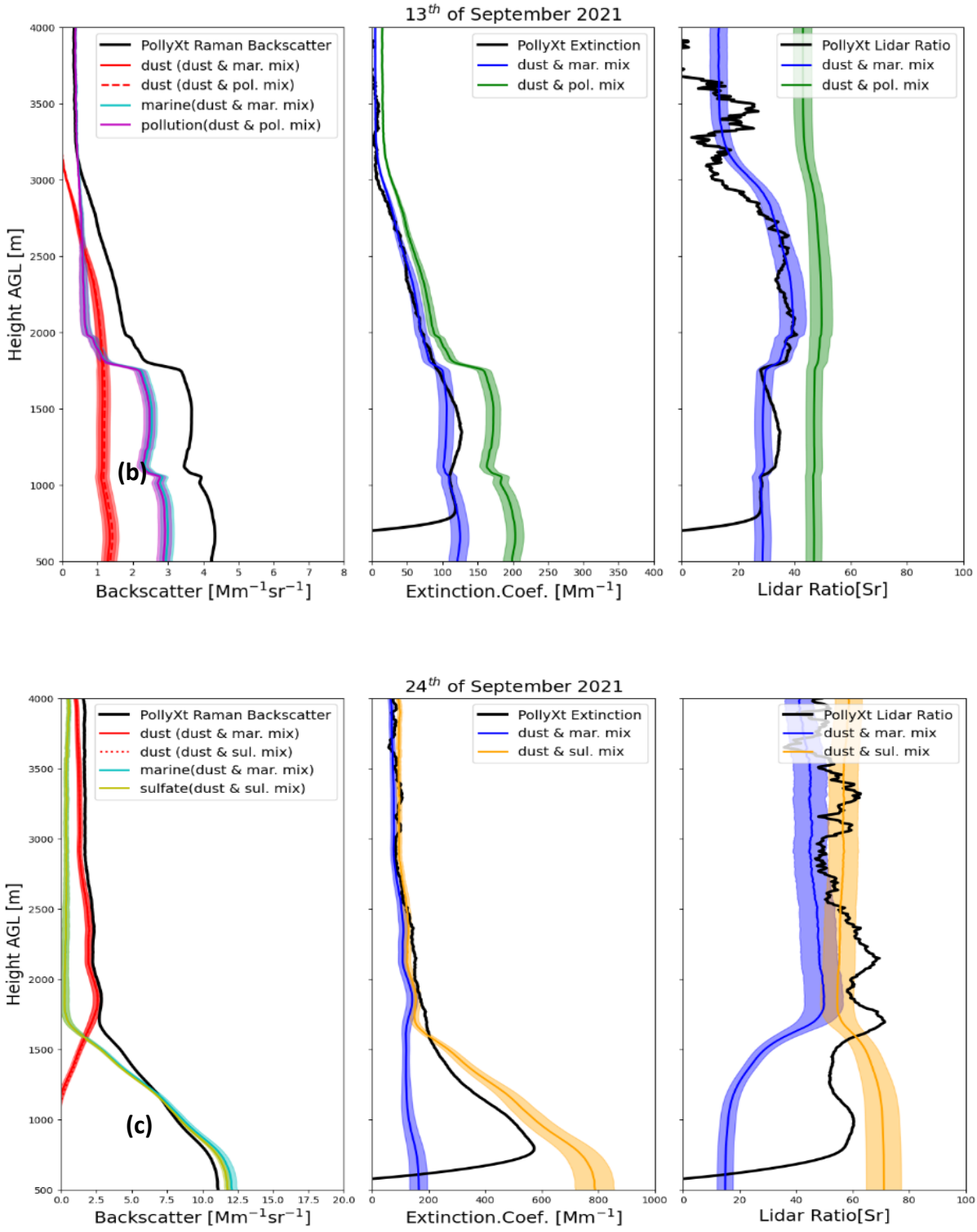

Figure 27: Comparison of the PollyXT Raman-derived products (black) with the EIEx backscatter coefficients, extinction coefficient and lidar ratio profiles: (a) For the 10th September 2021, (b) for the 13th September and (c) for the 24th September 2021.

For all three cases considered, between the PollyXT profiles and the EIEx method profiles, there is a good agreement for the free troposphere, even if the lidar ratio indicates lower values than those observed previously in the eVe case. Nevertheless, the validation of the

method is problematic in the MBL (<1.5 km), where we find several inconsistencies when comparing the profiles. This situation can be explained by different factors impacting the PollyXT data. The most influential aspect is the problem of overlap between the near and the far range. Indeed, the data used is derived from the far range, which is reliable at around 900 m, so products collected below 900 m should not be trusted as a reference for this type of investigation. Also, the possible contamination of the data by low clouds is not a negligible aspect.

5. Conclusion and recommendation

Saharan dust plumes transported toward the Atlantic Ocean represent one of the most important aerosol systems on Earth. Cabo Verde islands are in a unique position to study dust aerosols, their interaction and mixture with marine and other aerosol types. Hence, this study searched to analyze the variability of column-integrated and lidars profiles of aerosol optical properties over São Vicente Island, Cabo Verde, during the first stage of ASKOS campaign, which occurred from July to September of 2021. Additionally, the eVe lidar system operation in the marine and dusty environment of Cabo Verde provides a singular opportunity to apply and evaluate the method ElEx (elastic extinction). Method recently developed, targeting the estimation of aerosols extinction coefficient profiles using only the information provided by the elastic and polarization channels of conventional lidar systems (Giannakaki et al., 2020).

The analyzed column-integrated aerosol optical properties, namely Aerosol Optical Depth (AOD), Angstrom Exponent (AE), Lidar ratio (Lr) and particle Depolarization ratio (Dp) revealed distinct scenarios of aerosols over São Vicente, in terms of both loading and intrinsic properties, suggesting the presence of a variety of aerosols mixture states. AOD showed strong intrusions of dust plumes over the island during ASKOS, with AOD at 500 nm reaching values up to two, alternating with relatively clean marine scenarios when AOD at 500 nm was below 0.2. Low values of AE (< 0.6) were observed most of the time during the campaign period, indicating a dominance of air mass enriched with coarse mode particles. However, from the end of September, there was a significant increase in AE, revealing a shift in the aerosol size distribution over Cabo Verde, suggesting an enhancement of fine mode contribution, which coincided with the lowering in the frequency of high dust aerosol loadings events over São Vicente. Depolarization ratio also varied significantly throughout the campaign, from values typical of pure marine and pollution (< 5%) to values consistent with pure dust (>15%).

However, during the ASKOS experiment period, columnar depolarization ratio between 15 and 30% were dominant, indicating a long presence of dust aerosols mixed with marine particles over São Vicente. These observations based on the AERONET sunphotometer retrievals were corroborated by the analysis of volume depolarization ratio (VLDR) and range-corrected profiles from the eVe and PollyXT lidar systems, which provided the vertical structure of aerosols loading and optical properties and revealed distinct aerosol mixtures structures over São Vicente. From the lidars VLDR profiles, it was possible to identify well-mixed layers of dust being transported in the free troposphere, above a Marine Boundary Layer (MBL)

dominated by marine particles, but also scenarios with dust inside and above the MBL. Additionally, profiles scenarios indicating non-dust components mixed with marine aerosols were spotted over São Vicente during the ASKOS experiment. A particular case was the one related to the presence of volcanic aerosols plume from the Cumbre Vieja volcano eruption in La Palma, Canary.

Several of these described aerosol mixed scenarios provided the requirements to apply and evaluate the ElEx methods, from which 3 cases (10th, 13th and 24th of September 2021) were selected to perform this goal. Further analysis of the origin of air masses over Mindelo for the three selected cases, based on backward trajectories arriving at São Vicente at different altitudes and regional maps of AOD, helped to identify the type of aerosols defining the vertical structure and mixture over the island. For instance, for the 10th September case, the identification of the aerosol layers between 3 and 4 km over São Vicente as Saharan dust in the lidar profiles of Dp was corroborated by the AOD regional distribution from MERRA-2 and air masses trajectories arriving over the island. The back trajectories analysis revealed that in general, air masses flowing over São Vicente in the free troposphere during the campaign came from the Saharan regions and those circulating at low altitudes within MBL, mostly were from the Atlantic Ocean, mainly from areas northeast of Cabo Verde. This explained the presence of volcanic particles from the eruption of the Cumbre Vieja volcano of Las Palma, Canary, recorded in the MBL over São Vicente during the experiment.

Based on the assumptions supported by the previous analysis, with the application of the ElEx using eVe and PollyXT retrievals as inputs, we were able to evaluate the combination of aerosol type backscattering profiles and depolarization ratio to explain the aerosol mixture states observed over São Vicente for the selected case studies. While for the 10th September case, a well-defined structure consisting of dominance of dust above the MBL and marine particles in the MBL was identified, 13th of September presented a more complex vertical state of mixture, with a relevant contribution of dust and non-dust components across all layers. The 13th of September case required a distinct and more challenging combination of different pure aerosol species to explain the aerosol profiles over São Vicente. The last case study, 24th of September, also represented a complex scenario of aerosol vertical distribution over São Vicente and a challenge for the application of ElEx, mainly due to the presence of an unusual aerosol type, which was volcanic aerosols, combined with dust and marine particles. This led to a complicated aerosol mixture, especially inside and on MBL top, where the volcanic plume was transported

toward Cabo Verde. Nevertheless, for all the three cases, lidar ratio and extinction coefficient profiles were derived from the EIEx.

The validation of both lidar ratio and extinction coefficient profiles derived from the EIEx against the eVe and PollyXT Raman retrievals showed that the method, in general provides valuable and consistent results. This conclusion indicated that the assumptions regarding the aerosol's types over Mindelo and the assumed pure aerosols lidar ratio and depolarization ratio, including their respective uncertainty, proved to be reasonable. The support for this conclusion is the general consistency observed between the extinction coefficient profiles estimated using the EIEx method and the reference retrievals based on both Raman lidar: eVe and PollyXT. Especially in the layers not affected by the overlap issue and those with larger aerosol loading.

However, limitations also have to be mentioned, especially when the method has to deal with two or several aerosols' species either with a high (dust, ash) or with low depolarization ratio (marine, pollution). Also, across the transition layer between MBL and free troposphere, the EIEx extinction coefficients presented important deviations compared with the eVe profile. These are some reasons why more investigation on the ElEx application needs to be done. Extending the ElEx application to longer term measurements could make it possible to identify seasonal differences in the aerosol mixture conditions in the region around São Vicente. And provide a more conclusive evaluation on the method performance, in periods where a mixture of dust and smoke might be expected. In this sense, extending the ElEx evaluation including comparison to the AERONET sun photometer retrievals is also recommended.

Regarding the further application of the ElEx results, the aerosol mass concentration profiles could be derived, which are important to evaluate aerosol sources contributions to the air pollution issue and also to evaluate climate model prediction of aerosol mass profiles.

6. Reference

Ackerman, A. S., Toon, O. B., Stevens, D. E., Heymsfield, A. J., Ramanathan, V., & Welton, E. J. (2000). Reduction of Tropical Cloudiness by Soot. *Science*, *288*(5468), 1042–1047. https://doi.org/10.1126/SCIENCE.288.5468.1042

Adesina, J. A., Piketh, S. J., Formenti, P., Maggs-Kölling, G., Holben, B. N., & Sorokin, M. G. (2019). Aerosol optical properties and direct radiative effect over Gobabeb, Namibia. *Clean Air Journal*, *29*(2), 1–11. https://doi.org/10.17159/CAJ/2019/29/2.7518

Alam, K., Trautmann, T., Blaschke, T., & Majid, H. (2012). Aerosol optical and radiative properties during summer and winter seasons over Lahore and Karachi. *Atmospheric Environment*, *50*, 234–245. https://doi.org/10.1016/J.ATMOSENV.2011.12.027

Althausen, D., Engelmann, R., Baars, H., Heese, B., Ansmann, A., Müller, D., & Komppula, M. (2009). Portable Raman Lidar PollyXT for Automated Profiling of Aerosol Backscatter, Extinction, and Depolarization. *Journal of Atmospheric and Oceanic Technology*, *26*(11), 2366–2378. https://doi.org/10.1175/2009JTECHA1304.1

Ansmann, A., Ohneiser, K., Chudnovsky, A., Baars, H., & Engelmann, R. (2021). CALIPSO Aerosol-Typing Scheme Misclassified Stratospheric Fire Smoke: Case Study From the 2019 Siberian Wildfire Season. *Frontiers in Environmental Science*, *9*. https://doi.org/10.3389/fenvs.2021.769852

Ansmann, A., Riebesell, M., Wandinger, U., Weitkamp, C., Voss, E., Lahmann, W., & Michaelis, W. (1992). Combined raman elastic-backscatter LIDAR for vertical profiling of moisture, aerosol extinction, backscatter, and LIDAR ratio. *Applied Physics B 1992 55:1*, *55*(1), 18–28. https://doi.org/10.1007/BF00348608

Ansmann, A., Wagner, F., Müller, D., Althausen, D., Herber, A., Von Hoyningen-Huene, W., & Wandinger, U. (2002). European pollution outbreaks during ACE 2: Optical particle properties inferred from multiwavelength lidar and star-Sun photometry. *Journal of Geophysical Research: Atmospheres*, *107*(D15), AAC 8-1. https://doi.org/10.1029/2001JD001109

Baars, H., Ansmann, A., Althausen, D., Engelmann, R., Artaxo, P., Pauliquevis, T., & Souza, R. (2011). Further evidence for significant smoke transport from Africa to Amazonia. *Geophysical Research Letters*, *38*(20). https://doi.org/10.1029/2011GL049200

Baars, H., Kanitz, T., Engelmann, R., Althausen, D., Heese, B., Komppula, M., Preißler, J., Tesche, M., Ansmann, A., Wandinger, U., Lim, J. H., Young Ahn, J., Stachlewska, I. S., Amiridis, V., Marinou, E., Seifert, P., Hofer, J., Skupin, A., Schneider, F., … Zamorano, F. (2016). An overview of the first decade of PollyNET: An emerging network of automated Raman-polarization lidars for continuous aerosol profiling. *Atmospheric Chemistry and Physics*, *16*(8), 5111–5137. https://doi.org/10.5194/ACP-16-5111-2016

Baars, H., Seifert, P., Engelmann, R., & Wandinger, U. (2017). Target categorization of aerosol and clouds by continuous multiwavelength-polarization lidar measurements. *Atmospheric Measurement Techniques*, *10*(9), 3175–3201. https://doi.org/10.5194/AMT-10-3175-2017

Bates, B., Kundzewicz, Z., & Wu, S. (2008). *Climate change and water*. Intergovernmental

Panel on Climate Change Secretariat.

Bohlmann, S., Baars, H., Radenz, M., Engelmann, R., & Macke, A. (2018). Ship-borne aerosol profiling with lidar over the Atlantic Ocean: from pure marine conditions to complex dust–smoke mixtures. *Atmospheric Chemistry and Physics*, *18*(13), 9661-9679./

Bourgeois, Q., Ekman, A. M. L., & Krejci, R. (2015). Aerosol transport over the Andes from the Amazon Basin to the remote Pacific Ocean: A multiyear CALIOP assessment. *Journal of Geophysical Research: Atmospheres*, *120*(16), 8411–8425. https://doi.org/10.1002/2015JD023254

Brindley, H. E., & Ignatov, A. (2006). Retrieval of mineral aerosol optical depth and size information from Meteosat Second Generation SEVIRI solar reflectance bands. *Remote Sensing of Environment*, *102*(3–4), 344–363. https://doi.org/10.1016/J.RSE.2006.02.024

Bristow, C. S., Hudson-Edwards, K. A., & Chappell, A. (2010). Fertilizing the Amazon and equatorial Atlantic with West African dust. *Geophysical Research Letters*, *37*(14), n/a-n/a. https://doi.org/10.1029/2010GL043486

D'Auria, L., Koulakov, I., Prudencio, J., Cabrera-Perez, I., Ibanez, J., Martinez, J. B., ... & Rodriguez, N. P. (2022). Voluminous Storage and Rapid Magma Ascent Beneath La Palma Revealed by Seismic Tomography.

Chouza, F., Leblanc, T., Barnes, J., Brewer, M., Wang, P., & Koon, D. (2020). Long-term (1999–2019) variability of stratospheric aerosol over Mauna Loa, Hawaii, as seen by two co-located lidars and satellite measurements. *Atmospheric Chemistry and Physics*, *20*(11), 6821-6839.

Kaduk, C. (2017). Characterization of the optical properties of complex aerosol mixtures observed with a multiwavelength–Raman–polarization lidar during the 6–weeks BACCHUS campaign in Cyprus in spring 2015.

Diarra, C., & Ba, A. (2014). Analyse des paramètres optiques des aérosols atmosphériques, de leur distribution et de leur albédo de diffusion par les mesures photométriques au Mali. *Afrique Science: Revue Internationale Des Sciences et Technologie*, *10*(2). https://doi.org/10.4314/afsci.v10i2.

Diner, D. J., Beckert, J. C., Reilly, T. H., Bruegge, C. J., Conel, J. E., Kahn, R. A., Martonchik, J. V., Ackerman, T. P., Davies, R., Gerstl, S. A. W., Gordon, H. R., Muller, J. P., Myneni, R. B., Sellers, P. J., Pinty, B., & Verstraete, M. M. (1998). Multi-angle imaging spectroradiometer (MISR) instrument description and experiment overview. *IEEE Transactions on Geoscience and Remote Sensing*, *36*(4), 1072–1087. https://doi.org/10.1109/36.700992

Dubovik, O., Holben, B., Eck, T. F., Smirnov, A., Kaufman, Y. J., King, M. D., Tanré, D., & Slutsker, I. (2002). Variability of Absorption and Optical Properties of Key Aerosol Types Observed in Worldwide Locations. *Journal of the Atmospheric Sciences*, *59*(3), 590–608. https://doi.org/10.1175/1520-0469(2002)059<0590:VOAAOP>2.0.CO;2

Dubovik, O., & King, M. D. (2000). A flexible inversion algorithm for retrieval of aerosol optical properties from Sun and sky radiance measurements. *Journal of Geophysical Research: Atmospheres*, *105*(D16), 20673–20696. https://doi.org/10.1029/2000JD900282

Dunion, J. P., & Velden, C. S. (2004). The Impact of the Saharan Air Layer on Atlantic Tropical Cyclone Activity. *Bulletin of the American Meteorological Society*, *85*(3), 353–366. https://doi.org/10.1175/BAMS-85-3-353

Fomba, K. W., Müller, K., Van Pinxteren, D., Poulain, L., Van Pinxteren, M., & Herrmann, H. (2014). Long-term chemical characterization of tropical and marine aerosols at the Cape Verde Atmospheric Observatory (CVAO) from 2007 to 2011. *Atmospheric Chemistry and Physics*, *14*(17), 8883–8904. https://doi.org/10.5194/ACP-14-8883-2014

Freudenthaler, V., Esselborn, M., Wiegner, M., Heese, B., Tesche, M., Ansmann, A., ... & Seefeldner, M. (2009). Depolarization ratio profiling at several wavelengths in pure Saharan dust during SAMUM 2006. *Tellus B: Chemical and Physical Meteorology*, *61*(1), 165-179.

Gama, C., Tchepel, O., Baldasano, J. M., Basart, S., Ferreira, J., Pio, C., ... & Borrego, C. (2015). Seasonal patterns of Saharan dust over Cape Verde–a combined approach using observations and modelling. *Tellus B: Chemical and Physical Meteorology*, *67*(1), 24410.

Giannakaki, E., Kokkalis, P., Marinou, E., Solomos, S., Amiridis, V., Ansmann, A., Bartsotas, N., Engelmann, R., and Komppula, M.: Extinction profile retrieval at Finokalia, Crete, in the proceedings of 28th International Laser and Lidar Conference, Bucharest, Romania, 2017.

Giannakaki, E., Balis, D. S., Amiridis, V., & Zerefos, C. (2010). Optical properties of different aerosol types: seven years of combined Raman-elastic backscatter lidar measurements in Thessaloniki, Greece. *Atmospheric Measurement Techniques*, *3*(3), 569–578. https://doi.org/10.5194/amt-3-569-2010

Giannakaki, E., Kokkalis, P., Marinou, E., Bartsotas, N. S., Amiridis, V., Ansmann, A., & Komppula, M. (2020). The potential of elastic and polarization lidars to retrieve extinction profiles. *Atmospheric Measurement Techniques*, *13*(2), 893–905. https://doi.org/10.5194/AMT-13-893-2020

Groß, S., Freudenthaler, V., Schepanski, K., Toledano, C., Schäfler, A., Ansmann, A., & Weinzierl, B. (2015). Optical properties of long-range transported Saharan dust over Barbados as measured by dual-wavelength depolarization Raman lidar measurements. *Atmospheric Chemistry and Physics*, *15*(19), 11067–11080. https://doi.org/10.5194/ACP-15-11067-2015

Gross, S., Freudenthaler, V., Wiegner, M., Gasteiger, J., Geiss, A., & Schnell, F. (2012). Dual-wavelength linear depolarization ratio of volcanic aerosols: Lidar measurements of the Eyjafjallajökull plume over Maisach, Germany. *Atmospheric Environment*, *48*, 85-96.

Groß, S., Gasteiger, J., Freudenthaler, V., Wiegner, M., Geiß, A., Schladitz, A., Toledano, C., Kandler, K., Tesche, M., Ansmann, A., & Wiedensohler, A. (2011). Characterization of the planetary boundary layer during SAMUM-2 by means of lidar measurements. *Tellus B: Chemical and Physical Meteorology*, *63*(4), 695–705. https://doi.org/10.1111/j.1600-0889.2011.00557.x

Guo, J., Liu, H., Wang, F., Huang, J., Xia, F., Lou, M., ... & Yung, Y. L. (2016). Three-dimensional structure of aerosol in China: A perspective from multi-satellite observations. *Atmospheric Research*, *178*, 580-589.

Haarig, M., Ansmann, A., Gasteiger, J., Kandler, K., Althausen, D., Baars, H., ... & Farrell, D. A. (2017). Dry versus wet marine particle optical properties: RH dependence of depolarization ratio, backscatter, and extinction from multiwavelength lidar measurements during SALTRACE. *Atmospheric Chemistry and Physics*, *17*(23), 14199-14217.

Haywood, J. M., Johnson, B. T., Osborne, S. R., Baran, A. J., Brooks, M., Milton, S. F., Mulcahy, J., Walters, D., Allan, R. P., Klaver, A., Formenti, P., Brindley, H. E., Christopher, S., & Gupta, P. (2011). Motivation, rationale and key results from the GERBILS Saharan dust measurement campaign. *Quarterly Journal of the Royal Meteorological Society*, *137*(658), 1106–1116. https://doi.org/10.1002/QJ.797

Haywood, J. M., Pelon, J., Formenti, P., Bharmal, N. A., Brooks, M. E., Capes, G., Chazette, P., Chou, C., Christopher, S. A., Coe, H., Cuesta, J., Derimian, Y., Desboeufs, K., Greed, G., Harrison, M., Heese, B., Highwood, E. J., Johnson, B., Mallet, M., … Tulet, P. (2008). Overview of the Dust and Biomass-burning Experiment and African Monsoon Multidisciplinary Analysis Special Observing Period-0. *Journal of Geophysical Research: Atmospheres*, *113*(D23), 0–17. https://doi.org/10.1029/2008JD010077

Holben, B. N., Eck, T. F., Slutsker, I., Tanré, D., Buis, J. P., Setzer, A., Vermote, E., Reagan, J. A., Kaufman, Y. J., Nakajima, T., Lavenu, F., Jankowiak, I., & Smirnov, A. (1998). AERONET—A Federated Instrument Network and Data Archive for Aerosol Characterization. *Remote Sensing of Environment*, *66*(1), 1–16. https://doi.org/10.1016/S0034-4257(98)00031-5

Hsu, N. C., Tsay, S. C., King, M. D., & Herman, J. R. (2004). Aerosol properties over bright-reflecting source regions. *IEEE transactions on geoscience and remote sensing*, *42*(3), 557-569.

Hu, Y., Winker, D., Vaughan, M., Lin, B., Omar, A., Trepte, C., ... & Kuehn, R. (2009). CALIPSO/CALIOP cloud phase discrimination algorithm. *Journal of Atmospheric and Oceanic Technology*, *26*(11), 2293-2309.

Huang, J., Minnis, P., Chen, B., Huang, Z., Liu, Z., Zhao, Q., Yi, Y., Ayers, J. K., Huang, C. :, Minnis, P., Chen, B., Huang, Z., Liu, Z., Zhao, Q., Yi, Y., & Ayers, J. K. (2008). Long-range transport and vertical structure of Asian dust from CALIPSO and surface measurements during PACDEX. *Journal of Geophysical Research: Atmospheres*, *113*(D23), 23212. https://doi.org/10.1029/2008JD010620

Huneeus, N., & Boucher, O. (2007). One-dimensional variational retrieval of aerosol extinction coefficient from synthetic LIDAR and radiometric measurements. *Journal of Geophysical Research: Atmospheres*, *112*(D14), 14303. https://doi.org/10.1029/2006JD007625

Illingworth, A. J., Barker, H. W., Beljaars, A., Ceccaldi, M., Chepfer, H., Clerbaux, N., Cole, J., Delanoë, J., Domenech, C., Donovan, D. P., Fukuda, S., Hirakata, M., Hogan, R. J., Huenerbein, A., Kollias, P., Kubota, T., Nakajima, T., Nakajima, T. Y., Nishizawa, T., … Van Zadelhoff, G. J. (2015). The earthcare satellite: The next step forward in global measurements of clouds, aerosols, precipitation, and radiation. *Bulletin of the American Meteorological Society*, *96*(8), 1311–1332. https://doi.org/10.1175/BAMS-D-12-00227.1

Kambezidis, H. D., & Kaskaoutis, D. G. (2008). Aerosol climatology over four AERONET sites: An overview. *Atmospheric Environment*, *42*(8), 1892–1906.

https://doi.org/10.1016/J.ATMOSENV.2007.11.013

Kanitz, T., Ansmann, A., Engelmann, R., & Althausen, D. (2013). North-south cross sections of the vertical aerosol distribution over the Atlantic Ocean from multiwavelength Raman/polarization lidar during Polarstern cruises. *Journal of Geophysical Research: Atmospheres*, *118*(6), 2643-2655.

Kanitz, T., Seifert, P., Ansmann, A., Engelmann, R., Althausen, D., Casiccia, C., & Rohwer, E. G. (2011). Contrasting the impact of aerosols at northern and southern midlatitudes on heterogeneous ice formation. *Geophysical Research Letters*, *38*(17).

Kaufman, Y. J., Tanré, D., & Boucher, O. (2002). A satellite view of aerosols in the climate system. *Nature*, *419*(6903), 215–223. https://doi.org/10.1038/nature01091

Klett, J. D. (1981). Stable analytical inversion solution for processing lidar returns. *Applied Optics, Vol. 20, Issue 2, Pp. 211-220*, *20*(2), 211–220. https://doi.org/10.1364/AO.20.000211

Klüser, L., & Holzer-Popp, T. (2010). Relationships between mineral dust and cloud properties in the West African Sahel. *Atmospheric Chemistry and Physics*, *10*(14), 6901–6915. https://doi.org/10.5194/ACP-10-6901-2010

Knippertz, P., & Todd, M. C. (2012). Mineral dust aerosols over the Sahara: Meteorological controls on emission and transport and implications for modeling. *Reviews of Geophysics*, *50*(1). https://doi.org/10.1029/2011RG000362

Koren, I., Kaufman, Y. J., Remer, L. A., & Martins, J. V. (2004). Measurement of the Effect of Amazon Smoke on Inhibition of Cloud Formation. *Science*, *303*(5662), 1342–1345. https://doi.org/10.1126/SCIENCE.1089424/SUPPL_FILE/KOREN.SOM.PDF

Koren, I., Kaufman, Y. J., Washington, R., Todd, M. C., Rudich, Y., Martins, J. V., & Rosenfeld, D. (2006). The Bodélé depression: a single spot in the Sahara that provides most of the mineral dust tothe Amazon forest. *Environmental Research Letters*, *1*(1), 014005. https://doi.org/10.1088/1748-9326/1/1/014005

Krinner, G., Boucher, O., & Balkanski, Y. (2006). Ice-free glacial northern Asia due to dust deposition on snow. *Climate Dynamics*, *27*(6), 613–625. https://doi.org/10.1007/s00382-006-0159-z

Lambert, F., Delmonte, B., Petit, J. R., Bigler, M., Kaufmann, P. R., Hutterli, M. A., Stocker, T. F., Ruth, U., Steffensen, J. P., & Maggi, V. (2008). Dust-climate couplings over the past 800,000 years from the EPICA Dome C ice core. *Nature*, *452*(7187), 616–619. https://doi.org/10.1038/nature06763

Léon, J. F., Tanré, D., Pelon, J., Kaufman, Y. J., Haywood, J. M., & Chatenet, B. (2003). Profiling of a Saharan dust outbreak based on a synergy between active and passive remote sensing. *Journal of Geophysical Research: Atmospheres*, *108*(D18). https://doi.org/10.1029/2002JD002774

Liu, D., Zhao, T., Boiyo, R., Chen, S., Lu, Z., Wu, Y., & Zhao, Y. (2019). Vertical Structures of Dust Aerosols over East Asia Based on CALIPSO Retrievals. *Remote Sensing 2019, Vol. 11, Page 701*, *11*(6), 701. https://doi.org/10.3390/RS11060701

Lopes, F., Silva, J., Marrero, J., Taha, G., & Landulfo, E. (2019). Synergetic Aerosol Layer Observation After the 2015 Calbuco Volcanic Eruption Event. *Remote Sensing*, *11*(2), 195. https://doi.org/10.3390/rs11020195

Mamouri, R. E., & Ansmann, A. (2017). Potential of polarization/Raman lidar to separate fine dust, coarse dust, maritime, and anthropogenic aerosol profiles. *Atmospheric Measurement Techniques*, *10*(9), 3403–3427. https://doi.org/10.5194/AMT-10-3403-2017

Marais, E., & Chance, K. (2015). A Geostationary Air Quality Monitoring Platform for Africa. *Clean Air Journal*, *25*(1). https://doi.org/10.17159/2410-972X/2015/V25N1A3

Meningococcal Meningitis. (n.d.). Retrieved July 8, 2022, from https://www.who.int/teams/health-product-policy-and-standards/standards-and-specifications/vaccine-standardization/meningococcal-meningitis

Milford, C., Cuevas, E., Marrero, C. L., Bustos, J. J., Gallo, V., Rodríguez, S., Romero-Campos, P. M., & Torres, C. (2019). Impacts of Desert Dust Outbreaks on Air Quality in Urban Areas. *Atmosphere 2020, Vol. 11, Page 23*, *11*(1), 23. https://doi.org/10.3390/ATMOS11010023

Molero, F., Pujadas, M., & Artíñano, B. (2020). Study of the Effect of Aerosol Vertical Profile on Microphysical Properties Using GRASP Code with Sun/Sky Photometer and Multiwavelength Lidar Measurements. *Remote Sensing 2020, Vol. 12, Page 4072*, *12*(24), 4072. https://doi.org/10.3390/RS12244072

Mona, L., Liu, Z., Müller, D., Omar, A., Papayannis, A., Pappalardo, G., Sugimoto, N., & Vaughan, M. (2012). Lidar measurements for desert dust characterization: An overview. *Advances in Meteorology*, *2012*. https://doi.org/10.1155/2012/356265

Haarig, M., Ansmann, A., Althausen, D., Klepel, A., Groß, S., Freudenthaler, V., ... & Baars, H. (2017). Triple-wavelength depolarization-ratio profiling of Saharan dust over Barbados during SALTRACE in 2013 and 2014. *Atmospheric Chemistry and Physics*, *17*(17), 10767-10794. Moutin, T., Thingstad, T. F., Van Wambeke, F., Marie, D., Slawyk, G., Raimbault, P., & Claustre, H. (2002). Does competition for nanomolar phosphate supply explain the predominance of the cyanobacterium Synechococcus? *Limnology and Oceanography*, *47*(5), 1562–1567. https://doi.org/10.4319/LO.2002.47.5.1562

Müller, D., Ansmann, A., Mattis, I., Tesche, M., Wandinger, U., Althausen, D., & Pisani, G. (2007). Aerosol-type-dependent lidar ratios observed with Raman lidar. *Journal of Geophysical Research Atmospheres*, *112*(16). https://doi.org/10.1029/2006JD008292

Murayama, T., Sugimoto, N., Uno, I., Kinoshita, K., Aoki, K., Hagiwara, N., Liu, Z., Matsui, I., Sakai, T., Shibata, T., Arao, K., Sohn, B. J., Won, J. G., Yoon, S. C., Li, T., Zhou, J., Hu, H., Abo, M., Iokibe, K., … Iwasaka, Y. (2001). Ground-based network observation of Asian dust events of April 1998 in east Asia. *Journal of Geophysical Research: Atmospheres*, *106*(D16), 18345–18359. https://doi.org/10.1029/2000JD900554

Naeger, A. R., Gupta, P., Zavodsky, B. T., & McGrath, K. M. (2016). Monitoring and tracking the trans-Pacific transport of aerosols using multi-satellite aerosol optical depth composites. *Atmospheric Measurement Techniques*, *9*(6), 2463–2482. https://doi.org/10.5194/AMT-9-2463-2016

NASA Study Predicts Less Saharan Dust in Future Winds | NASA. (n.d.). Retrieved July 7, 2022, from https://www.nasa.gov/feature/esnt/2021/nasa-study-predicts-less-saharan-dust-in-future-winds

Nishizawa, T., Okamoto, H., Sugimoto, N., Matsui, I., Shimizu, A., & Aoki, K. (2007). An algorithm that retrieves aerosol properties from dual-wavelength polarized lidar measurements. *Journal of Geophysical Research: Atmospheres*, *112*(D6), 6212. https://doi.org/10.1029/2006JD007435

Sima, A., Rousseau, D., Kageyama, M., Ramstein, G., Schulz, M., Balkanski, Y., ... & Hatté, C. (2008, December). North-Atlantic millennial-timescale variability imprint on Western European loess deposits: a modeling study. In *AGU Fall Meeting Abstracts* (Vol. 2008, pp. PP12A-07).

Paschou, P., Siomos, N., Tsekeri, A., Louridas, A., Georgoussis, G., Freudenthaler, V., Binietoglou, I., Tsaknakis, G., Tavernarakis, A., Evangelatos, C., Von Bismarck, J., Kanitz, T., Meleti, C., Marinou, E., & Amiridis, V. (2022). The eVe reference polarisation lidar system for the calibration and validation of the Aeolus L2A product. *Atmospheric Measurement Techniques*, *15*(7), 2299–2323. https://doi.org/10.5194/AMT-15-2299-2022

Pio, C. A., Cardoso, J. G., Cerqueira, M. A., Calvo, A., Nunes, T. V., Alves, C. A., Custódio, D., Almeida, S. M., & Almeida-Silva, M. (2014). Seasonal variability of aerosol concentration and size distribution in cape verde using a continuous aerosol optical spectrometer. *Frontiers in Environmental Science*, *2*(MAY), 15. https://doi.org/10.3389/FENVS.2014.00015/BIBTEX

Polymenakou, P. N., Mandalakis, M., Stephanou, E. G., & Tselepides, A. (2008). Particle Size Distribution of Airborne Microorganisms and Pathogens during an Intense African Dust Event in the Eastern Mediterranean. *Environmental Health Perspectives*, *116*(3), 292–296. https://doi.org/10.1289/EHP.10684

Pöschl, U., & Shiraiwa, M. (2015). Multiphase Chemistry at the Atmosphere-Biosphere Interface Influencing Climate and Public Health in the Anthropocene. *Chemical Reviews*, *115*(10), 4440–4475. https://doi.org/10.1021/CR500487S/ASSET/IMAGES/LARGE/CR-2014-00487S_0003.JPEG

Prata, A. T., Young, S. A., Siems, S. T., & Manton, M. J. (2017). Lidar ratios of stratospheric volcanic ash and sulfate aerosols retrieved from CALIOP measurements. *Atmospheric Chemistry and Physics*, *17*(13), 8599–8618. https://doi.org/10.5194/ACP-17-8599-2017

Prospero, J. M., Ginoux, P., Torres, O., Nicholson, S. E., & Gill, T. E. (2002). Environmental characterization of global sources of atmospheric soil dust identified with the Nimbus 7 Total Ozone Mapping Spectrometer (TOMS) absorbing aerosol product. *Reviews of geophysics*, *40*(1), 2-1.

Qiu, H., Zhong, J., & Dong, X. (2003, July). Land-use and land-cover changes and dust storms in Tarim Basin, northwest China. In *Ecosystems Dynamics, Ecosystem-Society Interactions, and Remote Sensing Applications for Semi-Arid and Arid Land* (Vol. 4890, pp. 652-656). SPIE.

Rajot, J. L., Formenti, P., Alfaro, S., Desboeufs, K., Chevaillier, S., Chatenet, B., Gaudichet, A., Journet, E., Marticorena, B., Triquet, S., Maman, A., Mouget, N., & Zakou, A. (2008).

AMMA dust experiment: An overview of measurements performed during the dry season special observation period (SOP0) at the Banizoumbou (Niger) supersite. *Journal of Geophysical Research: Atmospheres*, *113*(D23). https://doi.org/10.1029/2008JD009906

Ramanathan, V., Ramana, M. V., Roberts, G., Kim, D., Corrigan, C., Chung, C., & Winker, D. (2007). Warming trends in Asia amplified by brown cloud solar absorption. *Nature 2007 448:7153*, *448*(7153), 575–578. https://doi.org/10.1038/nature06019

Randles, C. A., da Silva, A. M., Buchard, V., Colarco, P. R., Darmenov, A., Govindaraju, R., Smirnov, A., Holben, B., Ferrare, R., Hair, J., Shinozuka, Y., & Flynn, C. J. (2017). The MERRA-2 Aerosol Reanalysis, 1980 Onward. Part I: System Description and Data Assimilation Evaluation. *Journal of Climate*, *30*(17), 6823–6850. https://doi.org/10.1175/JCLI-D-16-0609.1

Rizzolo, J. A., Barbosa, C. G. G., Borillo, G. C., Godoi, A. F. L., Souza, R. A. F., Andreoli, R. V., Manzi, A. O., Sá, M. O., Alves, E. G., Pöhlker, C., Angelis, I. H., Ditas, F., Saturno, J., Moran-Zuloaga, D., Rizzo, L. V., Rosário, N. E., Pauliquevis, T., Santos, R. M. N., Yamamoto, C. I., … Godoi, R. H. M. (2017). Soluble iron nutrients in Saharan dust over the central Amazon rainforest. *Atmospheric Chemistry and Physics*, *17*(4), 2673–2687. https://doi.org/10.5194/ACP-17-2673-2017

Rogers, R. R., Vaughan, M. A., Hostetler, C. A., Burton, S. P., Ferrare, R. A., Young, S. A., Hair, J. W., Obland, M. D., Harper, D. B., Cook, A. L., & Winker, D. M. (2014). Looking through the haze: Evaluating the CALIPSO level 2 aerosol optical depth using airborne high spectral resolution lidar data. *Atmospheric Measurement Techniques*, *7*(12), 4317–4340. https://doi.org/10.5194/AMT-7-4317-2014

Rosenfeld, D., Rudich, Y., & Lahav, R. (2001). Desert dust suppressing precipitation: A possible desertification feedback loop. *Proceedings of the National Academy of Sciences of the United States of America*, *98*(11), 5975–5980. https://doi.org/10.1073/PNAS.101122798

Roskovensky, J. K., & Liou, K. N. (2005). Differentiating airborne dust from cirrus clouds using MODIS data. *Geophysical Research Letters*, *32*(12), 1–5. https://doi.org/10.1029/2005GL022798

Sakai, T., Nagai, T., Zaizen, Y., & Mano, Y. (2010). Backscattering linear depolarization ratio measurements of mineral, sea-salt, and ammonium sulfate particles simulated in a laboratory chamber. *Applied optics*, *49*(23), 4441-4449.

Saltzman, E. S. (2009). Marine Aerosols. *Geophysical Monograph Series*, *187*, 17–35. https://doi.org/10.1029/2008GM000769

Seifert, P. (2010). *Dust-related ice formation in the troposphere: A statistical analysis based on 11 years of lidar observations of aerosols and clouds over Leipzig* (Doctoral dissertation, Universität Leipzig).

Shimizu, A., Sugimoto, N., Matsui, I., Arao, K., Uno, I., Murayama, T., Kagawa, N., Aoki, K., Uchiyama, A., Yamazaki, A., Shimizu, C. :, Sugimoto, N., Matsui, I., Arao, K., Uno, I., Murayama, T., Kagawa, N., Aoki, K., Uchiyama, A., & Yamazaki, A. (2004). Continuous observations of Asian dust and other aerosols by polarization lidars in China and Japan during ACE-Asia. *Journal of Geophysical Research: Atmospheres*, *109*(D19), 19–36.

https://doi.org/10.1029/2002JD003253

Shin, H. C., Tenenholtz, N. A., Rogers, J. K., Schwarz, C. G., Senjem, M. L., Gunter, J. L., Andriole, K. P., & Michalski, M. (2018). Medical image synthesis for data augmentation and anonymization using generative adversarial networks. *Lecture Notes in Computer Science (Including Subseries Lecture Notes in Artificial Intelligence and Lecture Notes in Bioinformatics)*, *11037 LNCS*, 1–11. https://doi.org/10.1007/978-3-030-00536-8_1/COVER/

Stocker, T. F., Qin, D., Plattner, G. K., Tignor, M. M. B., Allen, S. K., Boschung, J., Nauels, A., Xia, Y., Bex, V., & Midgley, P. M. (2013). Climate change 2013 the physical science basis: Working Group I contribution to the fifth assessment report of the intergovernmental panel on climate change. *Climate Change 2013 the Physical Science Basis: Working Group I Contribution to the Fifth Assessment Report of the Intergovernmental Panel on Climate Change*, *9781107057999*, 1–1535. https://doi.org/10.1017/CBO9781107415324

Sugimoto, N., & Lee, C. H. (2006). Characteristics of dust aerosols inferred from lidar depolarization measurements at two wavelengths. *Applied Optics, Vol. 45, Issue 28, Pp. 7468-7474*, *45*(28), 7468–7474. https://doi.org/10.1364/AO.45.007468

Sugimoto, N., Uno, I., Nishikawa, M., Shimizu, A., Matsui, I., Dong, X., Chen, Y., & Quan, H. (2003). Record heavy Asian dust in Beijing in 2002: Observations and model analysis of recent events. *Geophysical Research Letters*, *30*(12). https://doi.org/10.1029/2002GL016349

Swap, R., Garstang, M., Greco, S., Talbot, R., & Kållberg, P. (1992). Saharan dust in the Amazon Basin. *Tellus B*, *44*(2), 133-149.

Tan, D. G., Andersson, E., Kloe, J. D., Marseille, G. J., Stoffelen, A., Poli, P., ... & Nett, H. (2008). The ADM-Aeolus wind retrieval algorithms. *Tellus A: Dynamic Meteorology and Oceanography*, *60*(2), 191-205.

Tesche, M., Ansmann, A., Müller, D., Althausen, D., Engelmann, R., Freudenthaler, V., & Groß, S. (2009). Vertically resolved separation of dust and smoke over Cape Verde using multiwavelength Raman and polarization lidars during Saharan Mineral Dust Experiment 2008. *Journal of Geophysical Research*, *114*(D13), D13202. https://doi.org/10.1029/2009JD011862

Tesche, M., Gross, S., Ansmann, A., Müller, D., Althausen, D., Freudenthaler, V., & Esselborn, M. (2011). Profiling of Saharan dust and biomass-burning smoke with multiwavelength polarization Raman lidar at Cape Verde. *Tellus, Series B: Chemical and Physical Meteorology*, *63*(4), 649–676. https://doi.org/10.1111/J.1600-0889.2011.00548.X

Tesche, M., Müller, D., Gross, S., Ansmann, A., Althausen, D., Freudenthaler, V., Weinzierl, B., Veira, A., & Petzold, A. (2011). Optical and microphysical properties of smoke over Cape Verde inferred from multiwavelength lidar measurements. *Taylor & Francis*, *63*(4), 677–694. https://doi.org/10.1111/j.1600-0889.2011.00549.x

Textor, C., Schulz, M., Guibert, S., Kinne, S., Balkanski, Y., Bauer, S., Berntsen, T., Berglen, T., Boucher, O., Chin, M., Dentener, F., Diehl, T., Easter, R., Feichter, H., Fillmore, D., Ghan, S., Ginoux, P., Gong, S., Grini, A., … Tie, X. (2006). Analysis and quantification

of the diversities of aerosol life cycles within AeroCom. *Atmospheric Chemistry and Physics*, *6*(7), 1777–1813. https://doi.org/10.5194/acp-6-1777-2006

Thomas, G. E., Poulsen, C. A., Curier, R. L., de Leeuw, G., Marsh, S. H., Carboni, E., Grainger, R. G., & Siddans, R. (2007). Comparison of AATSR and SEVIRI aerosol retrievals over the Northern Adriatic. *Quarterly Journal of the Royal Meteorological Society*, *133*(S1), 85–95. https://doi.org/10.1002/QJ.126

Vaughan, G., Wareing, D., & Ricketts, H. (2021). Measurement Report: Lidar measurements of stratospheric aerosol following the 2019 Raikoke and Ulawun volcanic eruptions. *Atmospheric Chemistry and Physics*, *21*(7), 5597–5604. https://doi.org/10.5194/acp-21-5597-2021

Villani, M. G., Mona, L., Maurizi, A., Pappalardo, G., Tiesi, A., Pandolfi, M., D'Isidoro, M., Cuomo, V., & Tampieri, F. (2006). Transport of volcanic aerosol in the troposphere: The case study of the 2002 Etna plume. *Journal of Geophysical Research: Atmospheres*, *111*(D21). https://doi.org/10.1029/2006JD007126

Wandinger, U., Seifert, P., Engelmann, R., Bühl, J., Wagner, J., Schmidt, J., ... & Ansmann, A. (2012, September). Observations of aerosol-cloud-turbulence interaction with integrated remote-sensing instrumentation. In *Proceedings of the 9th International Symposium on Tropospheric Profiling, edited by: Cimini, D., Di Girolamo, P., Marzano, FS, and Rizi* (Vol. 50, p. 20).

Wandinger, U., & Ansmann, A. (2002). Experimental determination of the lidar overlap profile with Raman lidar. *Applied Optics*, *41*(3), 511-514.

Weitkamp, C. (Ed.). (2006). *Lidar: range-resolved optical remote sensing of the atmosphere* (Vol. 102). Springer Science & Business.

Wang, S., Fang, L., Zhang, X., & Wang, W. (2015). Retrieval of aerosol properties for fine/coarse mode aerosol mixtures over Beijing from PARASOL measurements. *Remote Sensing*, *7*(7), 9311-9324.Weitkamp, D. C. (2004). *Lidar Range-Resolved Optical Remote Sensing of the Atmosphere* (W. T. Rhodes, T. Asakura, K.-H. Brenne, T. W. Hänsch, T. Kamiya, F. Krausz, B. Monemar, H. Venghaus, H. Weber, & H. Weinfurter (Eds.)).

Winckler, G., Anderson, R. F., Fleisher, M. Q., McGee, D., & Mahowald, N. (2008). Covariant glacial-interglacial dust fluxes in the equatorial Pacific and Antarctica. *Science*, *320*(5872), 93–96. https://doi.org/10.1126/SCIENCE.1150595

Yang, X., Zhao, C., Yang, Y., & Fan, H. (2021). Long-term multi-source data analysis about the characteristics of aerosol optical properties and types over Australia. *Atmospheric Chemistry and Physics*, *21*(5), 3803–3825. https://doi.org/10.5194/ACP-21-3803-2021

Yoon, C., Ryu, K., Kim, J., Lee, K., & Park, D. (2012). New approach for particulate exposure monitoring: determination of inhaled particulate mass by 24 h real-time personal exposure monitoring. *Journal of Exposure Science & Environmental Epidemiology*, *22*(4), 344–351. https://doi.org/10.1038/jes.2012.28

Zhang, X. Y., Gong, S. L., Zhao, T. L., Arimoto, R., Wang, Y. Q., & Zhou, Z. J. (2003). Sources of Asian dust and role of climate change versus desertification in Asian dust emission.

Geophysical Research Letters, *30*(24), 2272. https://doi.org/10.1029/2003GL018206